(2)

COMPUTER-CONTROLLED ION BEAM SPUTTER-DEPOSITION OF SUPERCONDUCTING OXIDE FILMS

DARPA Contract No. N00014-88-K-0525

Technical report covering the period July 1, 1988 - June 30, 1989

Principal Investigators:

Orlando H. Auciello* Angus I. Kingon Robert. F. Davis
North Carolina State University, Department of Materials Science and Engineering,
Raleigh, NC, 27695-7907
(919)-737-2347

*Also Microelectronics Center of North Carolina

Table of Contents

PROJECT SUMMARY

This technical report covers the first year of a three-year project. The goals of this project are: 1) the development of a new method for the fabrication of superconducting oxide thin films, viz computer controlled ion beam sputter deposition; and 2) the fabrication of $YBa_2Cu_3O_{7-\delta}$ thin films and devices using this method.

In the early stage of the project it was demonstrated that the use of complex *multicomponent* sputter targets (such as ceramic $YBa_2Cu_3O_{7-\delta}$) present significant problems for compositional control. During sputtering, the surface of the target may exhibit changes in both composition and morphology, resulting in changes in the sputtered flux with time. While these compositional control problems can be circumvented for developmental studies, they threaten to make the production of reproducible Josephson devices virtually impossible.

For these and other reasons (described previously), the new computer-controlled ion beam sputter deposition system was developed. The key features include: 1) a rotatable target holder assembly, which serves to position elemental targets under the ion beam in a rapid sequence, 2) a primary ion beam to produce a sputtered flux from the targets, 3) a secondary oxygen beam (ionic, atomic, or reactive oxygen (ozone)) to oxygenate the film and lower the required deposition temperature, 4) complete computer interfacing to provide real time feedback on the thickness of the depositing species and control of the above items, as well as additional operations such as mask insertion, contact deposition, etc.

In terms of the superconductor device objectives, the system is designed to allow for low temperature deposition for integrated devices, compositional control and flexibility, and for scaling to a commercial system. The capability of the system for controlled sequential deposition of layered structures is fundamental for the production of heterostructures and sandwich junctions (superconductor-insulator-superconductor and superconductor-normal-superconductor). This is demanding due to the short coherence lengths in the oxide superconductors.

It should also be noted that the ion beam sputter-deposition concept developed here presents various improvements over plasma sputter-deposition, such as the absence of the "negative ion effect", and the deleterious interaction of the plasma with the substrate.

The fundamental features of the computer-controlled ion beam sputter deposition concept were demonstrated during this year by constructing a prototype system. The system was used to deposit the first $YBa_2Cu_3O_{7-\delta}$ films by this method, which represents the major achievement for the first year of this research program. Films were polycrystalline, and a post-deposition anneal was employed to produce the superconducting structure.

The prototype system was also used for a fundamental study of the sputtering processes for $YBa_2Cu_3O_{7-\delta}$. Results were compared with calculations performed in conjunction with Argonne National Laboratory, and proved to be invaluable for establishing an optimum system geometry. Particular attention was given to ion backscattering processes which proved to be deleterious to film growth. In addition, sputter yields for the relevant oxides and metals were measured.

The sputtering and ion scattering studies, coupled with the development of the prototype system, have permitted the optimization of the design and construction of the dedicated computer controlled ion beam sputter-deposition system. This system is presently being commissioned. It has the additional important facility for in-situ structural analysis.

Clearly, the method is dependent upon an accurate, rapid method of feedback control. This can presently be achieved at high deposition rate by the use of a quartz crystal microbalance for layer thicknesses down to about 5 Å. This thickness value can be decreased at lower deposition rates without sacrificing accuracy. We currently are working on achieving layer thickness control down to one angstrom at deposition rates of up to 0.5 Å/sec.

It should be clear that the developments of the system during the past year has been rapid. The research team is now in a position to study in detail the deposition of $YBa_2Cu_3O_{7-\delta}$ films using the new technique, which represents the major objective for year 2. The third year will focus upon fabrication of devices.

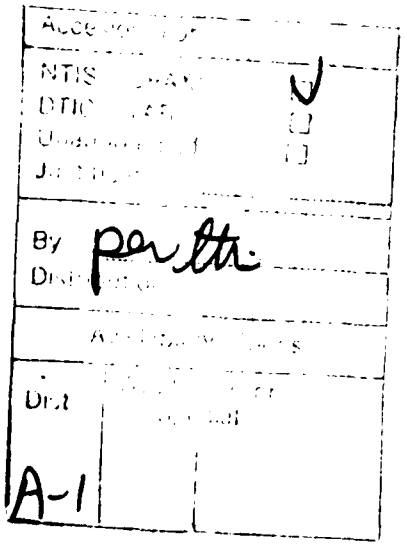

1. INTRODUCTION

The major goals of the present three-year research program are :(1) the development of a new method for the fabrication of superconducting oxide thin films, viz computer-controlled ion beam sputter deposition; and (2) the fabrication of $YBa_2Cu_3O_{7-\delta}$ thin films and devices using this method.

Key features of the new ion beam sputter-deposition technique under computer control include: (1) a rotatable target holder, which serves to position elemental target materials under the ion beam in a rapid sequence, (2) a primary ion beam for sputtering the targets and a secondary oxygen beam (either an ion or a neutralized atomic oxygen beam or an ozone jet) to oxygenate the films; (3) a shutter and a mask interposable between the targets and the substrate, which will be useful for patterning the films and producing simple device structures. The rationale for this approach has been detailed separately, in both the project proposal and in recent publications (see publications and presentations section). The technique allows one to overcome many specific problems associated with alternative methods such as magnetron sputter-, laser ablation-, and plasma assisted-deposition. In addition, it has the potential for producing as deposited high temperature superconducting thin films at relatively low substrate temperatures compatible with integrated device processing; provides in-process compositional control; allows compositional flexibility; and allows the fabrication of heterostructures, particularly sandwich junctions, which are difficult to achieve owing to the short coherence lengths in the oxide superconductors.

This document details the significant progress which has been achieved in the first year of the project towards the two main objectives mentioned above. Figure 1 shows a project flow diagram which emphasizes the tasks undertaken during the year. Year 2 and 3 projected tasks are shown in summary form only.

Section 2 describes an experimental study on sputtering from single, multicomponent ceramic $YBa_2Cu_3O_{7-\delta}$ targets. It is clearly shown that compositional control is difficult. This is largely due to changes in the target surface morphology during sputtering, and thus the composition of the sputtered flux similarly changes with time. This result,in particular, confirmed our hypothesis that a new deposition procedure is required for the synthesis of complex multicomponent oxides.

Section 3 describes the development of our proposed novel ion beam sputter-deposition system which makes use of multiple single component or single oxide targets. The system is shown schematically in Figure 2.

The Fabrication of High Tc Oxide Superconductor Thin Films and Devices via Computer-Controlled Dual Ion Beam Sputter Depostion and In-Situ Processing

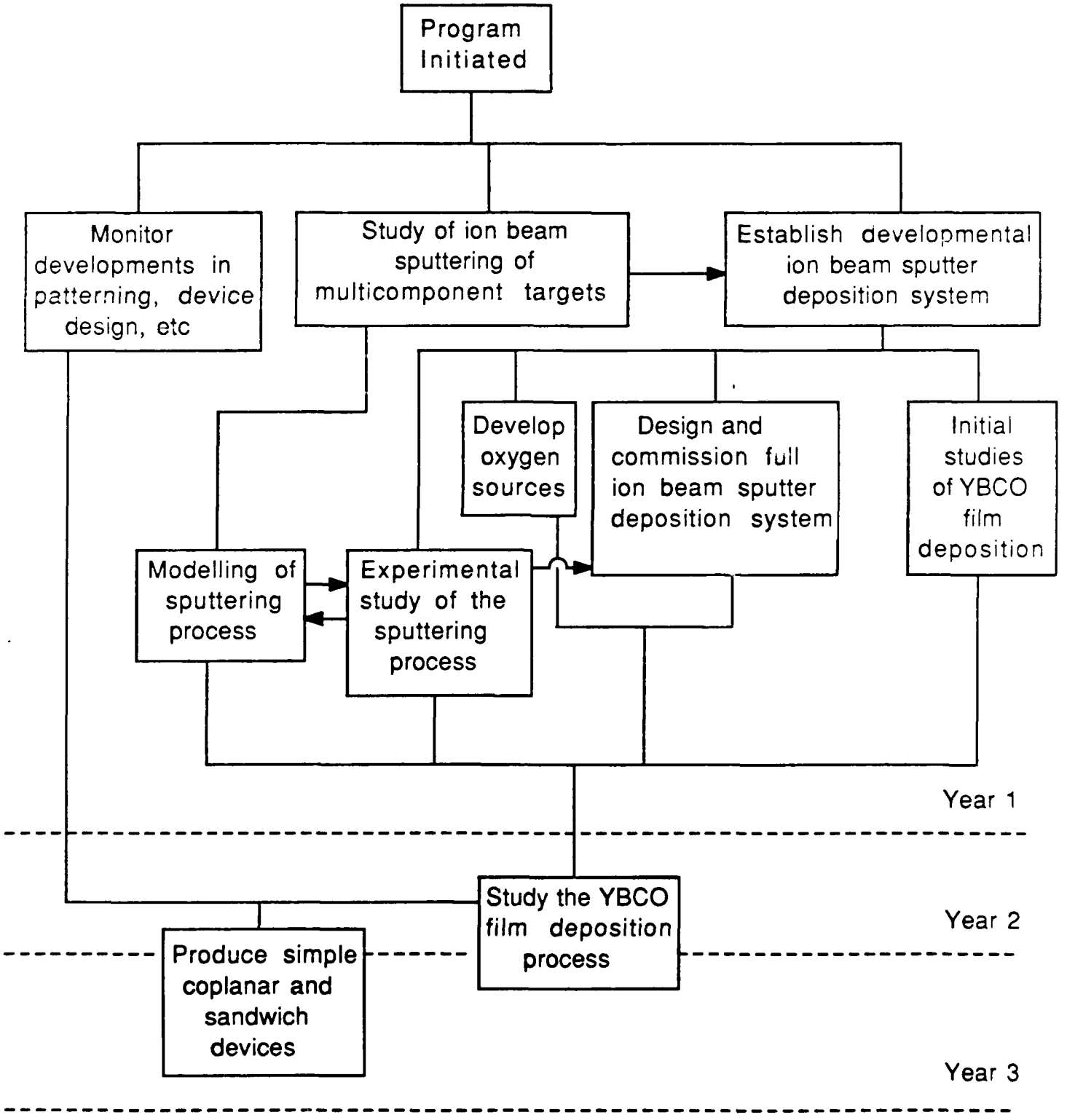

Figure 1. Project flow diagram for work under DARPA.

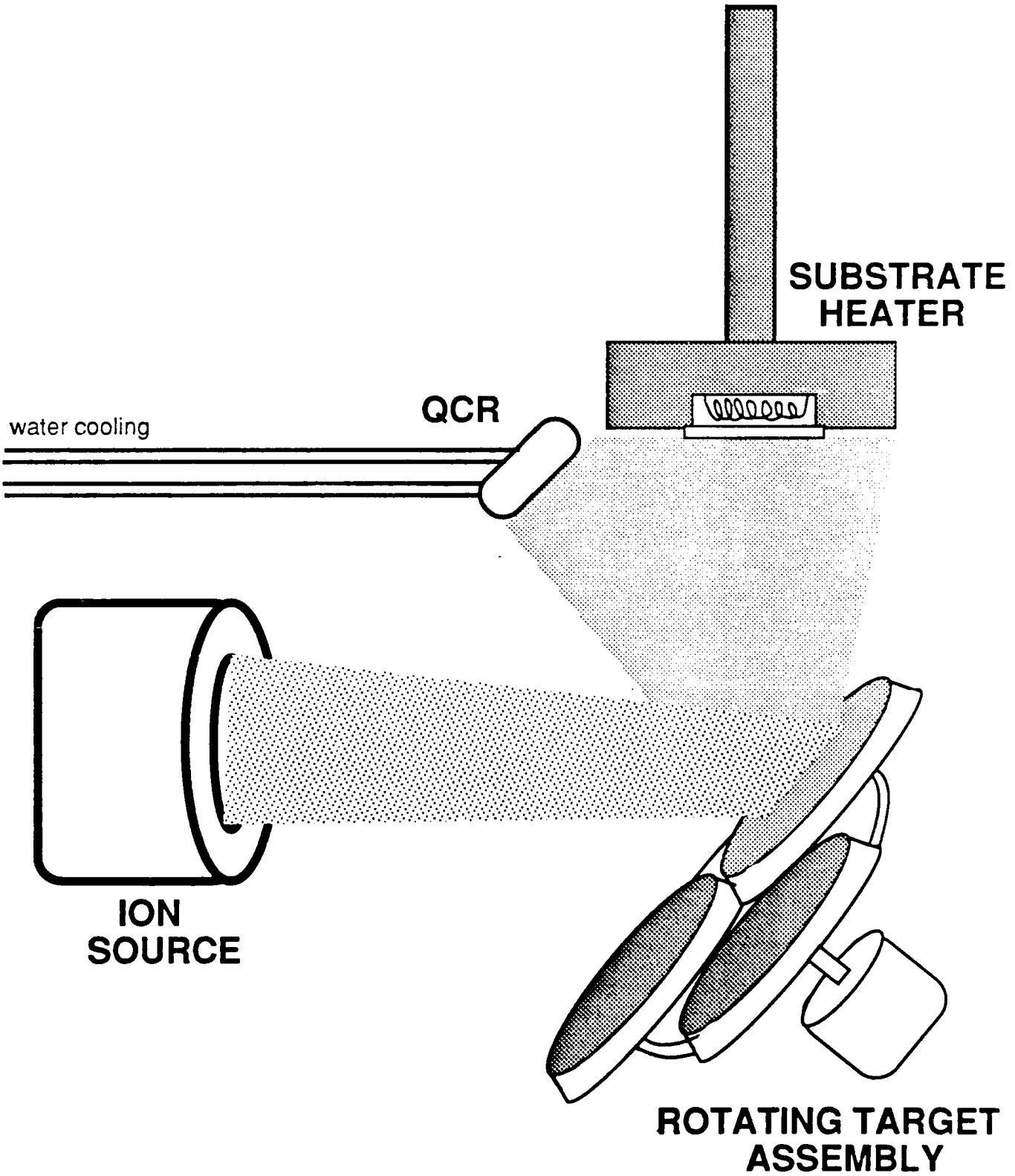

Figure 2. System geometry of the computer-controlled ion beam sputter deposition system. The computer controls the ion source, rotating targets, and quartz crystal resonator feedback loop.

Experiments and computer simulations were performed on sputtering and ion scattering processes from the targets in order to obtain a better understanding of the underlying physical phenomena and to use this knowledge for optimizing the system geometry. These studies provided a time-effective means for system optimization. The details, and the significance of the results are presented in Section 4.

In Section 5, the deposition and characterization of superconducting $YBa_2Cu_3O_{7-\delta}$ thin films is described. For this initial work, a developmental deposition system was constructed. The system has served the valuable purpose of verifying the proposed concepts for the deposition.

In Section 6, the real-time process control system is discussed, and some developments which should allow "layer-by layer" growth (with the layer thickness of atomic dimensions) are proposed. Section 7 contains the references cited in the report, and section 8 lists the publications and presentations made during the past year.

2. SPUTTERING FROM MULTICOMPONENT $YBa_2Cu_3O_{7-\delta}$ TARGETS

Initial studies on film deposition were performed with a $YBa_2Cu_3O_{7-x}$ bulk superconductor target, an unheated substrate, and an unfocused (collimated) 3 cm ion beam. This simple system configuration was useful for studying fundamental sputtering processes, an understanding of which is essential for determining important parameters such as system geometry, identity of sputtering target species, ion beam parameters, etc. Consequently, the influence of ion beam energy and flux on the morphology and composition of the ion impacted target was studied in relation to their effects on the deposited film characteristics. Results of this work have recently been published elsewhere.[1] These preliminary results served to confirm (1) the need for the ability to *individually* control the cation concentrations in the film and (2) the necessity for a thorough understanding of the ion-solid interaction physics involved in the sputtering process. Also, it clearly established the need for using a focused ion beam (<2 cm diameter) to minimize or eliminate impurity incorporation into the growing film from both the chamber sidewalls and target holder, and cross-contamination from adjacent targets, due to sputtering by ions from the tail of the ion beam gaussian profile spilling off the temporarily irradiated target.

The ion beam focusing problem was addressed by obtaining a commercially available Kaufman type ion source fitted with focusing grids, which generates a pseudo-focal point of ions at the target position, thereby confining the impingement area. The beam profile and current density were measured by sweeping a Faraday cup across the beam at the target position, which yielded the beam profile depicted in Figure 3. The ion source grid alignment was found to be critical for obtaining a properly directed beam with a reliable performance for extended period of times as demonstrated throughout several experiments.

The studies on ion beam sputtering of $YBa_2Cu_3O_{7-\delta}$ targets were directed at obtaining information on ion bombardment-induced surface topographical and compositional changes occurring during ion impact on the target and their possible influence on the composition and characteristics of the sputter-deposited films. Ar^+ ion beams of 600 to 1350 eV and 100 mA were used to irradiate the targets and deposit films on MgO or 3% yittria stabilized zirconia (YSZ), which were kept at room temperature. The deposited films were annealed in O_2 at 900 ^oC and slowly cooled in the furnace. Typical film thicknesses were < 2000 Angstroms. Secondary electron emission microscopy (SEM) was used to study topographical changes induced on the target surface by ion bombardment during the sputtering processes, while Auger electron spectroscopy (AES) analysis were performed on targets and films to correlate compositional changes on the targets with compositional variations observed in the films. The results appear summarized in table 2.1.

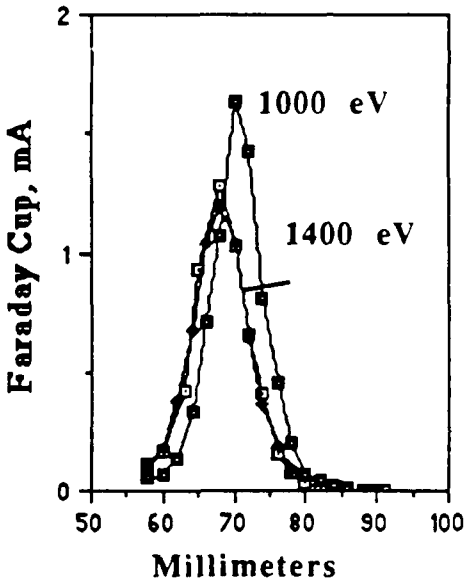

Figure 3. Ion beam profile of the primary beam used for ion beam sputter deposition of high temperature superconducting films. The profiles correspond to Ar^+ ion beams of 1000 and 1400eV, respectively.

Table 2.1

Results from AES Analyses of Irradiated Targets and Deposited Films

		Ba/Cu	Ba/O	Cu/O
Unsputtered Target Surface		1.56	.35	.23
Target	1350 eV	2.38	.25	.11
	1000 eV	3.93	.49	.12
	800 eV	1.05	.34	.32
	600 eV	3.46	.37	.11
Film	1350 eV	.86	.26	.30
	1000 eV	1.22	.27	.22
	800 eV	1.31	.31	.24
	600 eV	1.29	.20	.25

The analysis of table 2.1 indicates that the copper content is consistently lower on the sputtered target surface than on the unbombarded one. On the other hand, a general copper enrichment occurs in the deposited films. Table 2.1 also shows that the compositional changes depend on the energy of the ion beam. On the other hand, it was observed that the ion bombardment-induced surface topographical changes on the target surface depended on the ion beam current in the range of 5 to 25 mA. Further details of these studies can be seen in ref. 1. These studies served to confirm the need for new alternative ion beam sputter-deposition methods such as the one proposed and presently under development in the present research program.

3. DEVELOPMENT OF COMPUTER-CONTROLLED ION BEAM/ ROTATABLE MULTIPLE TARGET HOLDER DEPOSITION SYSTEM

3.1. Background

The results described in section 2 have emphasized the need for a new or modified method for sputter deposition. Key features of the new computer-controlled ion beam sputter deposition system have been described in the introduction. In this section, we describe particular aspects of the system which we have developed during the reporting period.

3.2. Development of the Deposition Chamber

An ultra-high vacuum chamber has been designed and manufactured for automated deposition and in-situ analysis of high Tc superconducting oxide thin films. A spherical system design was selected because its symmetry allows it to easily distribute many ports aimed at a central point in the chamber. As an example, 14 of the 29 ports have a direct relationship with the substrate when properly aligned for a deposition sequence. Ports are available to accommodate a variety of sputtering hardware and analytical instrumentation to assess vacuum and film deposition conditions including (see Figure 4):

1) 3 cm Kaufman ion source
2) Rotating multiple target assembly
3) Precision manipulator with substrate heater assembly
4) Load lock vacuum transfer and sample loading
5) RHEED ion gun and screen
6) Residual Gas Analyzer
7) Quartz Crystal Resonator
8) DPCMA and X-ray source for surface analysis
9) Second ion source or active flux species such as oxygen plasma or ozone

The chamber is 16 inches in diameter and the spherical shape assures a minimum surface area to volume ratio which is advantageous during chamber evacuation by the turbomolecular/ rotary vane pump station . The station itself is connected to the bottom of the chamber via an elbow which eliminates any possibility of extraneous debris from the chamber entering the turbo pump and damaging the blades. An electro-pneumatic gate valve is inserted into a position just below the chamber and equipped with a solid state relay circuit such that in the case of power interruption the gate valve will close and the chamber will

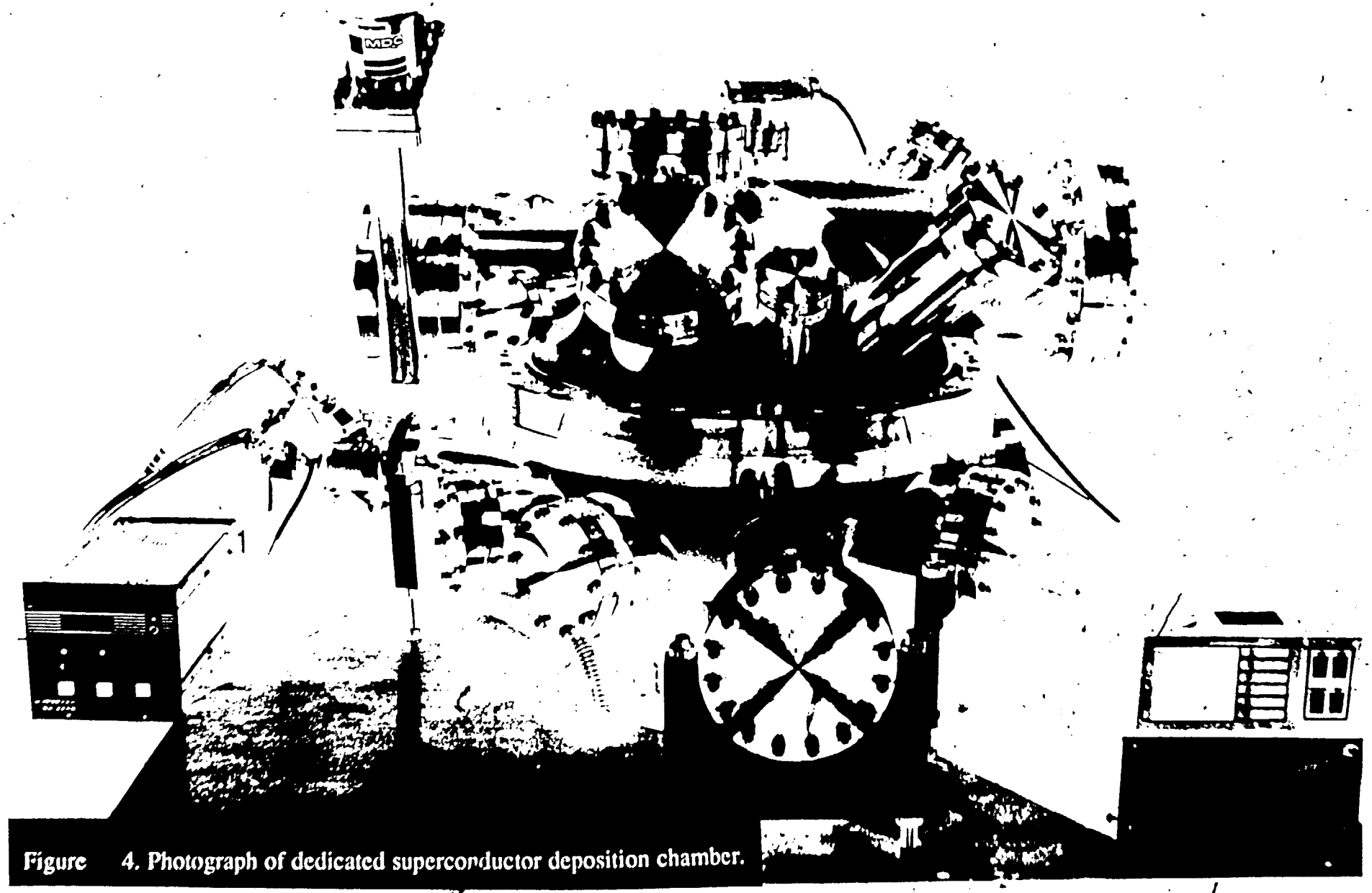

Figure 4. Photograph of dedicated superconductor deposition chamber.

remain under vacuum. Power can not be restored to reopen the valve until a manual reset button has been depressed.

Note that the construction of the target chamber is such that it can be separated into two hemispheres with the primary vacuum seal along the centerline. This seal, depending upon vacuum requirements, can be made with either a reusable viton 0-ring (10^{-8} Torr range) or high purity copper wire seal (10^{-10} Torr range). The ability to completely separate the upper and lower hemispherical portions of the chamber results in a convenient method to access internal areas of the chamber which provides the operator of the deposition system the flexibility to make necessary adjustments to sputtering hardware, install appropriate shielding to minimize chamber contamination, and allow for easy routine maintenance and cleaning to assure that the chamber remains in good operating condition. A motorized hoist system utilizing a permanent magnet motor and a variable speed SCR controller has been designed (currently under construction) to assist separating the hemispheres, in order to maintain a smooth motion during movement of the top hemisphere and maintain the integrity of the flange sealing surfaces.

Substrate loading and removal after deposition is accomplished through the use of a specially designed load lock system, which is cycled between atmospheric and vacuum pressures utilizing a small turbomolecular pump. Figure 5 is a schematic representation of the load lock assembly. The system features a 5 way cross with appropriate vacuum gauges to monitor the pressure inside the cross assembly and a specially designed hinged door which is attached to one port of the cross to allow for efficient loading and unloading of substrates. The transfer of substrates between chambers is realized by opening a manual gate valve and utilizing a magnetically coupled linear feedthrough device to move the substrate holder into position for coupling with the heater assembly. One unique feature of this load lock design is the ability to decouple the entire assembly from the gate valve and move it along a linear motion track. This mechanism facilitates moving the upper hemisphere without having to carry the load lock system.

The events describing the system design and construction are presented chronologically in Table 3.1.

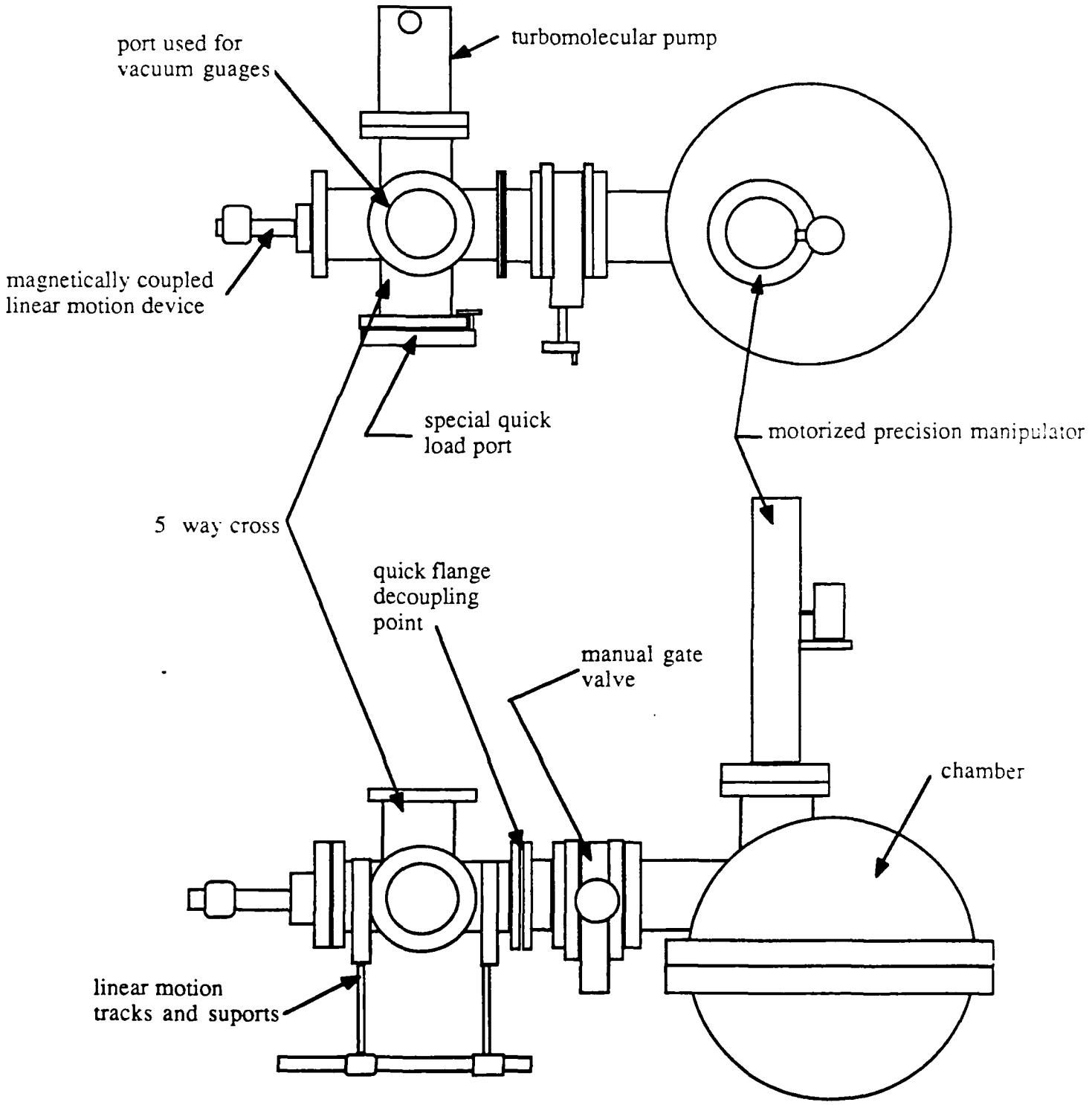

Figure 5. Schematic representation of the load lock design with detachable linear motion translation.

Table 3.1

Date	Event Description
8/88	Begin design of chamber using computer drafting software
10/88	Design completed, chamber construction contract out for bids
12/88	MDC, Inc. awarded contract
1/89	Design and order load lock components including turbomolecular pump package
4/89	Precision manipulator construction contract awarded to Thermionix Northwest
5/89	Chamber arrived at NCSU labs
6/89	Chamber assembled , initial vacuum obtained on 6-6-89 in order to begin leak test. A small turbomolecular pump (50 l/s) purchased for the load lock system was used and a pressure of 5×10^{-7} was achieved. Mounting hardware for ion gun and sputtering targets designed and under construction. Hoist mechanism design completed and under construction. Precision manipulator received.
*7/89	Substrate heater assembly design completed and delivered to NCSU shop for fabrication. Manipulator tested and implemented in system. Motor and target assemblies installed in the system. Computer interface completed.
*8/89	First room temperature thin film depositions made. Heater assembly completed and installed. First high temperature deposition completed. Load lock assembly completed and operational.

* anticipated scheduling of events.

3.3. Development of the Substrate Heater

Substrate heating is essential for fabricating crystalline as-deposited films. Deposition temperatures between 400 and 700°C are in principle necessary for producing as deposited high temperature superconducting films.[1] On the other hand, in-situ post deposition annealing of films can be required to improve crystallinity and/or attain the correct oxygen content necessary for producing the superconductive state; if oxygen-deficient, amorphous films are deposited. For cases in which a post-deposition anneal is necessary, the anneal may be best performed in the deposition chamber in order to reduce contamination which may occur during transfer to an external furnace. In this case, temperatures as high as 900°C may be required of a substrate heater. Considering the criteria discussed above, several substrate heaters have been designed and tested over the past year. These heaters represent a difficult design problem, because of the requirement for a vacuum and an oxygen (1 atmosphere) capability.

The first series of substrate heaters were based on resistive heating elements. The presence of oxygen in the chamber limits the choice of materials from which the element can be constructed. The earlier heater design incorporated Nichrome wire coiled within a Macor furnace block. The substrate holder was fabricated from boron nitride (a good thermal conductor at high temperature), and featured a mechanism which allowed rapid substrate introduction through the load lock. The substrates were fastened to a boron nitride plate, and clips for holding the substrates were attached to the surface of the plate.

The plate was heated by radiation from the filament and the substrate heated by thermal conduction through the boron nitride. Initial heating in vacuum was therefore slow, owing to the lack of convection processes. In addition, the Macor furnace block was susceptible to thermal fatigue cracking, although there was no problem attaining the required temperatures. The Nichrome element, however, was subject to "hot spots" and frequently failed. The cause of these hot spots was attributed to stresses induced in the Nichrome element during the coiling procedure.

The next substrate heater design involved substrate heating through direct contact with the heating element. To accomplish this, the heating element was placed directly on the surface of the support plate underneath the substrate. A strip of platinum mesh slightly larger than the substrate was chosen as the heating element . This platinum mesh heater performed well over a limited period of time, though its maximum temperature was only 500°C. After a number of depositions, a marked decrease in the maximum temperature of the furnace was observed. An inspection of the heating element revealed that components of the high Tc superconducting films (copper, barium, and yttrium) were deposited on the surface of

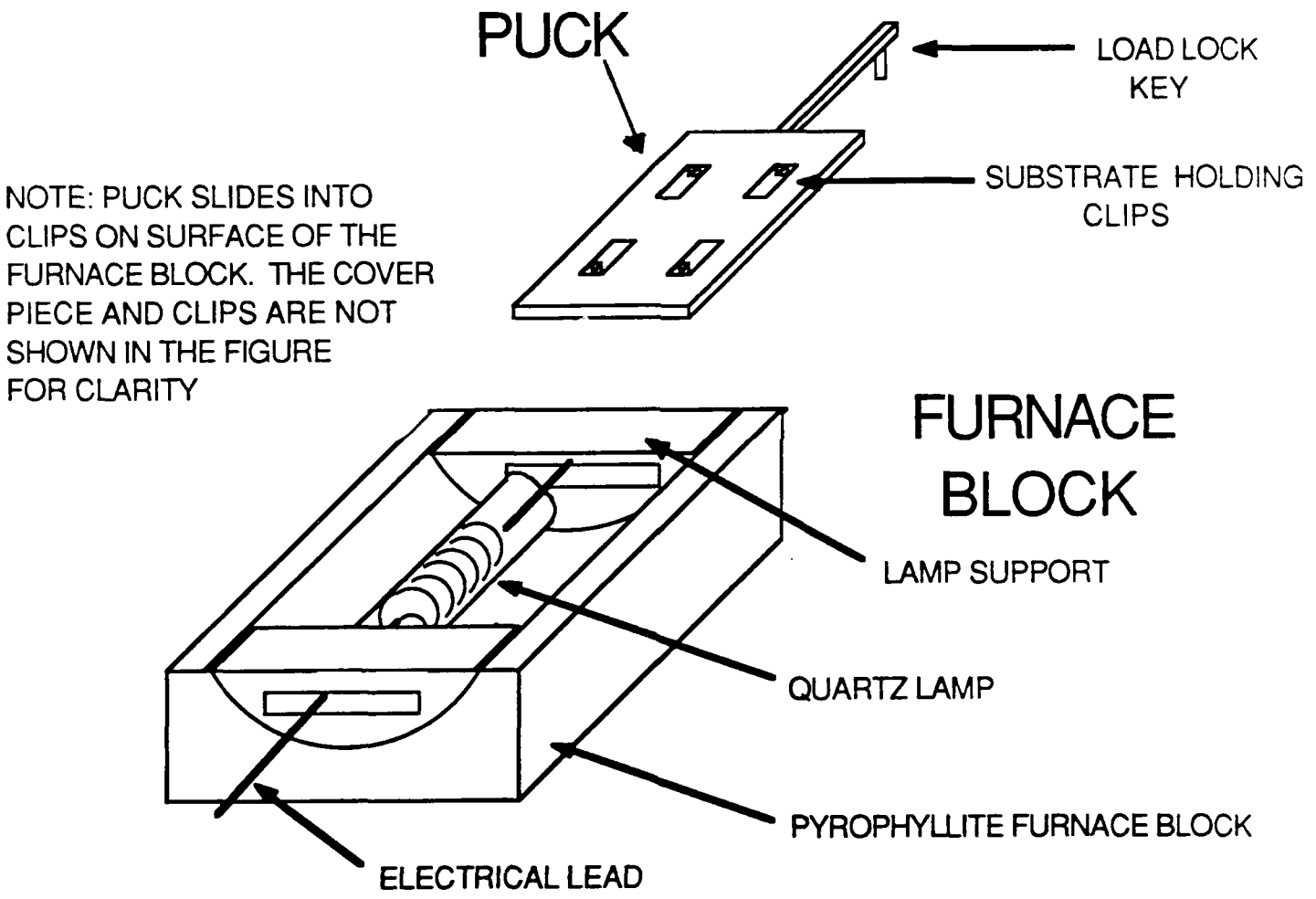

Figure 6. Diagram of the quartz lamp heated furnace block with load locking capabilities.

the support plate, creating new current paths, which effectively lowered the resistance of the element and limited the maximum achievable temperature.

The platinum mesh was subsequently replaced by tantalum foil hoping to increase the maximum temperature of the furnace. The tantalum foil possessed a higher resistance than the platinum allowing for a higher temperature since a limit of 20 amps was available to the furnace. Special care was taken to ensure that the tantalum was shadowed by the substrate so that no alternate current paths could be created due to sputtered material deposition. In addition, the support surface was cleaned between depositions to prevent build up of sputtered metals. This method produced some problems related to temperature non-uniformity across the surface of the substrate due to overheating of the areas in direct contact with the mesh, which had wires in a square grid pattern.

The current heater design is based on a quartz lamp heating element. This lamp attains very high temperatures and draws much less current than the resistive heaters discussed above. The lamp support consists of a pyrophyllite block (Figure 6), which houses a Sylvania 500 Watt tungsten halogen quartz lamp. A platinum reflector plate is positioned behind the lamp on a cylindrical concave surface of the pyrophyllite block. The radiation emanating from the lamp is thereby focused on the back side of the substrate support (labeled "puck" in Figure 6), which is machined from Inconel to facilitate thermal conduction through it. This furnace has easily attained temperatures above 600°C on the surface of magnesium oxide substrates while passing only half of the rated current through the lamp. The time required to reach these temperatures is less than one half hour, which make feasible the deposition of several films per day. The quartz lamp furnace is currently being used in the sputtering system and has performed well for several months.

3.4. Development of the Rotatable Target Holder

The rotating target holder initially designed and built featured a vacuum stepping motor and a cross-bar aluminum plate, holding three target supporting copper rings, which was directly attached to the motor shaft The targets were pressed into copper retaining rings. Due the the step size of the motor (7.5°) and the torque required to start and drive the rotating target assembly, an undesirable "jerky" movement was produced, which compromised both position reproducibility and target integrity when using oxide targets. Therefore, a pin with a "Teflon" head was positioned in contact with the back side of the rotating aluminum holder plate fulfilling the function of a friction brake. The brake friction force could be adjusted. This method initially worked well, but with extended use at elevated temperatures the brake would stick or show signs of erosion, resulting in failure of the rotating motion. This problem was solved by designing a gear driving mechanism such as

that shown in Figure 7. This rotational driving mechanism provides a smoother rotation with increased turning torque, allowing heavier target loads.

3.5. Oxygen Sources

The oxygen content of high T_c superconducting materials is critical for achieving the superconducting state. In the case of thin films, it is desirable to introduce the oxygen into the lattice during deposition at the lowest possible substrate temperature in order minimize interdiffusion between the film and substrate, which otherwise would occur in a high temperature (>900 ^{o}C) post-deposition anneal. This effect is particularly critical for the integration of high Tc superconducting thin films with Si-based semiconductor technology.[1] Different techniques have been developed to introduce oxygen into growing films, viz, low energy (50-100 eV) oxygen ion beams, ≤ 1 eV atomic oxygen species delivered as a beam or produced in a plasma generated in front of the substrate, and an ozone vapor jet. Each of these methods has advantages and disadvantages.

3.5.1 Low energy oxygen ion beam

The low energy oxygen ion beam (50-100 eV) impacting on the growing film may contribute to improve some film characteristics such as adhesion, density, and crystallization temperature. All these effects, already observed in ion-assisted film deposition of other materials, have been attributed, to some extent, to the extra energy supplied to the growing film by the impacting ions. On the other hand, this ion impact may lead to some radiation damage that even if low, because of the relatively low ion energy involved, may be enough to adversely affect the film characteristics. This may be a relevant factor to be considered when trying to produce high T_c Josephson junctions, where the energy of the oxygen ions may be enough to induce undesirable collisional processes in the very thin (10-100 Angstroms) insulating layer needed between two superconducting films, or may reduce Jc at the film interfaces. A Kaufman ion beam source has been purchased, which is fitted with an specially designed filament resistant to oxidation, and will be used to test the oxygen ion beam approach for film oxygenation as described above.

3.5.2 Sub-eV atomic oxygen beam

Alternatively to the method described in (i), atomic oxygen can be delivered into the growing film as ≤ 1 eV species produced in an r.f. or microwave plasma discharge and formed into a beam via an effusion process through a capillary exit from the plasma container. An advantage of this method, is that due to the thermal energy of the oxygen atoms no damage is

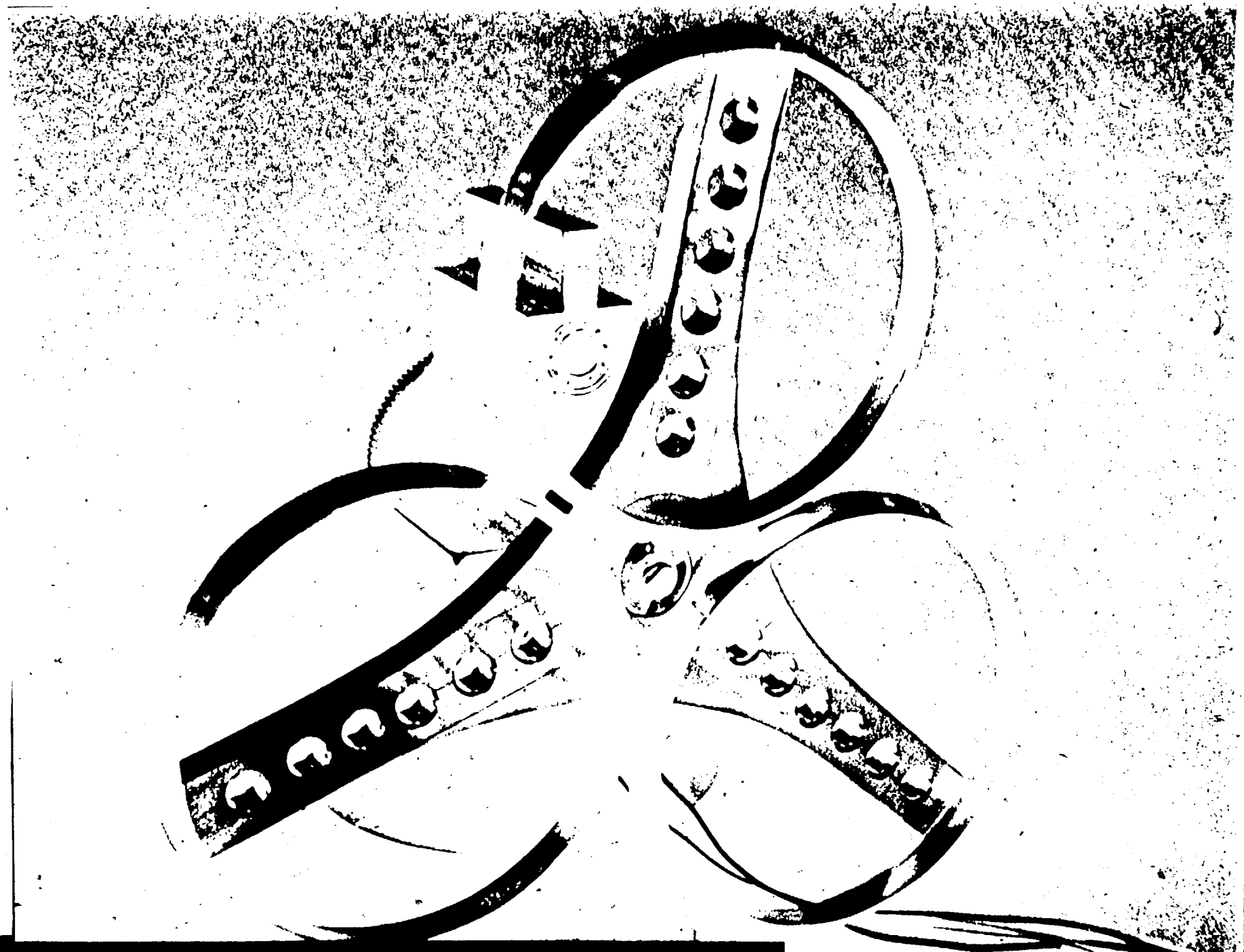

Figure 7. Photograph of the rotatable target holder with gear mechanism currently in use.

expected to occur in the films. However, the potentially beneficial effects of energetic ions described above would not exist in this case. A sub-eV energy atomic oxygen source has been built by one of the principal investigators (O.A.) for another related project and will be tested in the ion beam sputter-deposition system.

3.5.3 Ozone vapor jet

A third approach to dynamically introduce oxygen into the growing film makes use of an ozone vapor jet. This method has already been demonstrated by another group.[2] This ozone source has been used to produce as deposited high T_c superconducting films on substrates at about 600 ^{o}C. A system similar to that already demonstrated[2] has been constructed for use in our ion beam sputtering system.(Figure 8). Ozone is produced by passing pure oxygen through a silent discharge ozone generator. The generator is powered by a 12kV transformer controlled by an a.c. power supply. The ozone/oxygen mixture flows through Teflon tubing to a liquid nitrogen cooled condenser which is maintained at approximately 20 torr by a mechanical pump. At 20 Torr and 77K ozone condenses while oxygen remains in the vapor state. Liquid ozone, purple in color, is allowed to collect in the bottom of the condenser. Enough ozone for a deposition, approximately 1ml, can be collected in 15 minutes to one half hour. The only limit to the amount of liquid ozone that may be collected is the hazard of explosion that large quantities of the liquid represent.

After a sufficient amount of ozone is collected in the condenser, a valve in the line between the generator and the condenser (Figure 8) is closed. The remaining vapor in the system is then pumped by the mechanical pump down to a level below 1 mTorr. This ensures that no vapors except those from the condensed ozone are present in the system, since the vapor pressure of liquid ozone at 77K is approximately 3 mTorr. Following the operations described above, the ozone vapor jet is ready to be introduced into the deposition system. The depositions are carried out with ozone vapor pressures of about 100 - 400 mTorr, which result in a chamber pressure of 2.5 x 10^{-7} Torr. These pressures are attained by heating the liquid ozone with a resistive Nichrome wire heater wrapped around the condenser. The vapor pressure of ozone is an exponential function of temperature, so a specific vapor pressure can be achieved by precisely controlling the temperature of the condenser. This is accomplished by controlling the current being passed through the Nichrome wire by the feedback from a platinum resistive temperature detector (RTD) placed near the bottom of the condenser.

The ozone source has been characterized in conjunction with experiments aimed at depositing copper, yttrium, and barium films via organometallic MBE. The results indicate

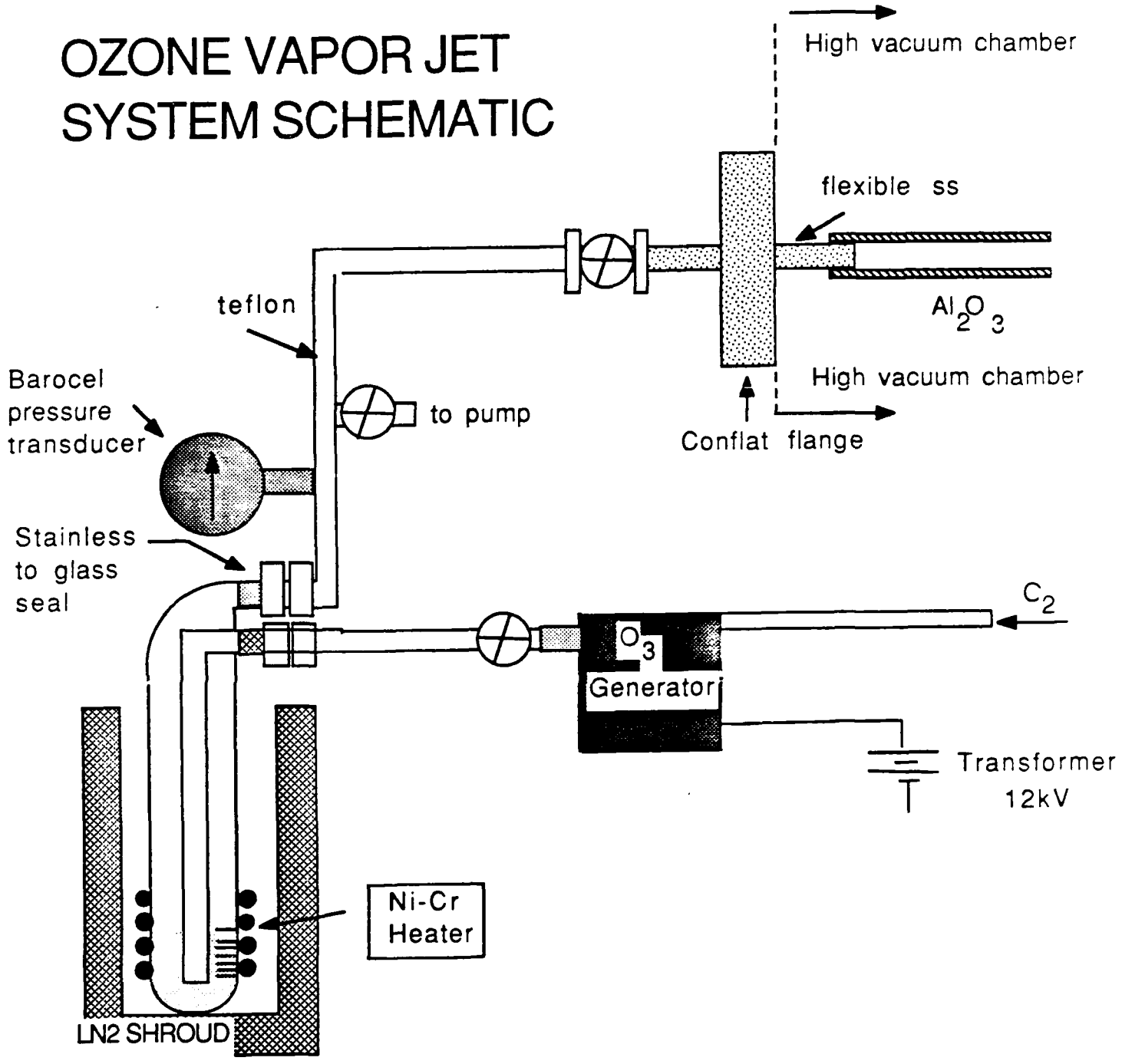

Figure 8. Schematic drawing showing the ozone vapor jet generator system.

that the source is in good operating condition and therefore it will shortly be incorporated in the ion beam sputter-deposition system.

3.6. Computer Control System

The design and implementation of the computer software which drives the ion beam sputter deposition system marks a major achievement in the program. The computer software and associated hardware interfaces play a crucial role in determining the flexibility of the system as both a research tool and as a prototype for potential upgrading to a manufacturing system. With these themes in mind, the software has been developed to allow the user options necessary for compatibility in a university research setting while also providing a testing mode for fully automatic, industrially-oriented applications. The following section describes the computer-related portions of the deposition system, including unique features in both the software and hardware which have been developed for the system.

The computer used to drive the system is a MacIntosh II system including a 40 kilobyte internal hard disk drive, 25K external back-up drive (from Jasmine), and internal floppy. The system has been up-graded to two megabytes of random access memory. We have also purchased a color monitor and phone modem as accessories. This system was chosen for its ease of programming, speed of operation, and user-friendliness.

Interfacing is performed through a National Instruments data acquisition board that features analog to digital, digital to analog, timing, and digital I/O ports, as well as a communications port (RS-232). The current system utilizes all of the features described above. The board can be easily configured and controlled through two software languages, either BASIC or through LABVIEW, a software package developed by National Instruments. Computer programs, described below, have been developed for both software languages. This data acquisition package has proven very adequate for the current demands in implementing the computer controlled ion beam sputter-deposition system.

The capabilities of the computer control software are now illustrated by detailing a typical film deposition. First, the following parameters are introduced into the computer program: (a) the number of sputtering targets necessary to produce a composite film, (b) the density of each target, (c) the thickness of each layer to be deposited (either in Angstroms or ions/cm^2), and (d) the currents and voltages of the beam to tailor the sputtering of each particular target, thus the film component deposition rate. Upon starting the program, the computer rotates the first target into position under the ion beam. The quartz crystal resonator (QCR), used for dynamic monitoring of the film thickness, is then programmed to the film density and is reset to a zero reading. The computer then switches the ion beam on to the specified current and voltage values and monitors the QCR until the film thickness

setpoint is reached. The ion beam is then switched off, to avoid sputtering of the target holder, and thus film contamination during rotation, and target two is brought into position. The cycle repeats itself with each element being sputtered as long as necessary to reach the preprogrammed elemental film set point, and the entire sequence is performed until the desired total film thickness is reached. The uniformity and reproducibility of film deposition from run to run are still being characterized, but initial measurements have shown < 1% deviation in thickness and composition (see Figure 9 for example).

Other parameters which can be controlled prior to and during deposition include gas flow rates, substrate temperature, and a shuttering capability for use in masking substrates, either for target pre-sputtering or metal contact deposition. In the fully automated system, control of pumping and purging cycles for loading and unloading wafers is also available. The design of the program is versatile enough to have instrument control and feedback loops added as the need arises without significant restructuring.

Figure 10 depicts the virtual instrument "panel"(not including many of auxiliary controls mentioned above) created by LABVIEW to drive the system. The grey boxes are for user input data on the targets and other physical parameters (beam energy and current, etc.), and the other windows display data being generated and collected by the computer during a run. The binary toggle switch is used to initiate and halt deposition. Other indicators and control instruments can be added as required.

The BASIC version of the automated control program has been developed primarily through collaboration with A. R. Krauss of Argonne National Labs. Figures 11a-b show the two main windows for programming the deposition in the BASIC program. The window shown in Figure 11a allows the operator to input the target parameters (elements, density, mass) and the mode of film measurements, while that shown in Figure 11b allows to input the parameters for controlling the oxygen flow into the activated species source, the thickness of each deposited element, the ion beam energy, and many other parameters. Additionally, many of the computer protection circuits and interface wiring schematics have been generated through Dr. Krauss' expertise. We are presently coauthoring a paper describing in detail the system hardware, software, and performance capabilities of the computer controlled ion beam deposition system.

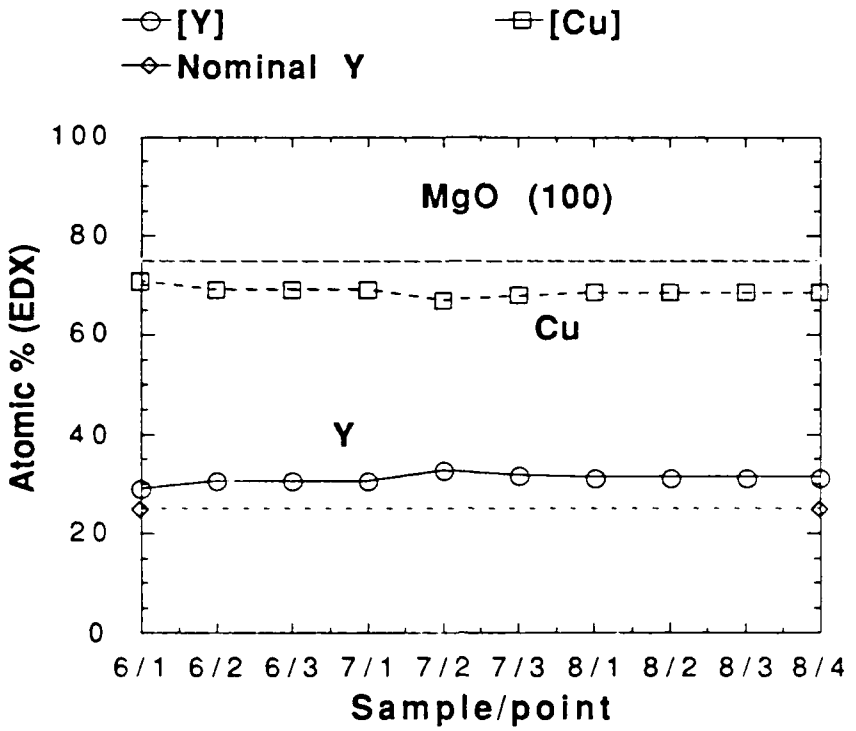

Figure 9. Y_1Cu_2 film deposited by computer-controlled ion beam sputter deposition to demonstrate the accuracy achieved (<1% deviation in thickness and composition) in a two-component film.

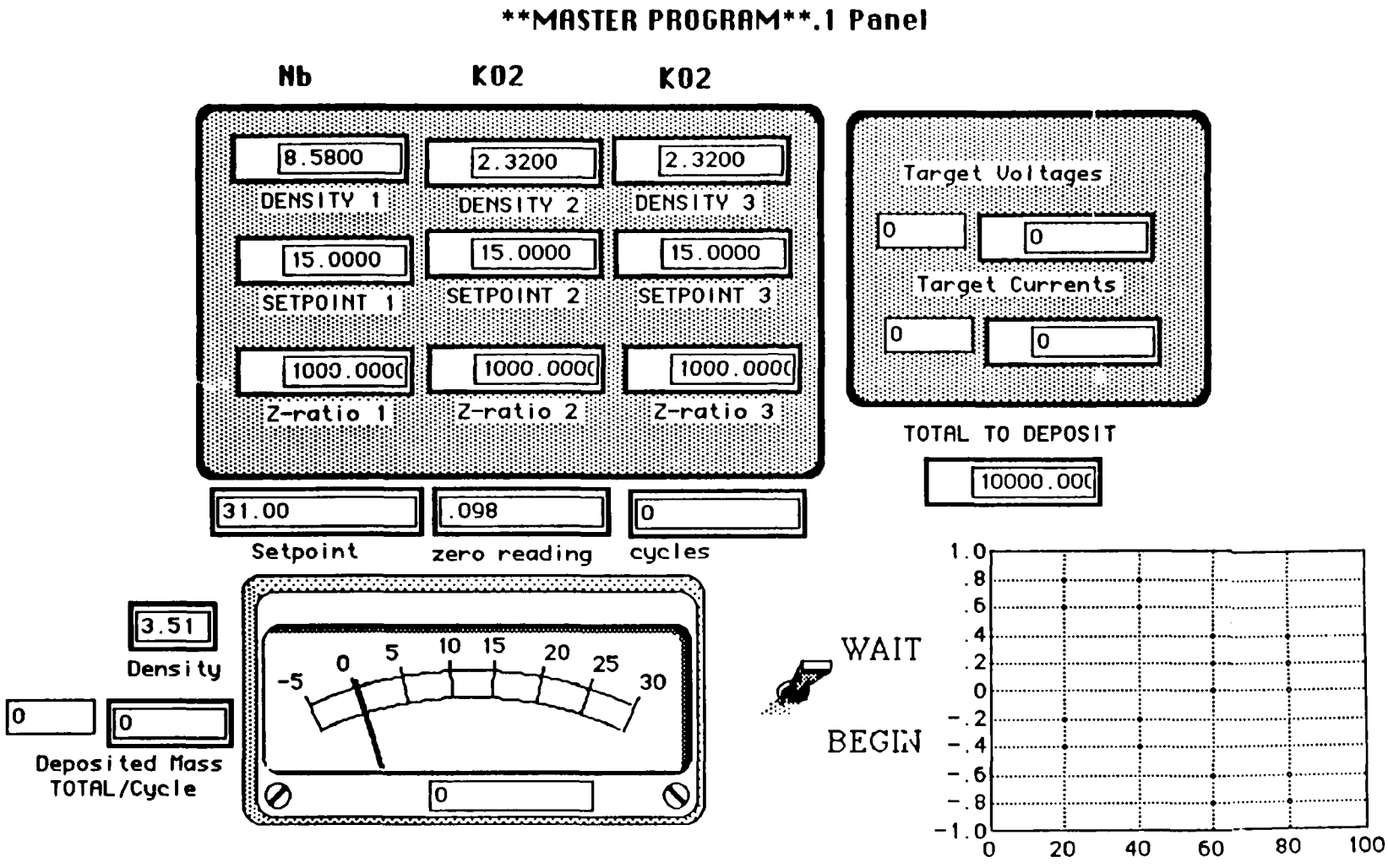

Figure 10. Computer screen generated using LABVIEW software package to control the deposition process. Areas in dark grey are data inputs, others are data output indicators. The binary switch toggles the deposition on and off.

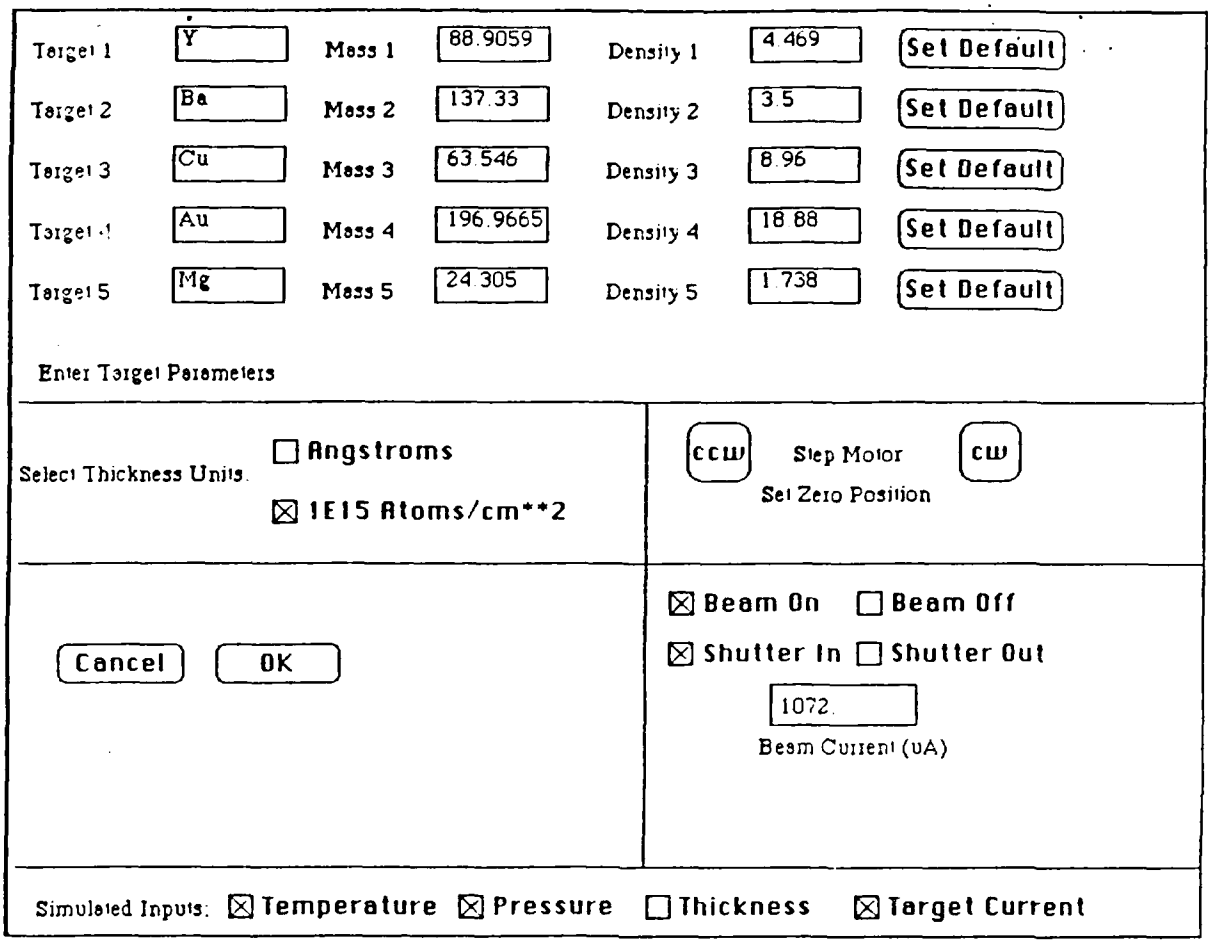

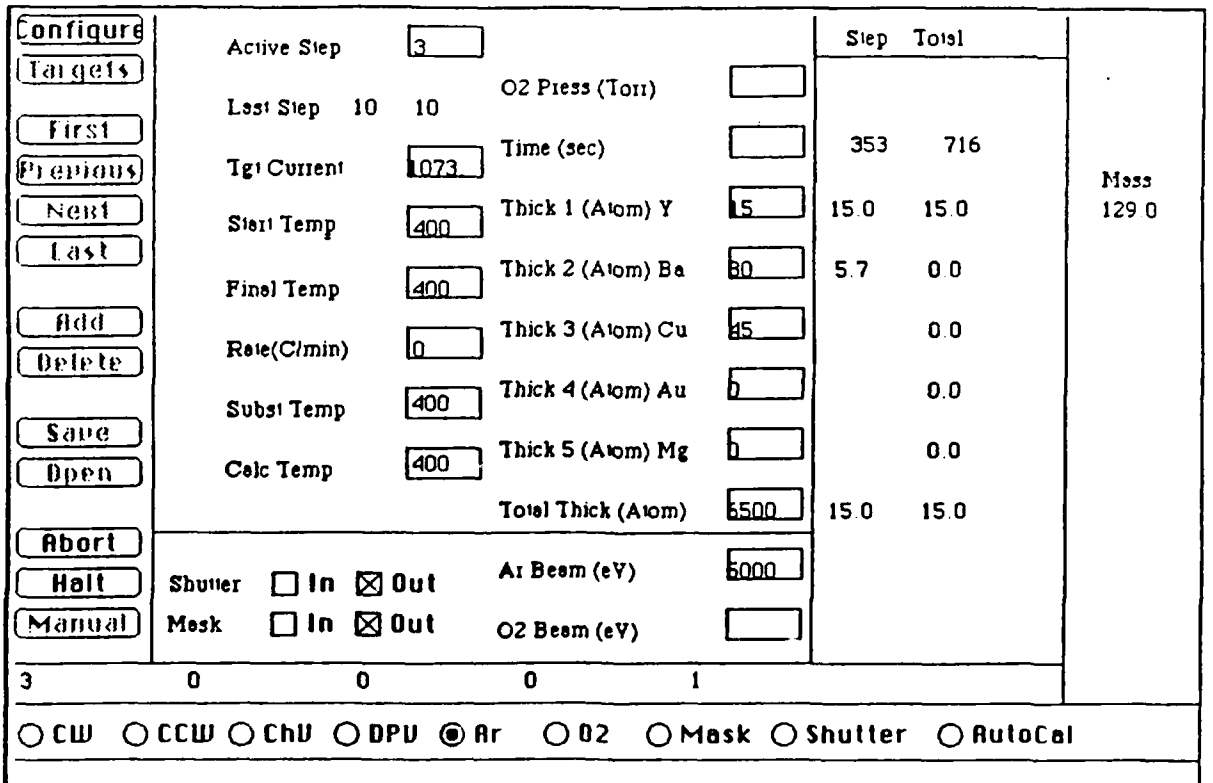

Figure 11. Computer screens generated using BASIC software. (A) Data input and set up parameters screen. (B) Deposition control and monitor screen.

4. COMPUTER MODELLING AND EXPERIMENTAL RESULTS ON ION SCATTERING AND SPUTTERING PROCESSES

4.1. Background

Several groups have been using high current (20-100 mA)/low energy (1000-2000 eV) ion beams to deposit high T_c superconducting films by ion beam-induced sputtering of bulk superconductor (e.g. $YBa_2Cu_3O_{7-x}$) targets.[3] Our group, as discussed in section 2 of this report, recognized limitations in that approach (preferential sputtering of multicomponent oxides, ion bombardment-induced deleterious surface topography, etc.) and therefore developed the automated ion beam sputter-deposition concept described in this report, which involves the use of elemental materials (e.g. Y, Ba, Cu) or their oxides as targets. We realized that little information was available on basic ion scattering and sputtering processes, occurring in ion-targets interaction during film deposition, and their influence on film characteristics at these ion beam energies and fluxes. It was clear that a good understanding of these phenomena was needed in order to determine the optimum deposition parameters (ion energy, ion beam angle of incidence on the target, substrate position with respect to targets, etc.) capable of yielding superconductor films with optimized characteristics.

First evidence for the need of studies discussed in this section were obtained when trying to measure the sputtering yield of Y, Ba, and Cu, a relevant parameter for the present research program. These measurements involved the following steps:

(1) ion beam sputter-deposition of films of each element on separate new gold coated quartz crystals, positioned as indicated in Figure 2, by erosion of the corresponding elemental target with an Ar^+ ion beam (1200 eV) directed at 45^o with respect to the target surface. This is the geometry most commonly used by most researchers in ion beam sputter-deposition of thin films,[4] which was adopted in the first stage of the present program. The material deposited on each crystal produce a decrease in its natural frequency of vibration, the change being proportional to the deposited mass. This is one of the most sensitive methods for in situ dynamical measurement of mass (thickness) of thin films.[5] (2) After deposition, each quartz crystal was positioned in front of the Ar^+ ion beam at normal incidence to measure the sputtering yield from the erosion of the deposited material, in this case by measuring the quartz crystal frequency increase due to the erosion of the previously deposited mass of each particular element.

Cu and Y films were easily obtained by Ar^+ ion beam-induced sputtering of the corresponding materials. However, a net erosion of the quartz crystal gold electrode was observed when trying to deposit Ba. An analysis of the physics of the collision between Ar^+ ions (40 amu) and much heavier Ba atoms (137 amu) on the surface of the target indicated

that the mass ratio is unfavorable for an effective energy transfer from Ar^+ ions to Ba atoms to initiate the collision cascades in the solid, which are necessary for an effective sputtering processes .[6] On the contrary, scattering of Ar^+ ions into an specular reflection direction with respect to the ion beam is favorable, particularly for $\geq 40^o$ angle of incidence as in the case discussed above. The scattered ions may retain enough energy as to produce a substantial erosion of the growing Ba film. Additionally, a substantial amount of scattered Ar^+ ions impacting on the growing film can be trapped in it and adversely affect the film characteristics. The previous analysis lead to the hypothesis that the use of ions of mass equivalent to Ba or higher (Xe for example) would reverse the situation previously described to one in which the energy transfer to Ba atoms would be favorable for producing substantial sputtering and little ion scattering on the target surface. In agreement with the proposed hypothesis, the irradiation of a Ba target by a Xe^+ ion beam (1200 eV) resulted in the production of reasonable thick Ba film, which was subsequently used for measuring the sputtering yield of Ba as previously described for the cases of Cu and Y.

It became evident, from the initial observations described above, that more systematic studies on ion scattering and sputtering were necessary in order to determine the optimum parameters for the ion beam sputter-deposition technique being developed in the present research program. Experimental measurements performed until now involved independent irradiations of Y, Ba, and Cu targets by Ar^+, Kr^+, or Xe^+ ions of 1000 or 1200 eV directed at 45^o with respect to the target surface. Three identical substrates were positioned, for each irradiation, as indicated in Figure 12, such that there surface normal were at 90^o, 60^o, and 30^o with respect to the ion beam direction. Several films were deposited on room temperature substrates by irradiating each target with each one of the ion beams indicated above. The following measurements were performed:

(i) Film thickness by step height profilometry to determine the amount of material deposited on each substrate, in order to obtain information that can be correlated with the angular distribution of the sputtered material.

(ii) Amount of scattered ions trapped in the films to obtain information on the angular distribution of scattered ions from the targets.

Film thickness measurement results are shown in Figure 13. For the case of Cu and Ba sputtered by Ar^+ or Xe^+ ion beams directed at 45^o to the target surface, the thickest films were deposited on substrates at 60^o, while for Y sputtered under the same conditions there was not clear trend. The same deposited films were subsequently analyzed by a semiquantitative secondary ion mass spectrometry technique to determine the relative amount of trapped scattered ions. Figure 14a-b shows results for the case of Ar and Xe incorporation in Cu and Y films respectively. As expected, from the collision dynamics that

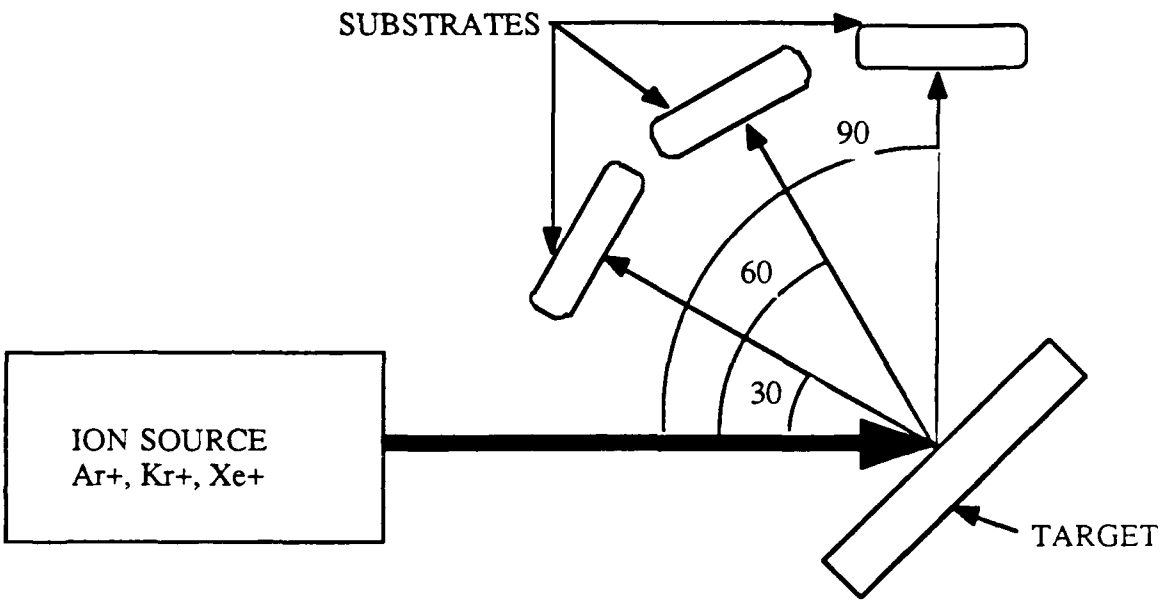

Figure 12. System geometry indicating the position of the ion beam, target, and substrates for studies on sputtering and ion scattering processes as well as experimental scattered ion incorporation into deposited films.

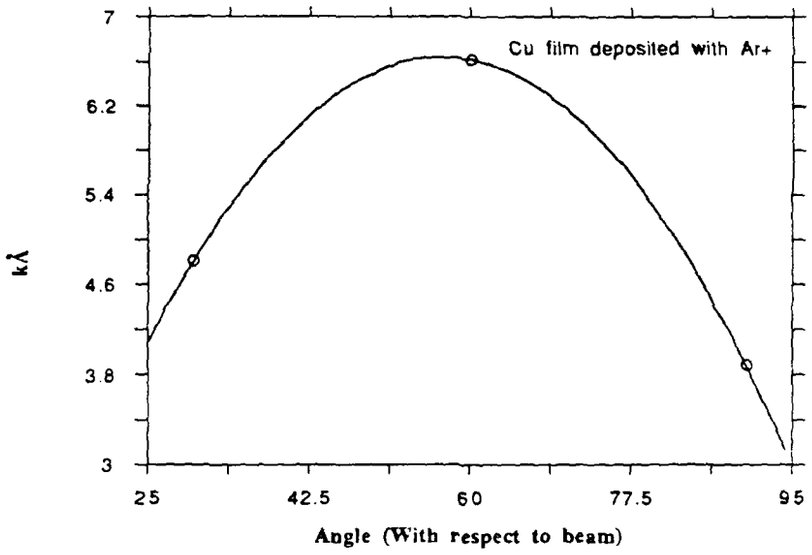

Figure 13. Film thickness as measured with a stylus verses position of the substrate. See Figure for the system configuration used for this study.

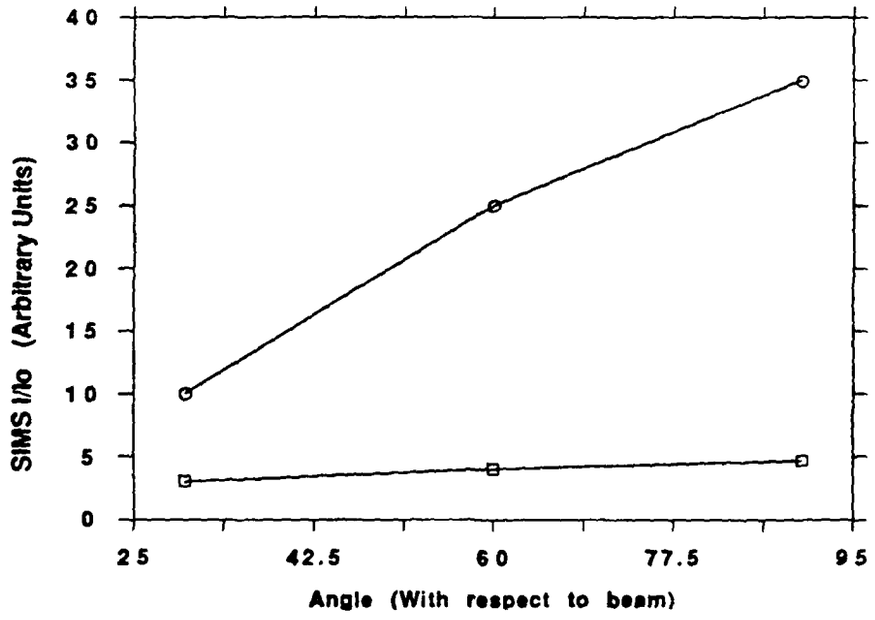

Figure 14. Gas incorporation as a function of substrate-to-beam angle for Ar^+ and Xe^+ bombardment of Cu targets (see Figure). Data was measured using the SIMS technique.

favours scattering into the ion beam specular reflection direction, films deposited at the 90° position contained the largest amount of Ar. On the contrary, the amount of Xe incorporated in films deposited at all three positions was negligible.

The sputtering and ion scattering phenomena were also studied by computer simulations with the TRIM code[7] involving the following parameters: (i) beam energy (1 keV and 9 keV, 1.4 keV in progress), (ii) ion beam angle of incidence with respect to the target surface (45° and 90°), (iii) ion mass (Ar, Kr, Xe, and He), (iv) target (Cu, Ba, Y still in progress). Figures 15-32 show results from extensive calculations on ion scattering yields (number of ions or neutralized ions scattered from the target surface per incident ion) and sputtering yields (number of atoms ejected from the target surface per incident ion) as a function of ion beam energy, angle of ejection (θ) from the target surface, and recoil energy of scattered species. The following general trends can be observed from the analysis of the data in Figures 15-32:

4.2. Sputtering Yield (Y_{sp})

(a) For the case of ions impacting normally to the target surface, Y_{sp} increases as a function of beam energy up to maximum energy calculated (9 keV) for Ar^+, Kr^+, and Xe^+ ions impacting on both Cu or Ba targets (Figures 15a and b). However, an extended range calculation beyond 9 keV should show a decreased in Y_{sp} values. This is generally due to a deeper penetration of the ions into the solid, which results in larger depth for collision cascade initiation and consequently larger energy dissipation in the cascade before it reaches the surface to produce the sputtering of atoms. The results presented in Figures 15a and b are in agreement with others already well stabilized both theoretically and experimentally for most materials.[6]

(b) For the case of ions impacting at 45° angle of incidence to the target surface, Y_{sp} is still increasing for the maximum beam energy used for these calculations (Figures 16a and b), although the sputtering yield curves present steeper slopes at 9 keV. This could be explained by considering that at this oblique angle of incidence the energy deposited in the target through the development of the collision cascade remains closer to the surface than in the normal bombardment case. Therefore, higher energies are required for the bombarding ions to penetrate deeper and produce a reduction in the sputtering yield as discussed for the normal bombardment case, which would lead to a maximum in the Y_{sp} vs. energy curve at a higher energy than for the normal bombardment case.

(c) The analysis of Figures 15 and 16 indicates that in general Y_{sp} is smaller for Ba than for Cu for a given bombarding ion. This depend to a some extent on the energy transferred by the

incident ion to the first impacted atom in the target, which is a function of the ion/target atom mass ratio, and the energy subsequently delivered by the latter to other target atoms in the collision cascade that finally leads to an sputtered atom from the surface.

(d) $\mathbf{Y_{sp}}$ increases as a function of bombarding ion mass (from Ar to Xe), although this increase is at a slower rate at normal than at 45° ion beam incidence. This can be rationalized in terms of similar arguments discussed in (a) and (b).

(e) The outstanding point of the results discussed in (a) and (b), regarding the optimization of parameters for ion beam sputter-deposition of multicomponent films, is that the difference in sputtering yield between Kr^+ and Xe^+ bombardment is relatively small, while both of them produce substantially higher sputtering yields than Ar^+ ion bombardment. This indicates that Kr^+ would be a suitable ion for producing reasonable deposition rates, which is very convenient considering that the production of Kr^+ ions is less costly than the generation of Xe^+.

(f) $\mathbf{Y_{sp}}$ is smaller for ion beam normal incidence than for the 45° incidence case by almost 50% for most ion beam energies (compare Figures 15 and 16) . This is in agreement with what is already well known for other materials.[6]

(g) The sputtering yield $\mathbf{Y_{sp}}$ of atoms ejected with energies > 100 eV increases as a function of bombarding ion energy and mass, the latter particularly noticeable for the 45° bombardment case (compare Figures 17a-b and 18a-b) and decreases, specially for 45° bombardment, as a function of increasing target mass (compare Figures 18a and b). As already shown in Figures 15 and 16, the slope of the $\mathbf{Y_{sp}}$ vs. energy curves, at the maximum energy calculated, in Figures 17a-b is also smaller than those in Figures 18a-b. Again, as in (a) and (b), the behavior described above can be explained in terms of the collision processes with energy transfer between the bombarding ions and the target atoms, with the mass ratio playing the same relevant role as in (a) and (b). The importance of determining the contribution of relatively energetic sputtered particles to the total sputtering flux relates to their effect on the growing film when impacting on the substrate, since energetic sputtered particles may contribute to produce some radiation damage and/or re-sputtering of the growing film. These results should be considered simultaneously with all the others presented in this section when determining which is the optimum geometry for ion beam sputter-deposition of thin films.

(h) The $\mathbf{Y_{sp}}$ vs. polar angle (θ) distributions of sputtered atoms with respect to the target surface normal have been calculated for two bombarding ion kinetic energies at normal incidence to the target surface (9 and 1 keV as shown in Figures 19a-b and 20a-b respectively). These Figures clearly show that the maximum sputtering flux is directed along the target surface normal (0° in Figures 18 and 20). However, the maximum yield, as well as

the decrease as a function of angle, is larger for 9keV than for 1 keV bombardment. Similar calculations for the 45° bombardment case show similar trends (Figures 21a-b and 22a-b)as for normal bombardment. However, the calculations for the 45° bombardment case at 1 keV (Fig. 22a-b) show slight changes in the yields up to about 40-45° and more pronounced changes from 45° to 90°, particularly for the Xe/Cu system. This behavior in principle agrees with previous results,[8] which indicate that the sputtered flux distribution from solids bombarded with ions of ≤ 5 keV energy would extend towards an specular reflection direction with respect to the ion beam incident direction. This effect can in principle be explained in terms of a collision cascade energy deposition closer to the surface for low energies, such that a memory effect of the initial ion beam incident direction exist within the cascade and leads to ejection of sputtered atoms along the mentioned specular direction. This result is important in that it may help in determining which would be the most appropriate ion beam energy for ion beam sputter-deposition of thin films.

4.3. Scattering Yield (Y_S)

(a) Y_S decreases slowly as a function of beam kinetic energy (Figures 23a-b and 24a-b). This is understandable, considering that the scattered ions always penetrate into the solid to a certain depth and suffer multiple collisions with target atoms during their inward and outward paths before they are re-ejected into the vacuum. Therefore, the higher the kinetic energy of the bombarding ions, the larger the penetration into the solid, which would result in a larger amount of ions that statistically will loose enough energy, in their way out as to remain trapped in the target contributing to reduce the number of scattered ions from the solid. This effect would be more pronounced for normal than for oblique bombardment, as in the latter case the ion path remain closer to the surface. Therefore, the scattering yield should be smaller for normal than for 45° angle of incidence as observed in Figures 23 and 24. Again, it is observed, as in the sputtering case, that the difference between the Kr^+ and Xe^+ scattering yields is generally smaller than that between them and the scattering yield for Ar^+ ions.

(b) Y_S decreases as the mass of the incident ions increases (Figures 25 and 24). This is understandable in terms of the physics of the collision between the impacting ions and the target atoms, such that more massive ions will generally be scattered less than lighter ones.

(c) Y_S is smaller for normal than for 45° ion beam incidence by about 50% (Figures 23 and 24), which is qualitatively explainable considering the smaller depth of penetration of ions impacting at oblique angle of incidence, therefore suffering less energy loss than those impacting at normal incidence.

(d) An important parametric dependence to be considered is the scattering yield Y_S vs. kinetic energy (also named recoil energy) of the scattered particles, since the energetic scattered particles impacting on the growing film can lead to substantial sputtering of deposited material, as observed in the experiments previously discussed. Figures 25 and 26 show this parametric dependence for 9 and 1 keV Ar^+ and Xe^+ ions respectively impacting normally to Cu and Ba targets, while Figures 27a-b and 28a-b show similar data for 45^o ion bombardment. It is clearly seen that the yields and energies of scattered Ar^+ ions are generally greater than for the Xe^+ ions. However, in both cases (9 and 1 keV bombarding energy ions) the energy of the scattered ions is not as high as it would be expected to explain the substantial scattered ions-induced sputtering of Ba films, when bombarding the Ba target at 45^o and depositing the film on a substrate at 90^o with respect to the bombarding ion beam direction (see Figure 2), as previously described in this section. One possible explanation to reconcile the apparent discrepancy between the experimental results from the Ba related experiments and the computer calculations presented here is the following. The TRIM code[7] may not properly include ions that are scattered after suffering one or a few collisions at the surface, which are those that will retain a large part of their initial energy and therefore be energetic enough as to produce sputtering of the growing film. A careful study of the TRIM code will be performed in the near future to investigate this problem.

One additional interesting point to be considered from the analysis of Figures 25a and 26a is that the scattering yield of Xe^+ ions from Cu is practically zero for both 9 and 1 keV ions impacting at normal incidence on the target, which is the reason why curves for the Xe/Cu system are not visible. This in principle is expected from the collision dynamics between such a massive ion as Xe and the less massive Cu atom.

(e) In relation to the scattering yield Y_S vs. polar angle (θ) distribution of scattered ions, Figures 29 and 30a-b show that the scattering yield as well as the Y_S vs. θ dependence is much more pronounced for Ar^+ ions than for Xe^+, when impacting at normal incidence, and the scattering yield is larger in the direction along the target surface normal (0^o angle in Figures 29 and 30). For 45^o ion beam incidence, on the other hand, the polar angle distribution of scattered ions show a fairly constant scattering yield, for Ar^+ ions impacting on Cu, up to about 50^o angle and a rapid decrease in the range to 90^o ejection angle (i.e. a direction parallel to the target surface) (see Figures 31 and 32). On the contrary, the scattering yield for Xe^+ ions is much smaller and the polar angle distribution more uniform than for the Ar/Cu case (see Figures 31 and 32).

The studies on sputtering and ion scattering discussed above have been very useful in helping to determine the most appropriate geometry, at least up to our present knowledge, that would be applicable for ion beam sputter-deposition of multicomponent oxides, not only

for superconductors but also optoelectronic and ferroelectric materials. Considering the present understanding of sputtering and scattering phenomena, the optimized geometry is that where the substrate is positioned with its surface almost parallel to the target surface and the ion beam is directed almost normal to the target. This geometry would in principle contribute to minimize ion scattering directed towards the substrate and produce a cosine-like sputtering flux distribution . The quartz crystal monitor, which is a critical component of the computer-controlled deposition system for tailoring the deposited amount of each film component, should be located either at the back of the substrate holder aligned with a central hole on it to allow the sputtered flux to pass through and deposit on the crystal, or at a symmetric position with respect to the normal to the target in relation to the substrate position. Measurements on the symmetry of the sputtered flux with respect to the target normal, not yet completed, will allow to determine which is the optimum mechanically feasible position.

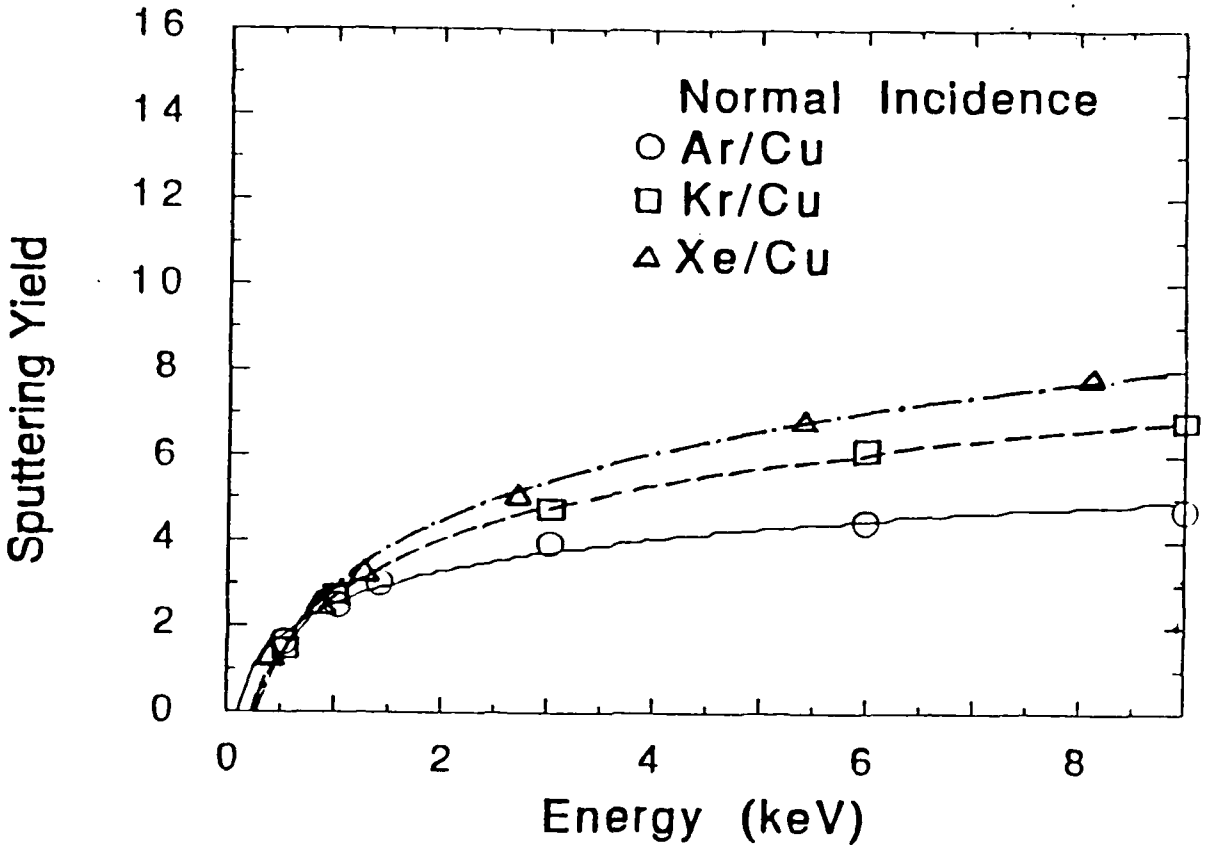
Normal Incidence
Ar/Cu
Kr/Cu
Xe/Cu
Sputtering Yield
Energy (keV)
0
2
4
6
8
10
12
14
16

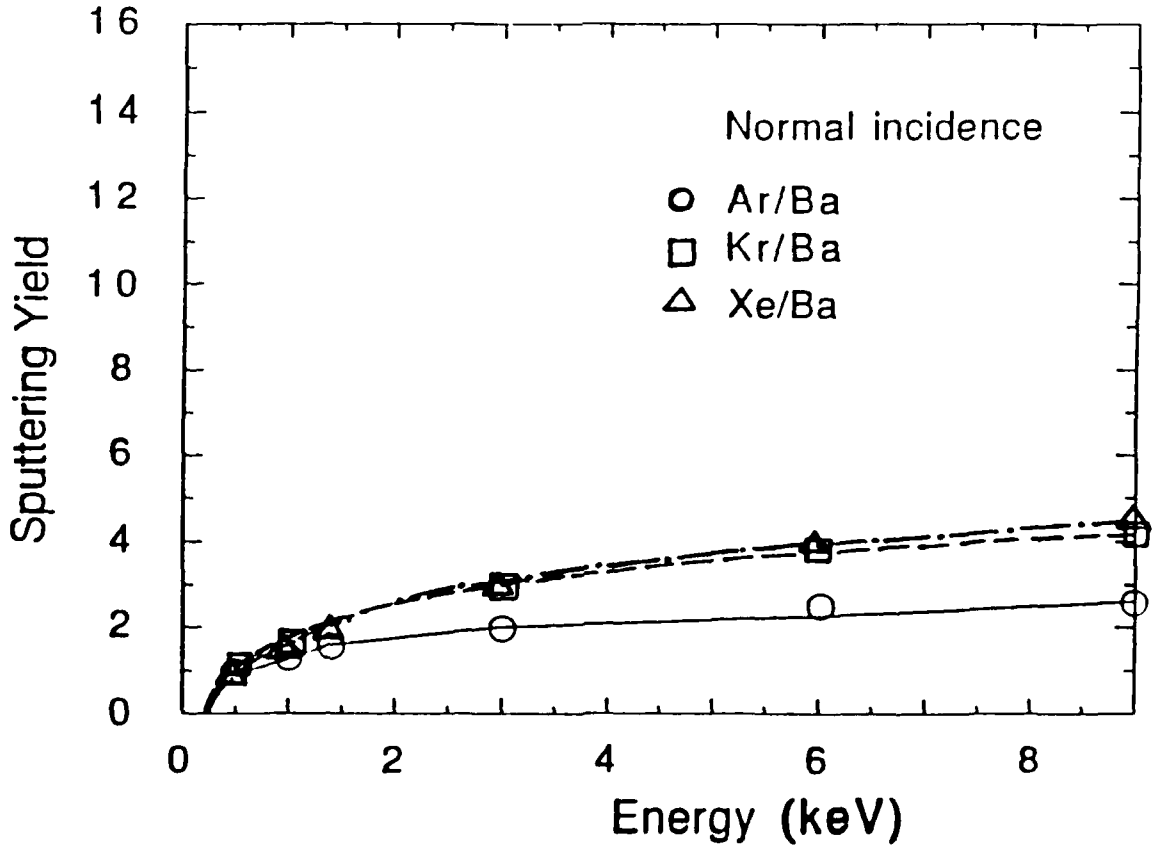
Normal incidence
Ar/Ba
Kr/Ba
Xe/Ba
Sputtering Yield
Energy (keV)
0
2
4
6
8
10
12
14
16

Figure 15.

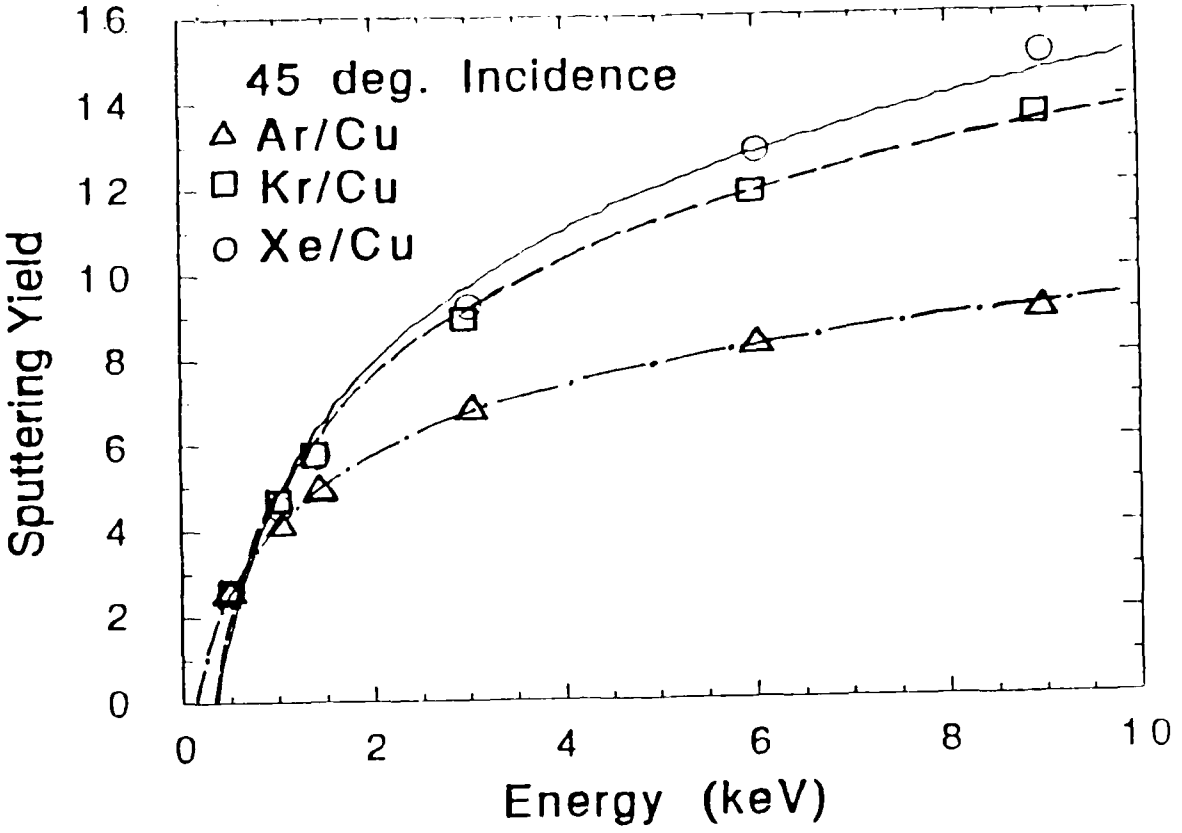
45 deg. Incidence
Ar/Cu
Kr/Cu
Xe/Cu
Sputtering Yield
Energy (keV)
0
2
4
6
8
10
12
14
16

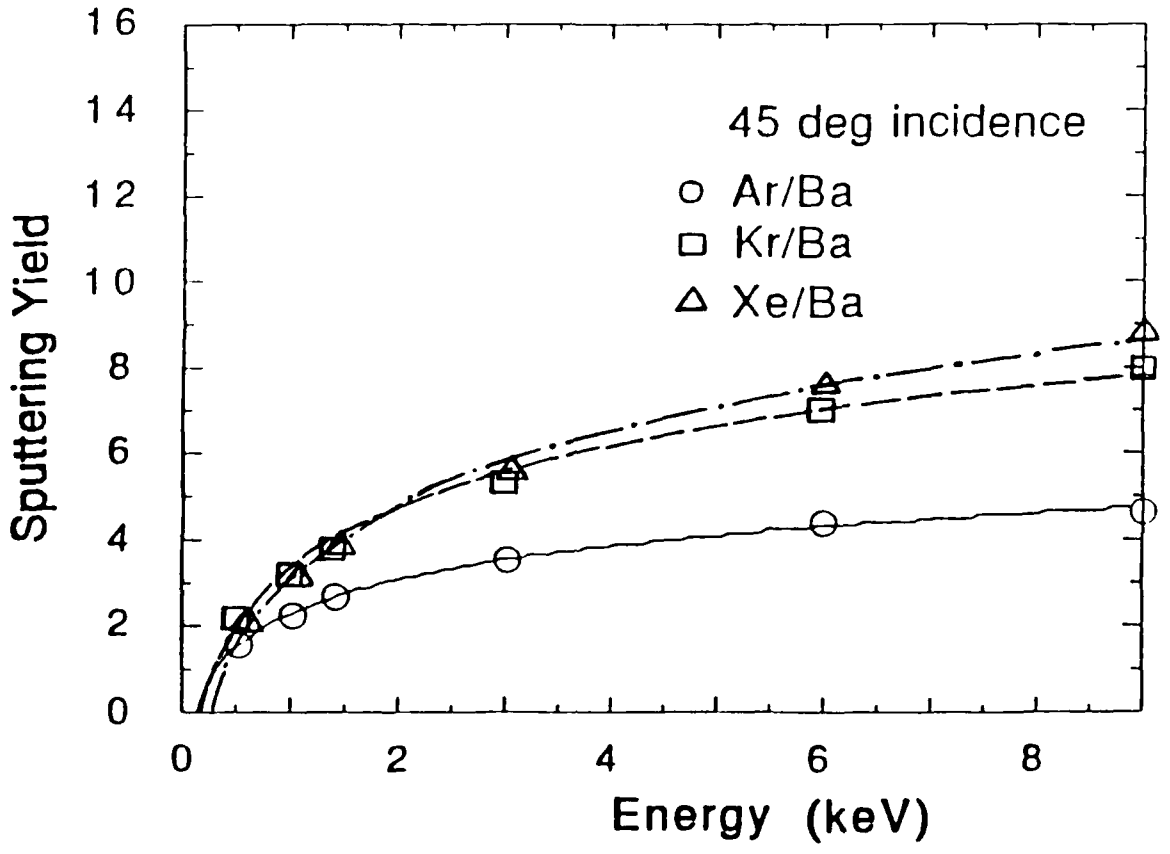
45 deg incidence
Ar/Ba
Kr/Ba
Xe/Ba
Sputtering Yield
Energy (keV)
0
2
4
6
8
10
12
14
16

Figure 16.

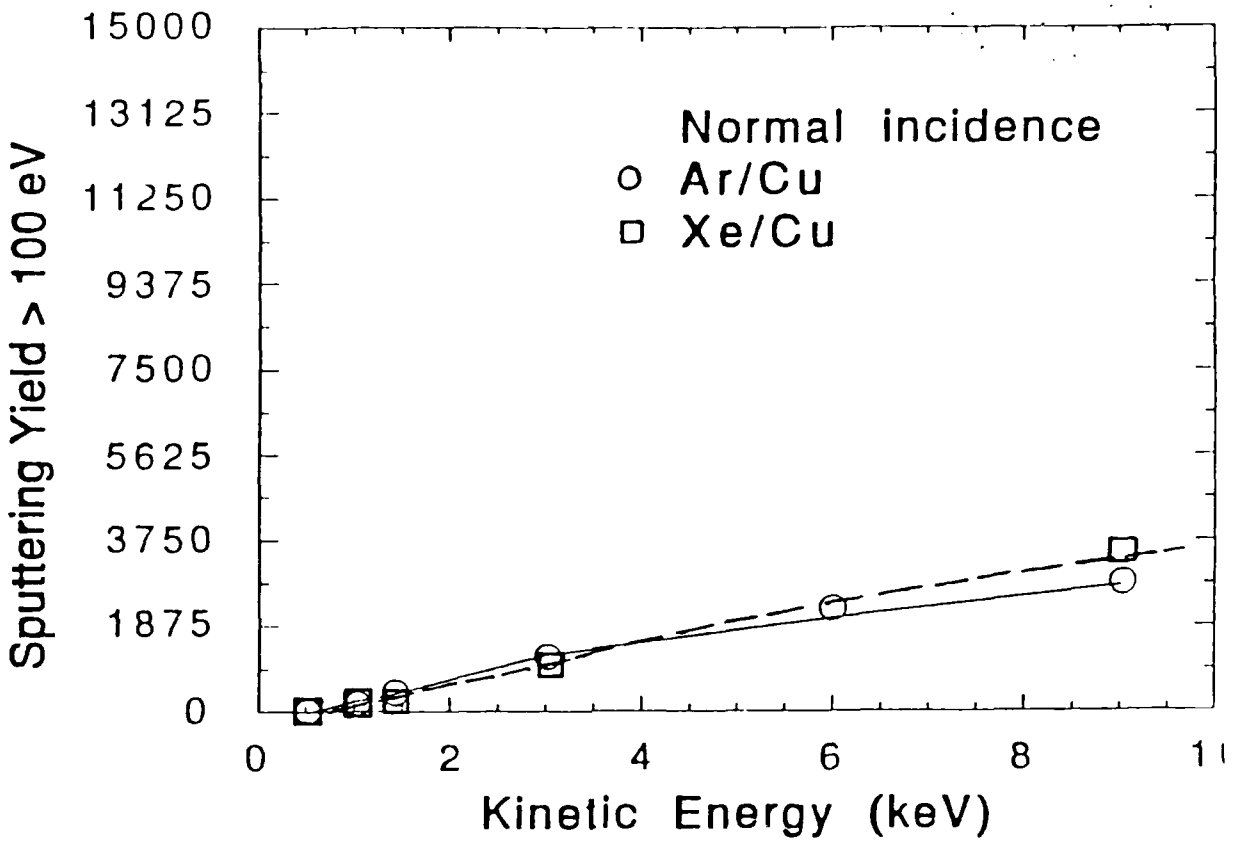
Normal incidence
Ar/Cu
Xe/Cu
Sputtering Yield > 100 eV
15000
13125
11250
9375
7500
5625
3750
1875
0
0
2
4
6
8
Kinetic Energy (keV)

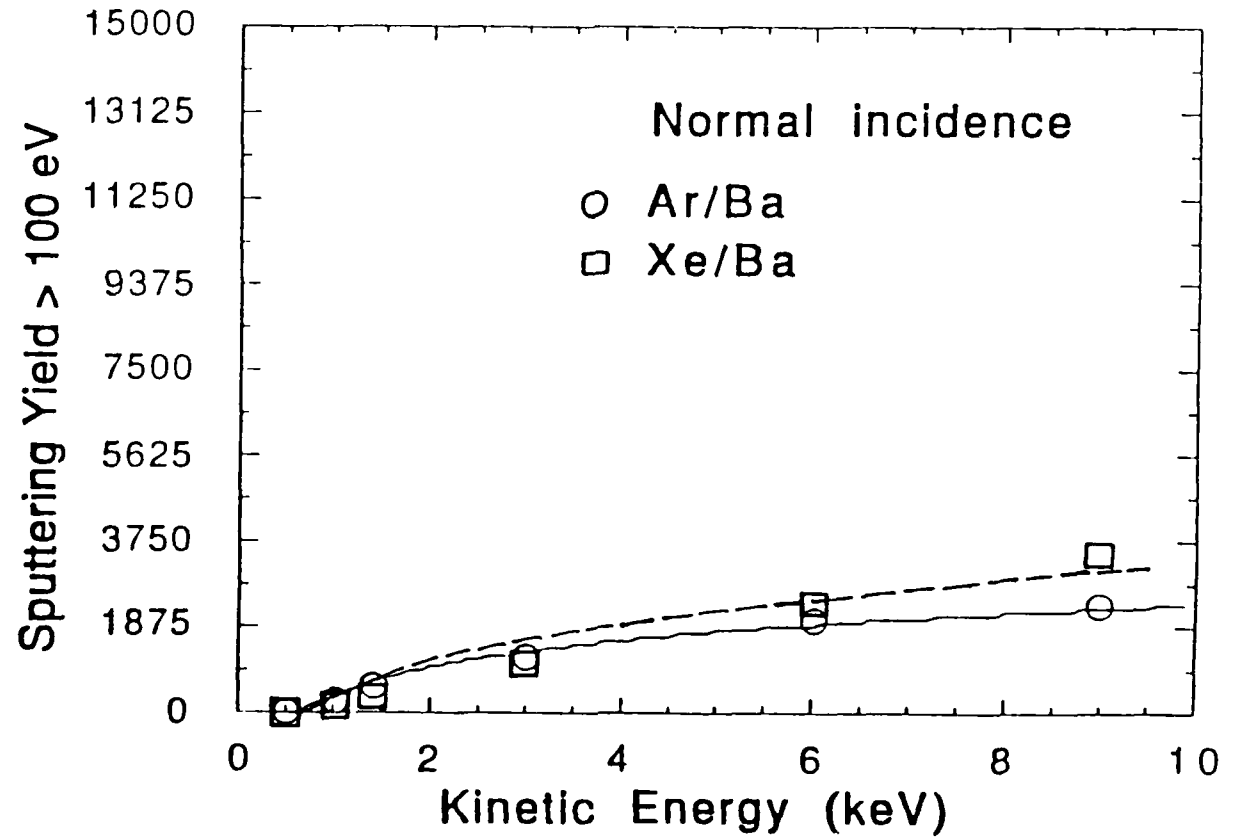
Normal incidence
Ar/Ba
Xe/Ba
Sputtering Yield > 100 eV
15000
13125
11250
9375
7500
5625
3750
1875
0
0
2
4
6
8
10
Kinetic Energy (keV)

Figure 17.

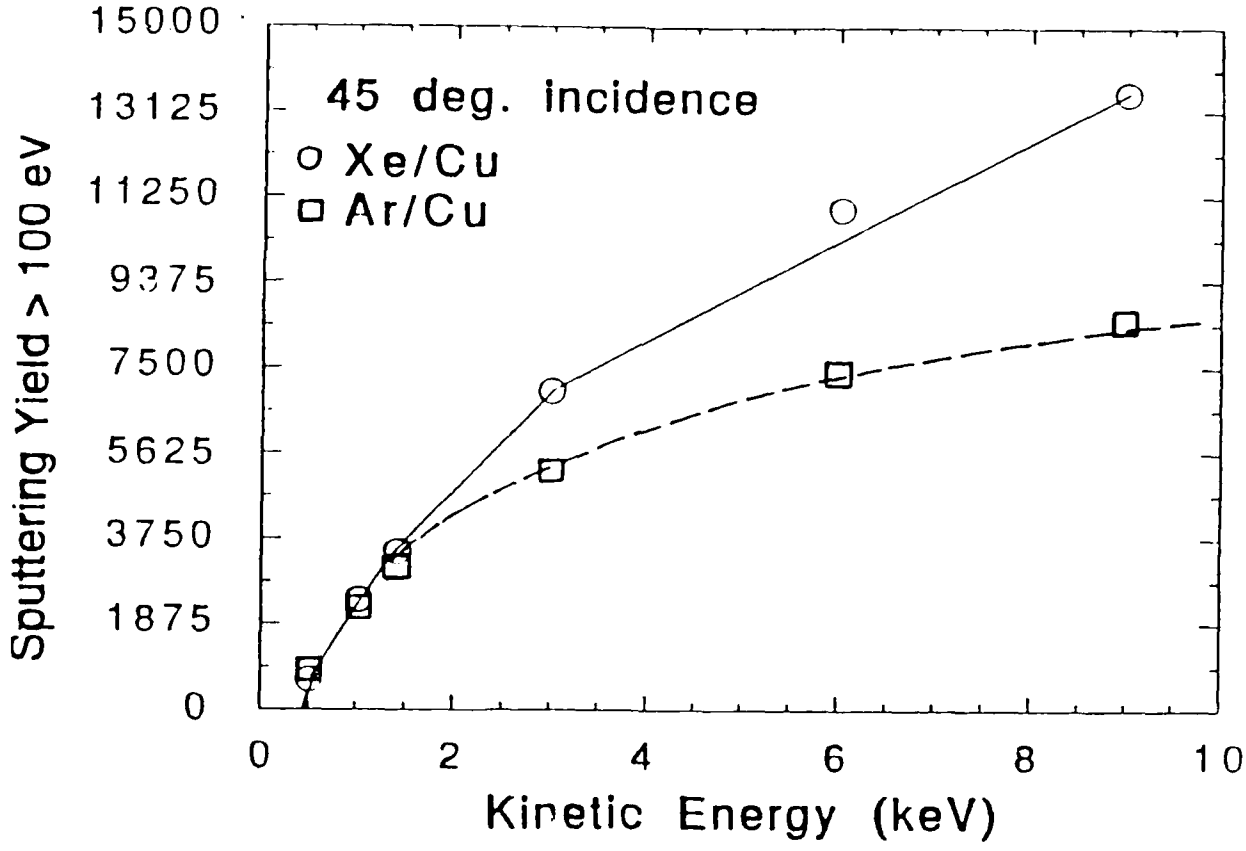
45 deg. incidence
Xe/Cu
Ar/Cu
Sputtering Yield > 100 eV
15000
13125
11250
9375
7500
5625
3750
1875
0
0
2
4
6
8
10
Kinetic Energy (keV)

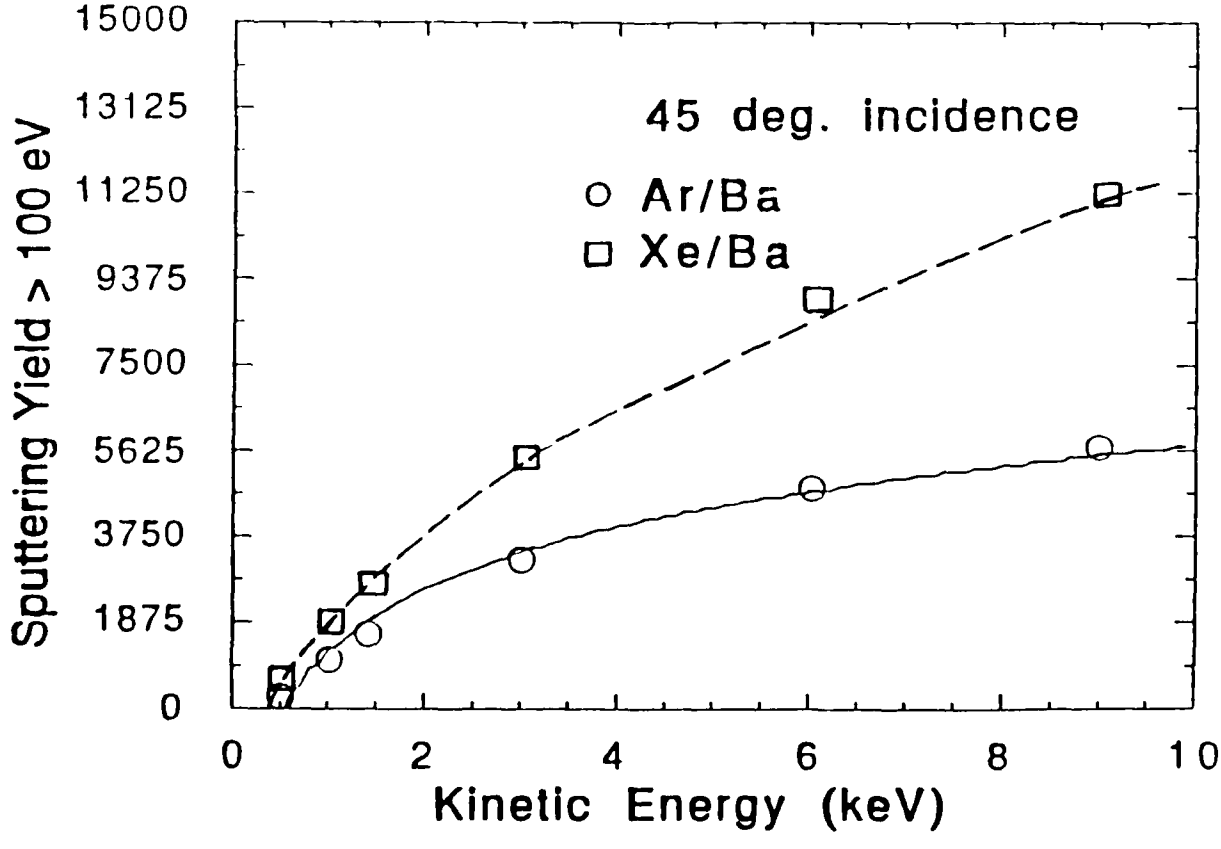
45 deg. incidence
Ar/Ba
Xe/Ba
Sputtering Yield > 100 eV
15000
13125
11250
9375
7500
5625
3750
1875
0
0
2
4
6
8
10
Kinetic Energy (keV)

Figure 18.

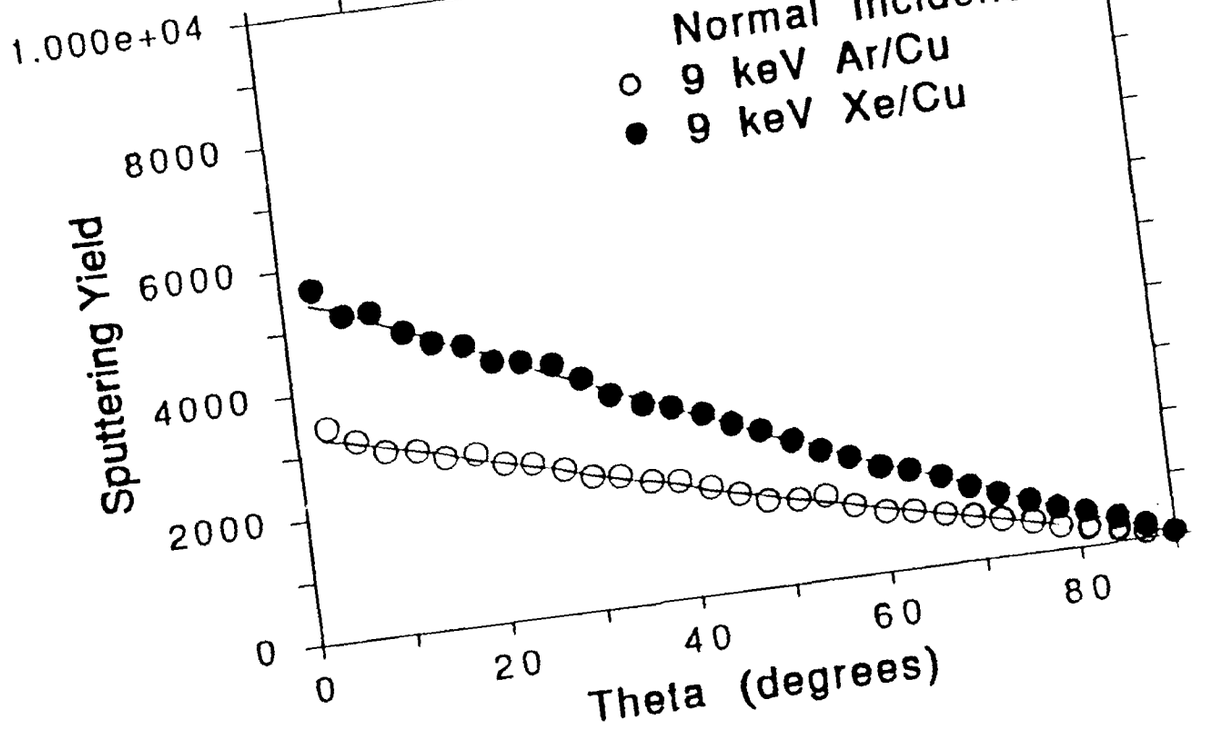
Normal Incidence
9 keV Ar/Cu
9 keV Xe/Cu
Sputtering Yield
1.000e+04
8000
6000
4000
2000
0
0
20
40
60
80
Theta (degrees)

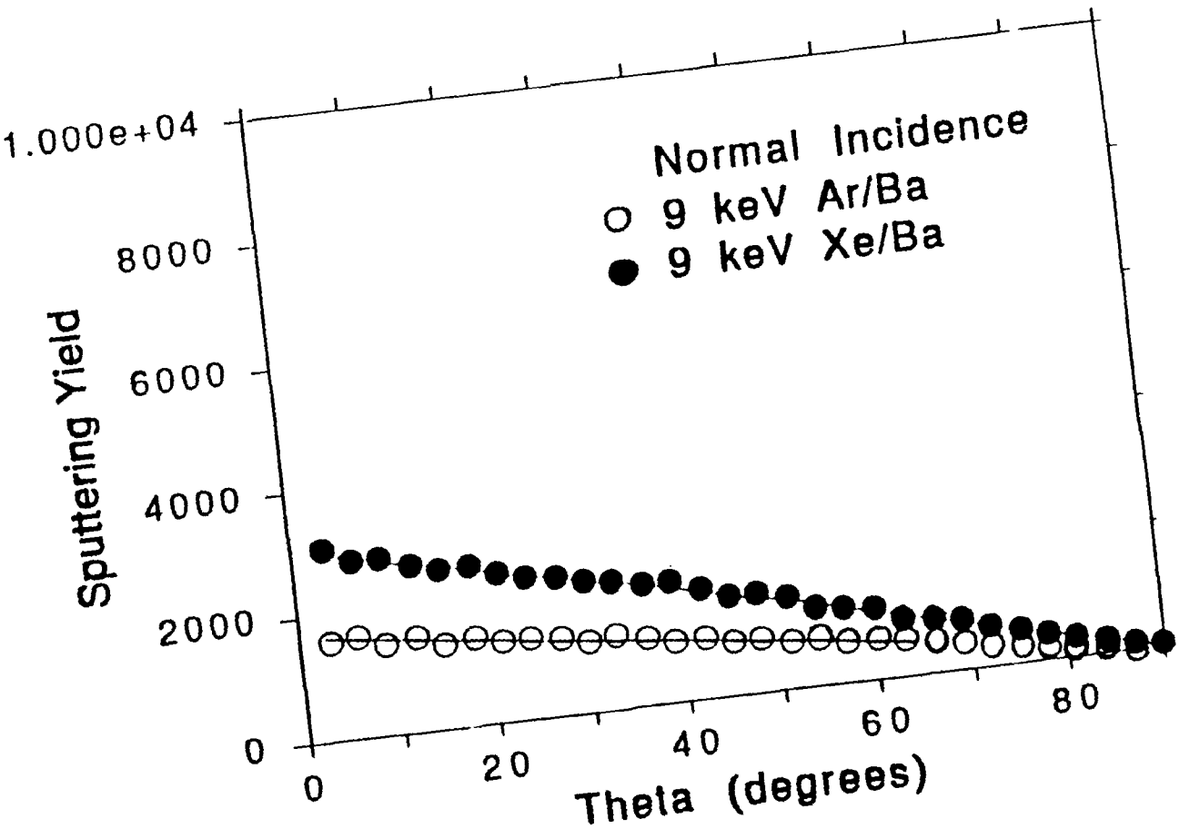
Normal Incidence
9 keV Ar/Ba
9 keV Xe/Ba
Sputtering Yield
1.000e+04
8000
6000
4000
2000
0
0
20
40
60
80
Theta (degrees)

Figure 19.

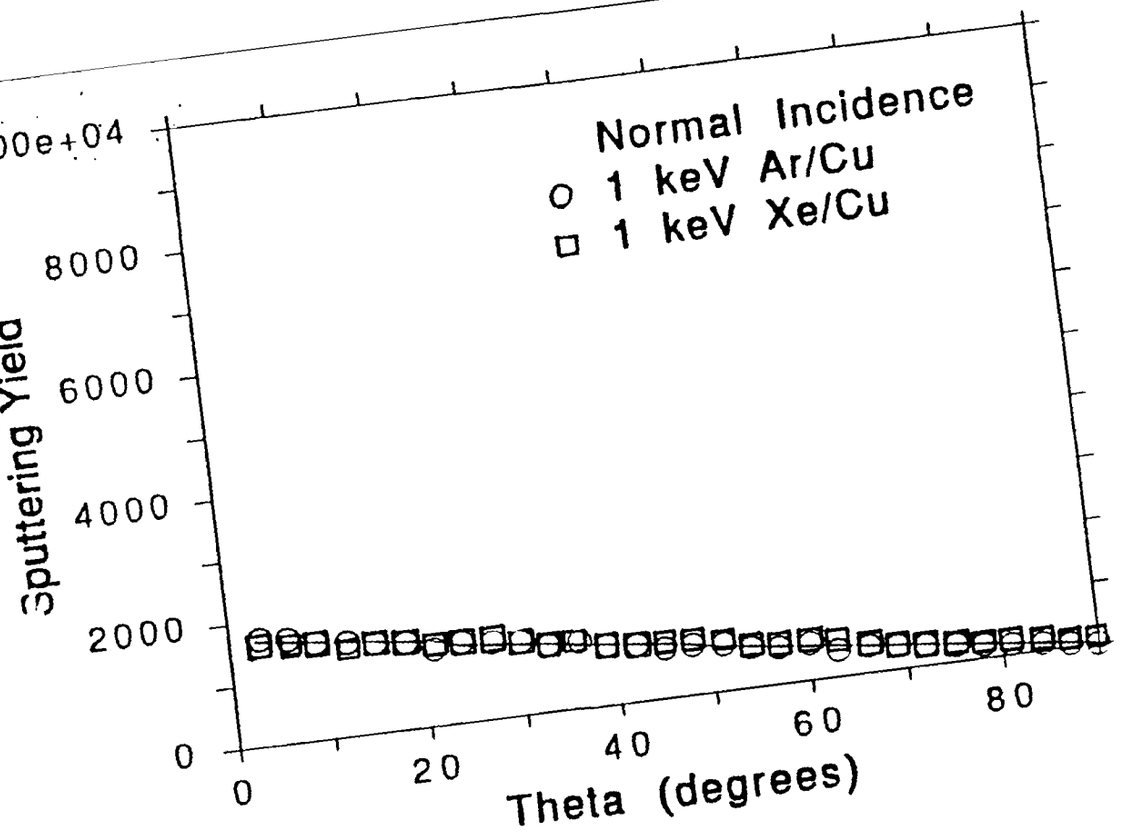
Normal Incidence
1 keV Ar/Cu
1 keV Xe/Cu
Sputtering Yield
1.000e+04
8000
6000
4000
2000
0
0
20
40
60
80
Theta (degrees)

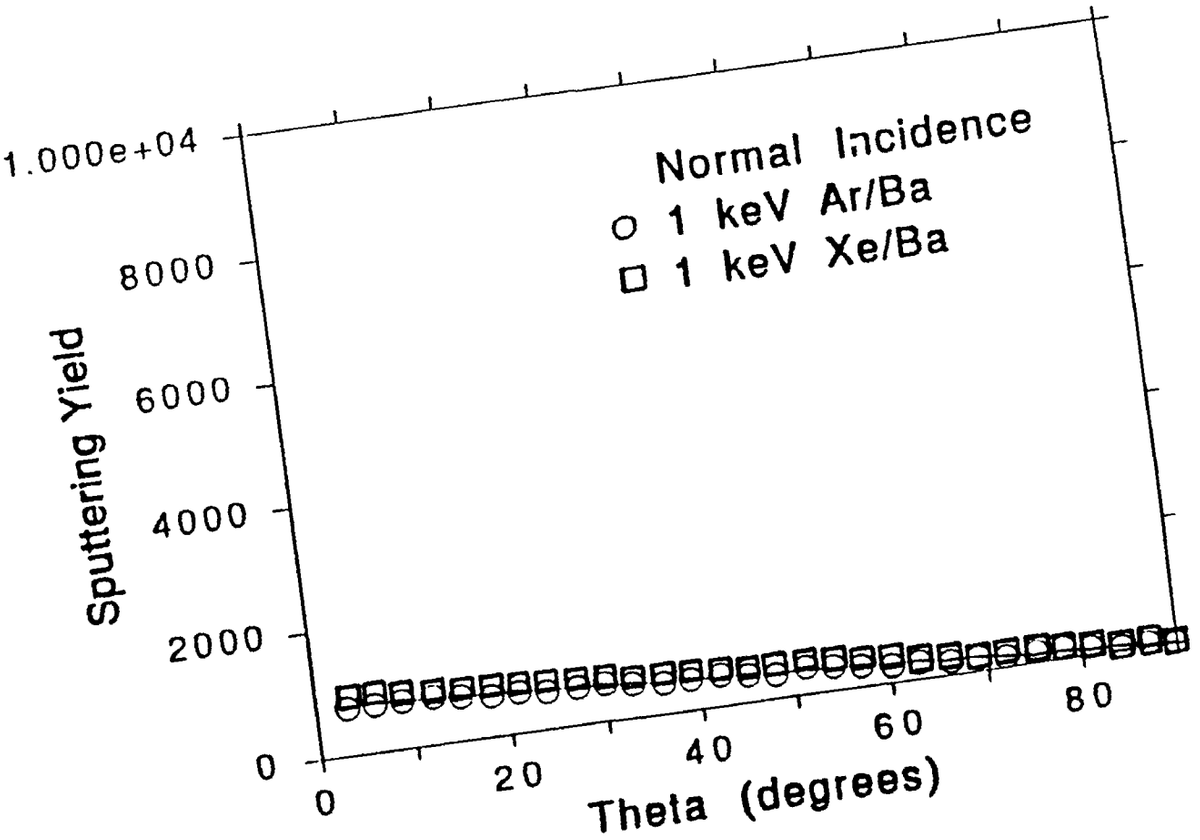
Normal Incidence
1 keV Ar/Ba
1 keV Xe/Ba
Sputtering Yield
1.000e+04
8000
6000
4000
2000
0
0
20
40
60
80
Theta (degrees)

Figure 20.

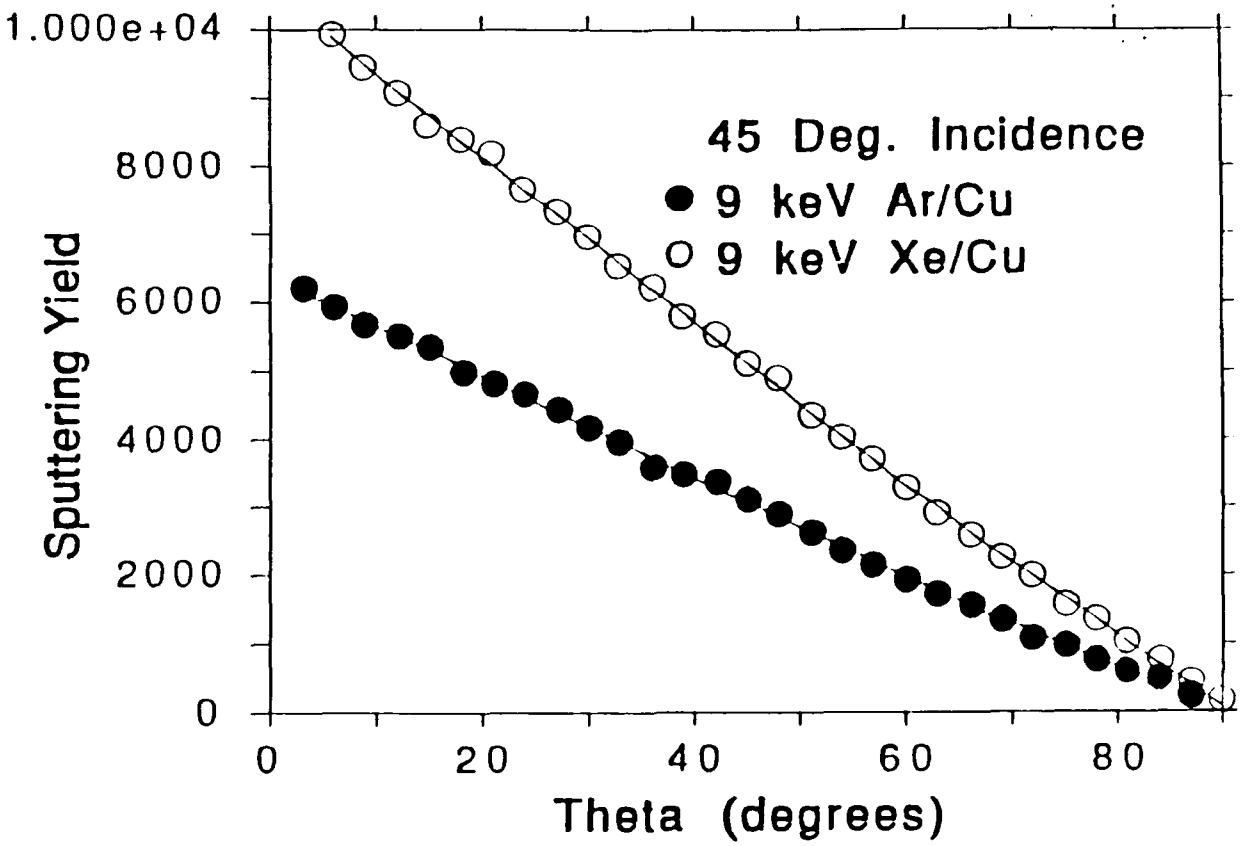
1.000e+04
8000
6000
4000
2000
0
Sputtering Yield
45 Deg. Incidence
9 keV Ar/Cu
9 keV Xe/Cu
0
20
40
60
80
Theta (degrees)

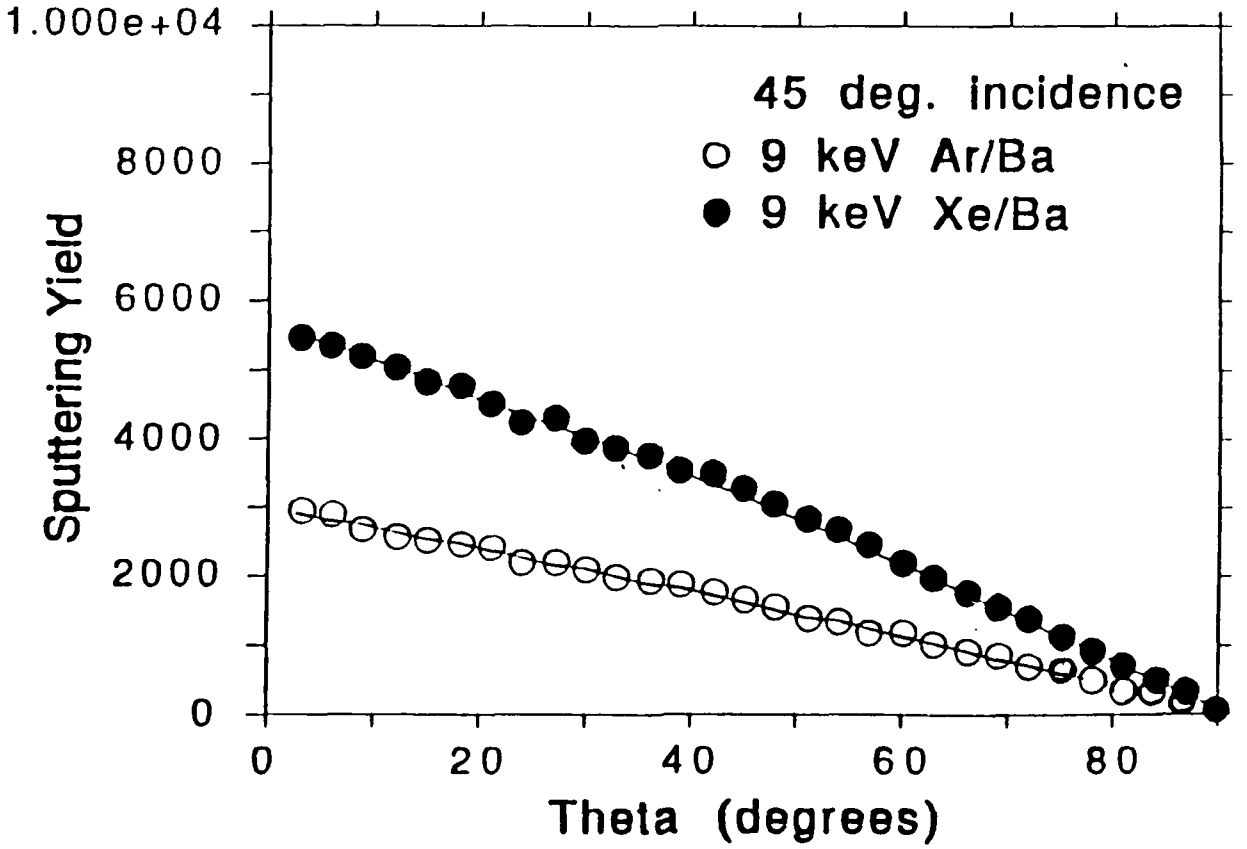
1.000e+04
8000
6000
4000
2000
0
Sputtering Yield
45 deg. incidence
9 keV Ar/Ba
9 keV Xe/Ba
0
20
40
60
80
Theta (degrees)

Figure 21.

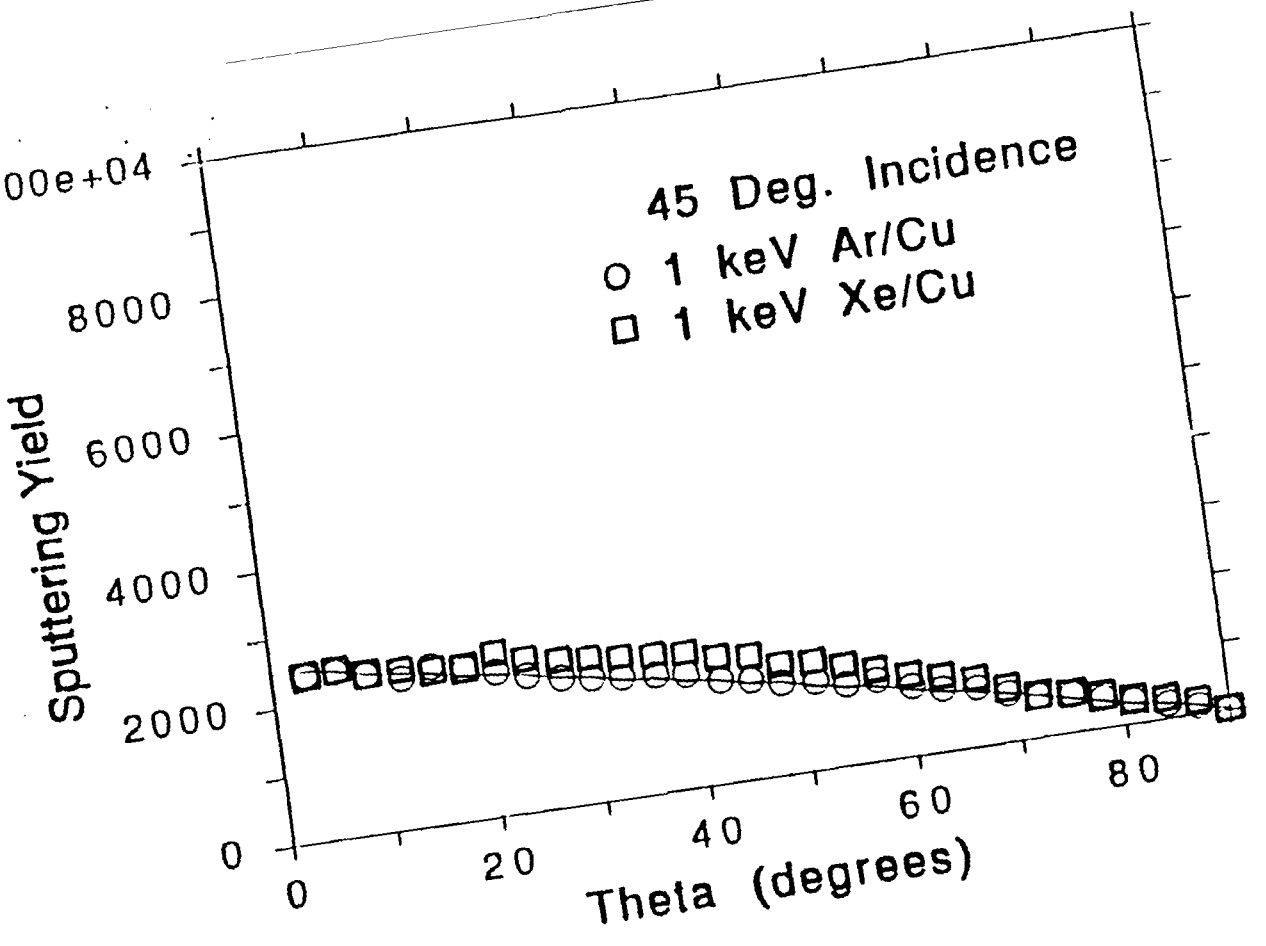
45 Deg. Incidence
1 keV Ar/Cu
1 keV Xe/Cu
Sputtering Yield
.000e+04
8000
6000
4000
2000
0
0
20
40
60
80
Thela (degrees)

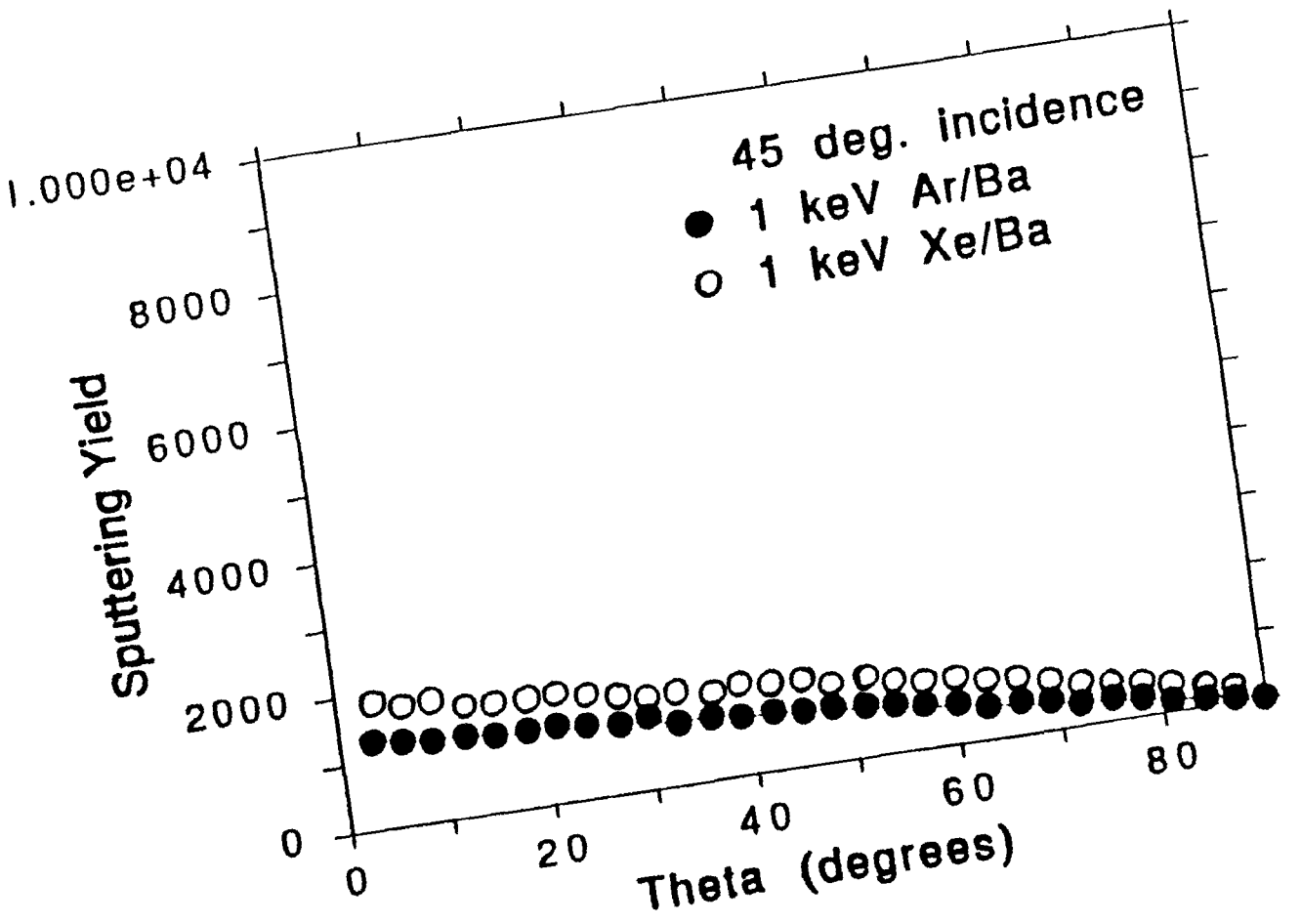
45 deg. incidence
1 keV Ar/Ba
1 keV Xe/Ba
Sputtering Yield
1.000e+04
8000
6000
4000
2000
0
0
20
40
60
80
Theta (degrees)

Figure 22.

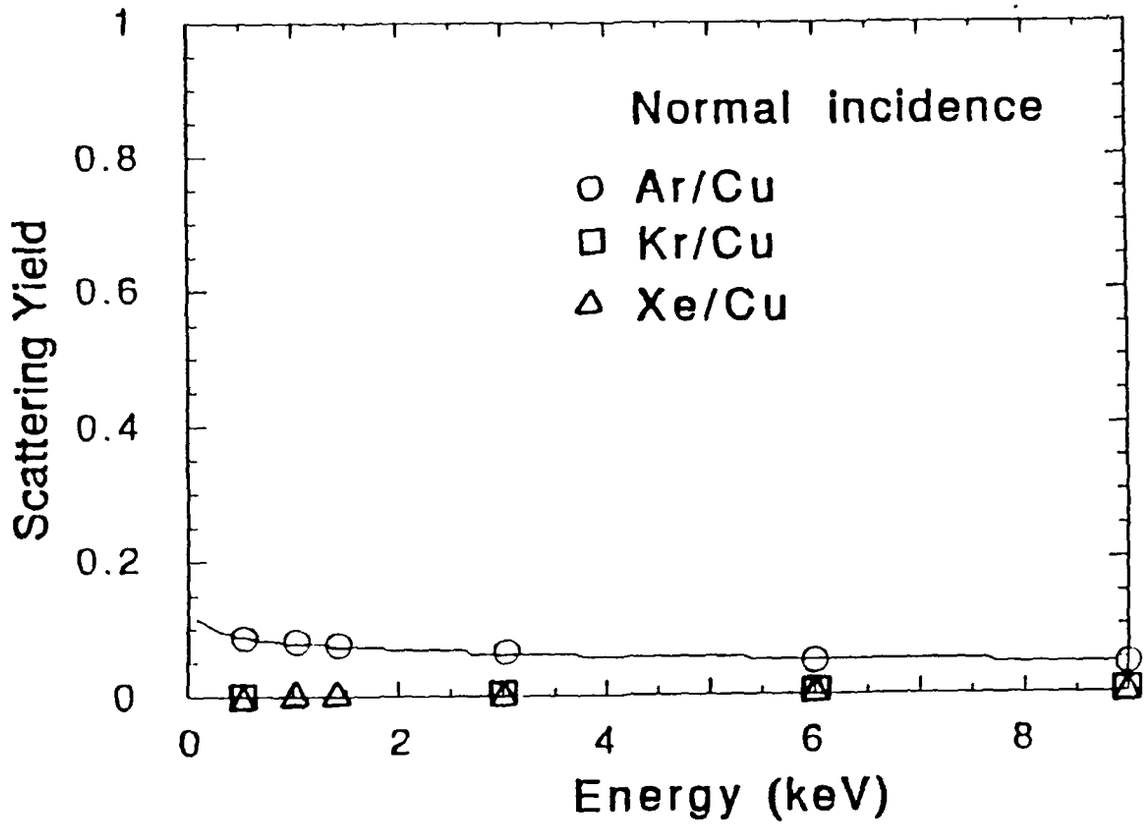
Normal incidence
Ar/Cu
Kr/Cu
Xe/Cu
Scattering Yield
Energy (keV)
0
0.2
0.4
0.6
0.8
1
0
2
4
6
8

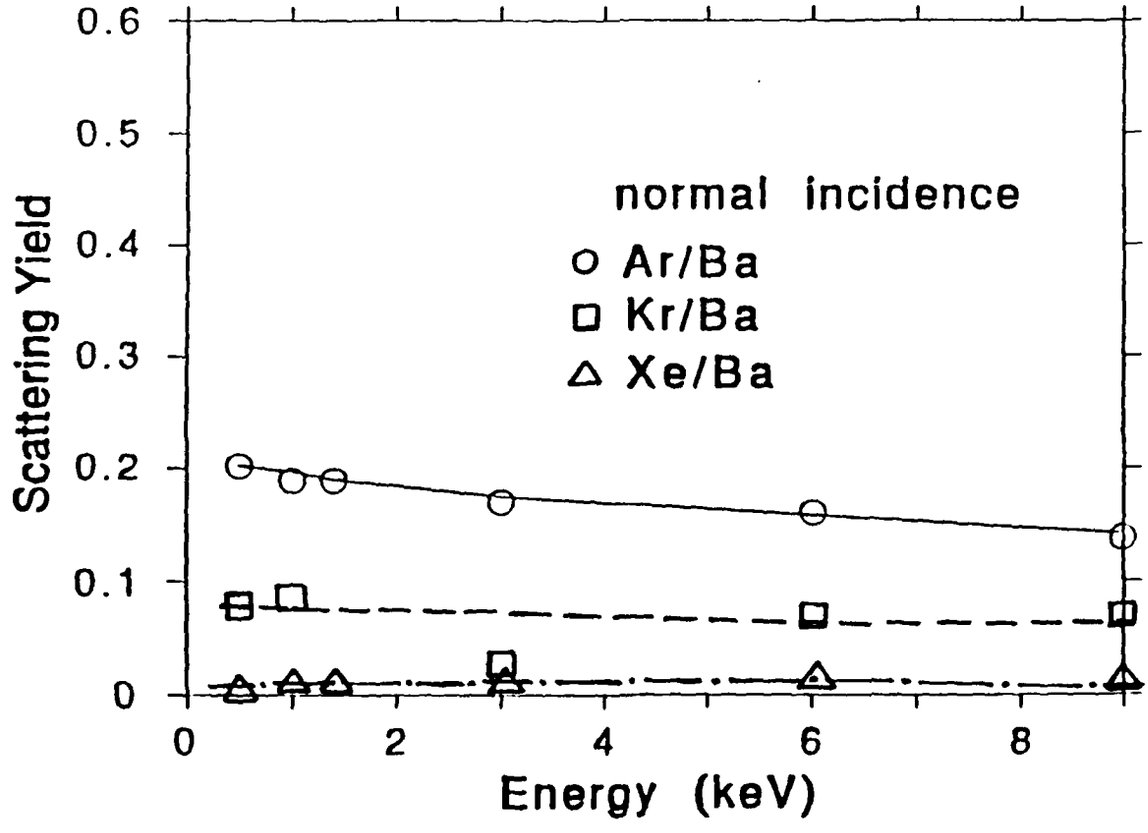
normal incidence
Ar/Ba
Kr/Ba
Xe/Ba
Scattering Yield
Energy (keV)
0
0.1
0.2
0.3
0.4
0.5
0.6
0
2
4
6
8

Figure 23.

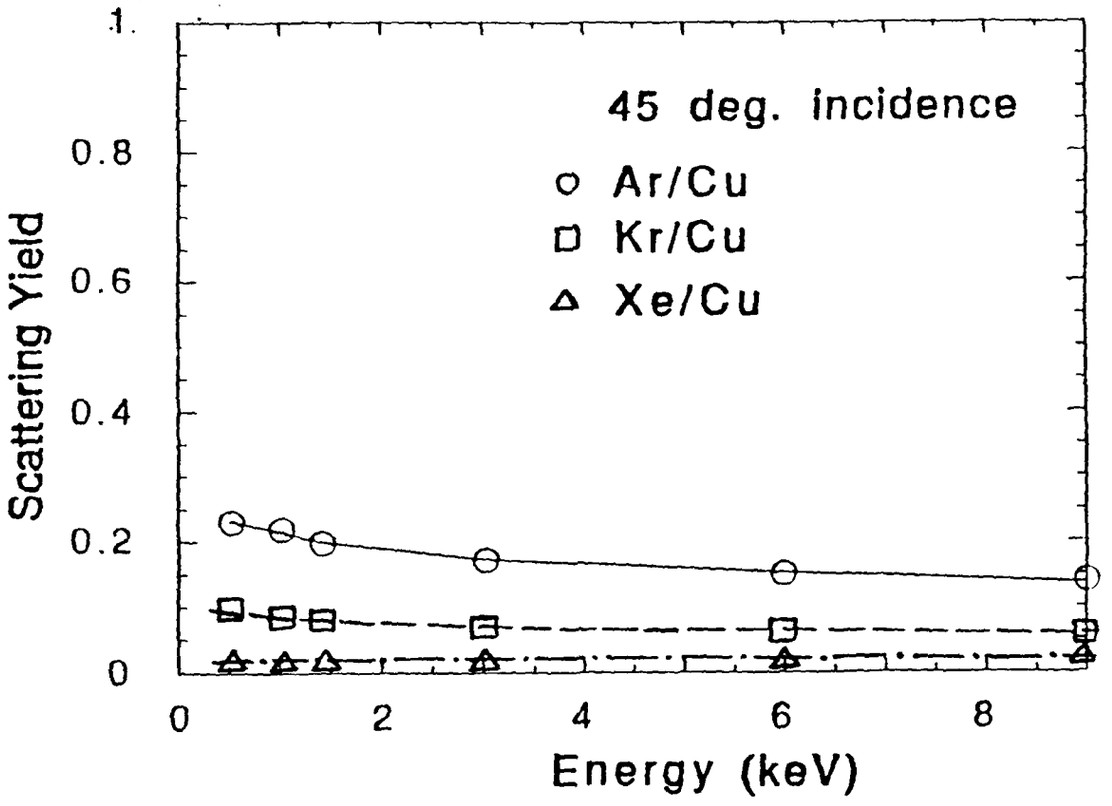
45 deg. incidence
Ar/Cu
Kr/Cu
Xe/Cu
Scattering Yield
Energy (keV)
0
0.2
0.4
0.6
0.8
1
0
2
4
6
8

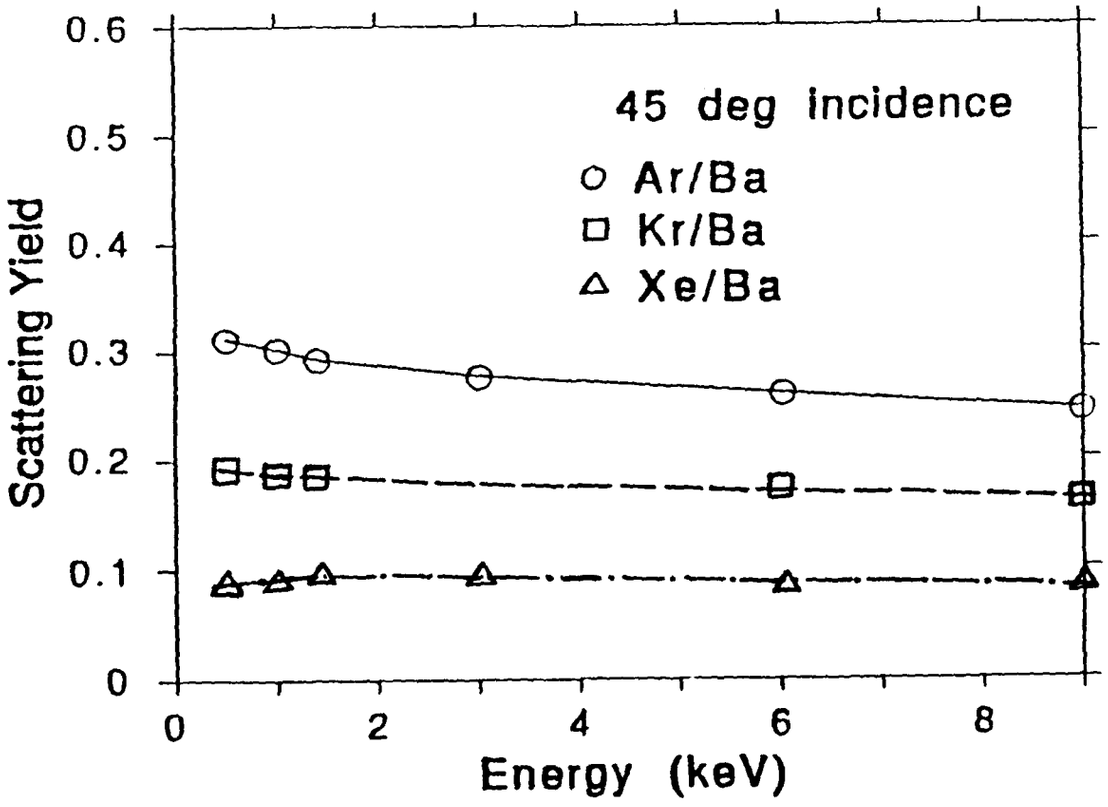
45 deg incidence
Ar/Ba
Kr/Ba
Xe/Ba
Scattering Yield
Energy (keV)
0
0.1
0.2
0.3
0.4
0.5
0.6
0
2
4
6
8

Figure 24.

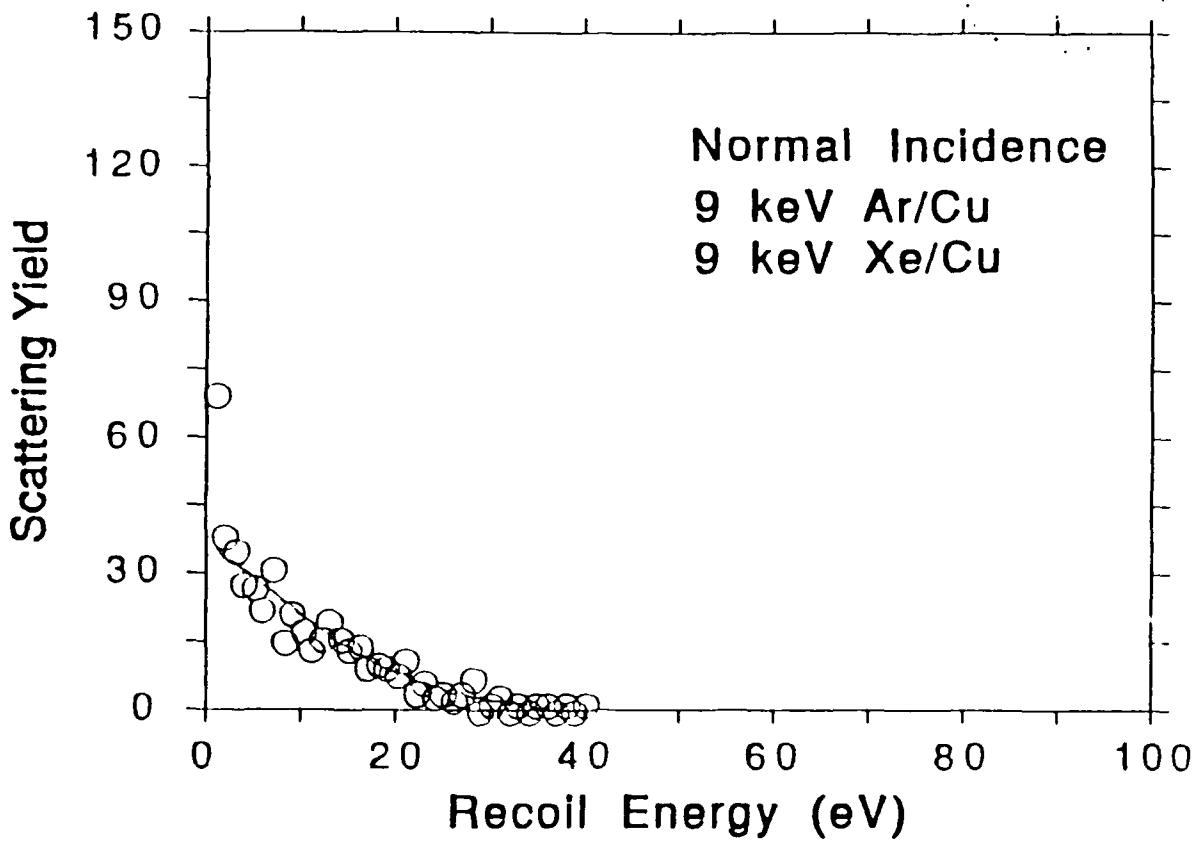
Normal Incidence
9 keV Ar/Cu
9 keV Xe/Cu
Scattering Yield
Recoil Energy (eV)
0
30
60
90
120
150
0
20
40
60
80
100

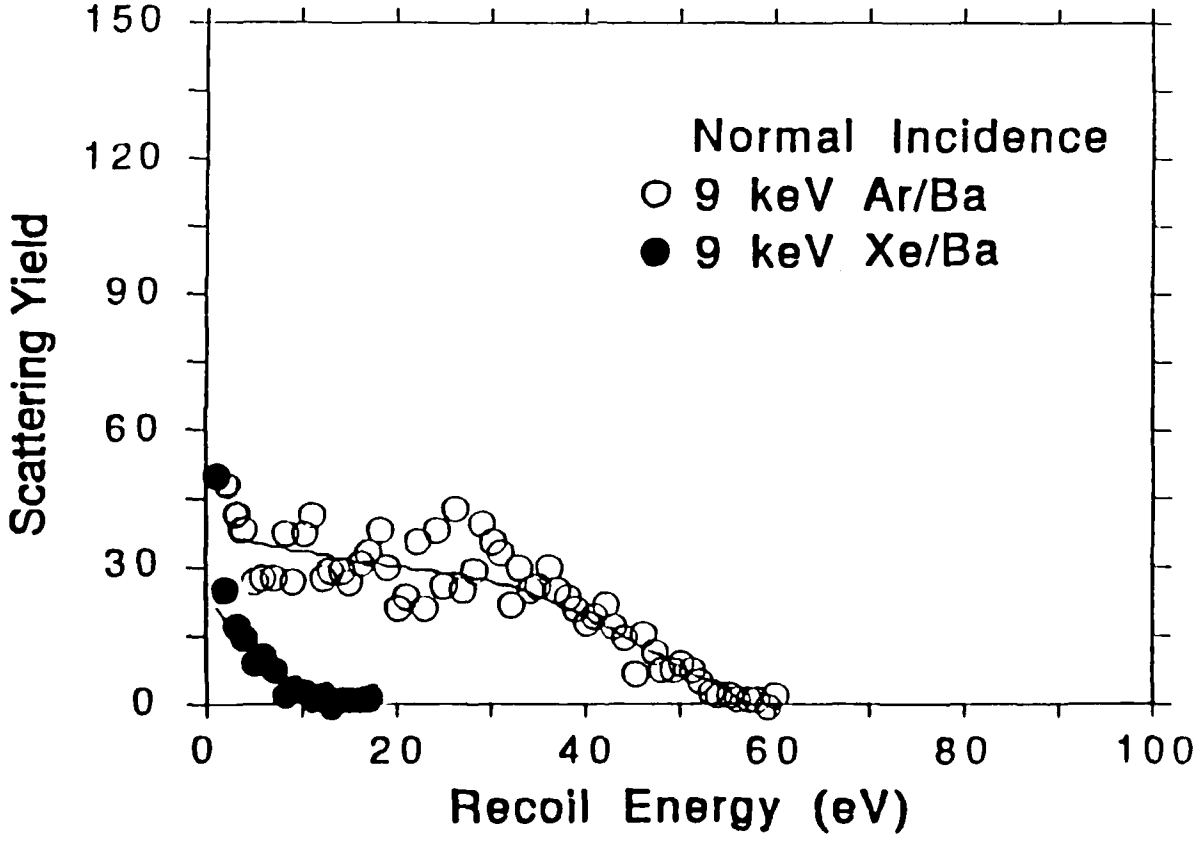
Normal Incidence
9 keV Ar/Ba
9 keV Xe/Ba
Scattering Yield
Recoil Energy (eV)
0
30
60
90
120
150
0
20
40
60
80
100

Figure 25.

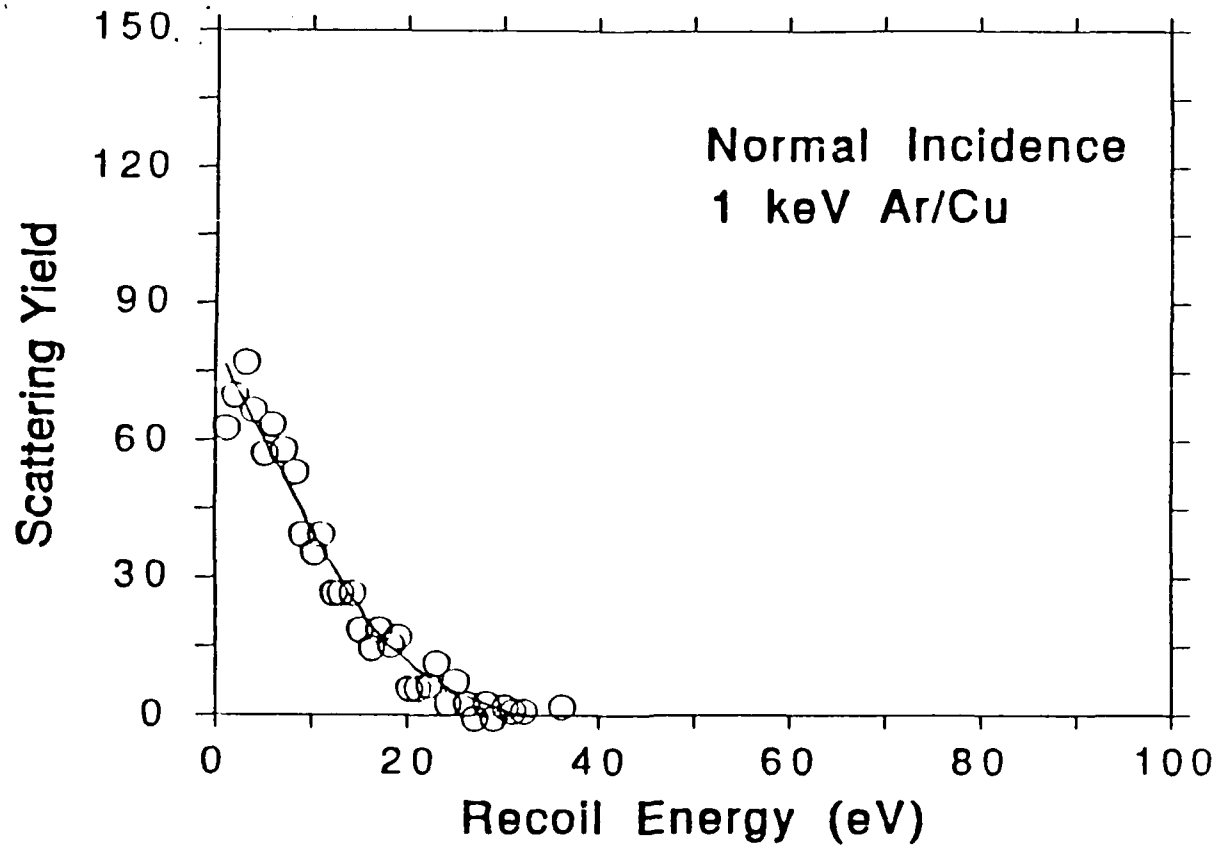
Normal Incidence
1 keV Ar/Cu
Scattering Yield
Recoil Energy (eV)
0
30
60
90
120
150
0
20
40
60
80
100

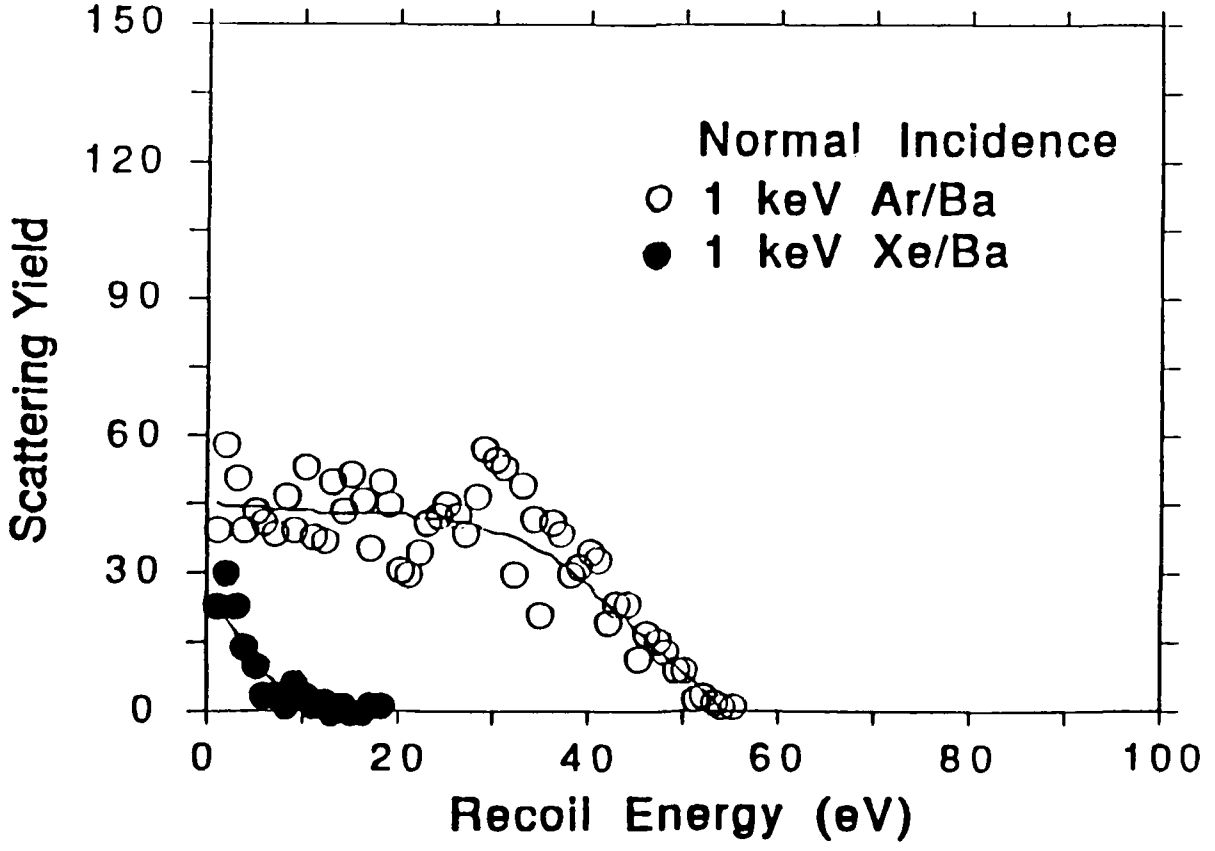
Normal Incidence
1 keV Ar/Ba
1 keV Xe/Ba
Scattering Yield
Recoil Energy (eV)
0
30
60
90
120
150
0
20
40
60
80
100

Figure 26.

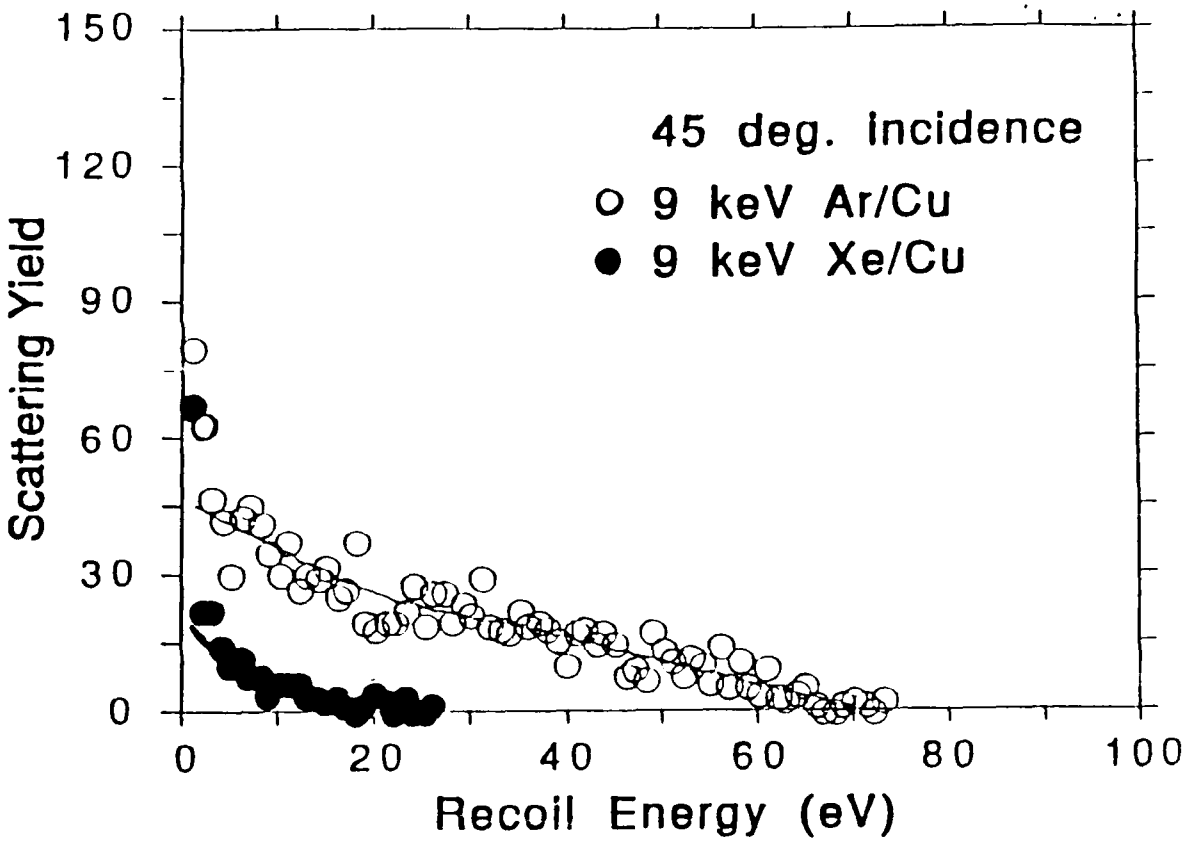
45 deg. incidence
9 keV Ar/Cu
9 keV Xe/Cu
Scattering Yield
Recoil Energy (eV)
0
30
60
90
120
150
0
20
40
60
80
100

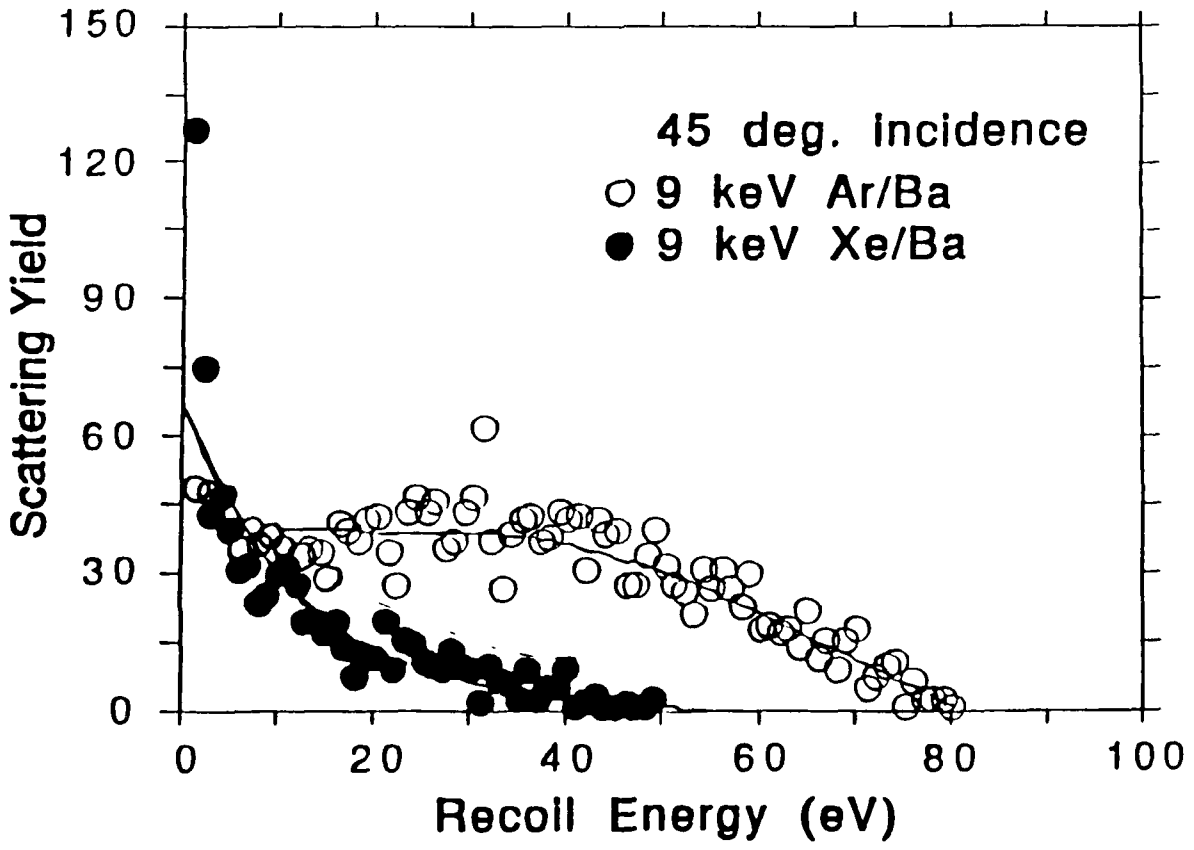
45 deg. incidence
9 keV Ar/Ba
9 keV Xe/Ba
Scattering Yield
Recoil Energy (eV)
0
30
60
90
120
150
0
20
40
60
80
100

Figure 27.

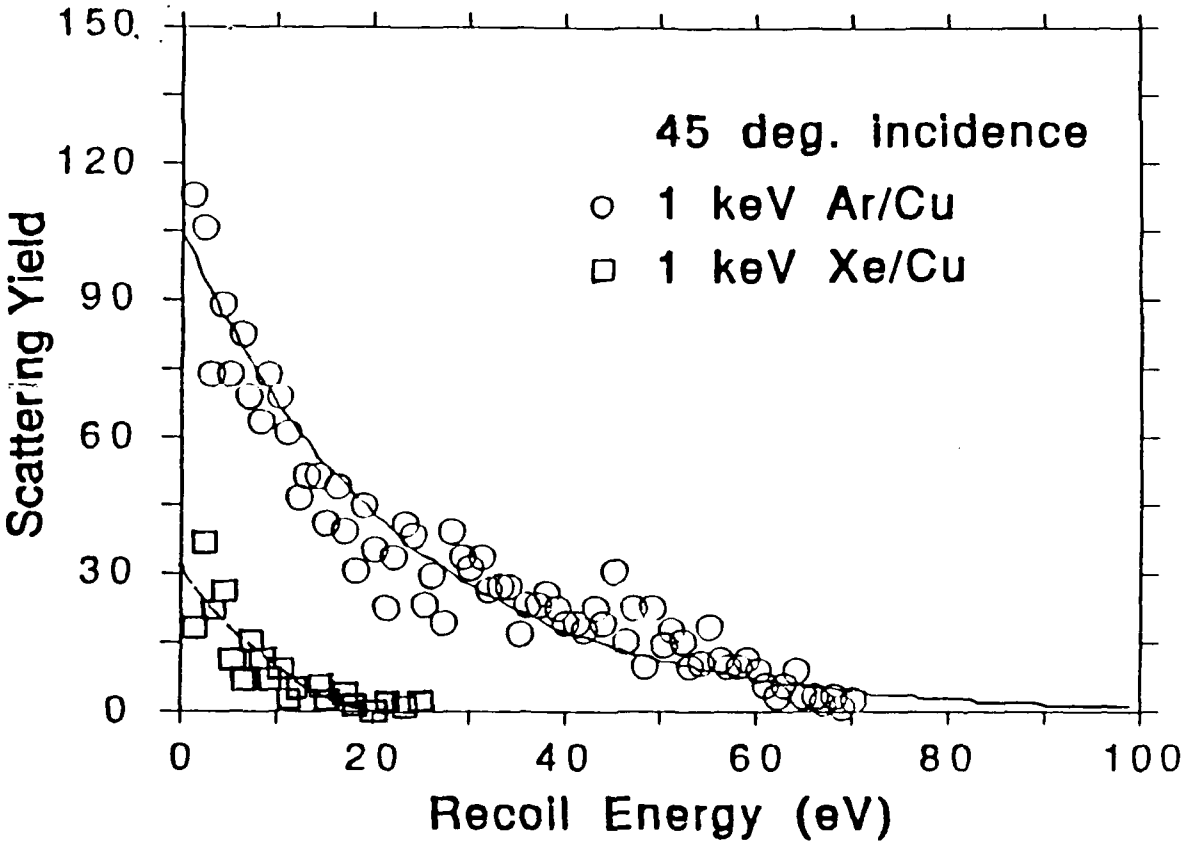
45 deg. incidence
1 keV Ar/Cu
1 keV Xe/Cu
Scattering Yield
Recoil Energy (eV)
0
30
60
90
120
150
0
20
40
60
80
100

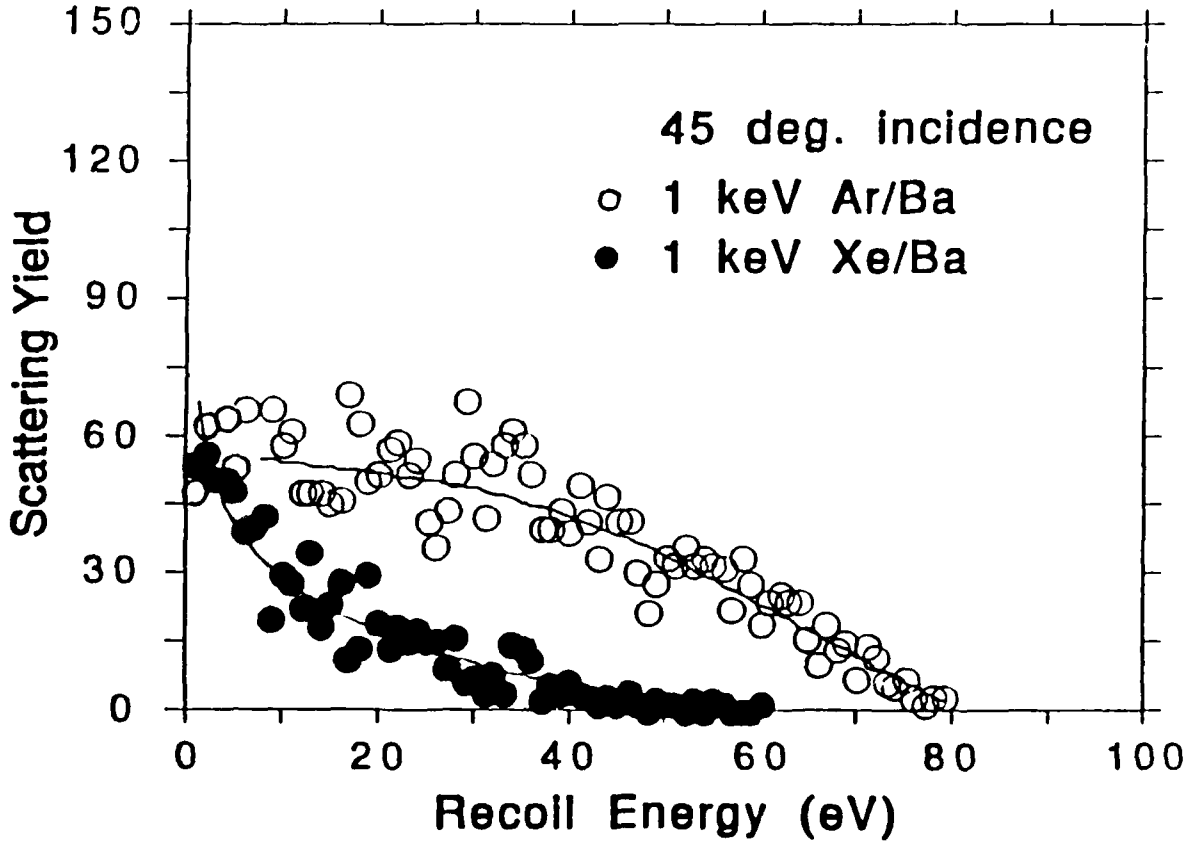
45 deg. incidence
1 keV Ar/Ba
1 keV Xe/Ba
Scattering Yield
Recoil Energy (eV)
0
30
60
90
120
150
0
20
40
60
80
100

Figure 28.

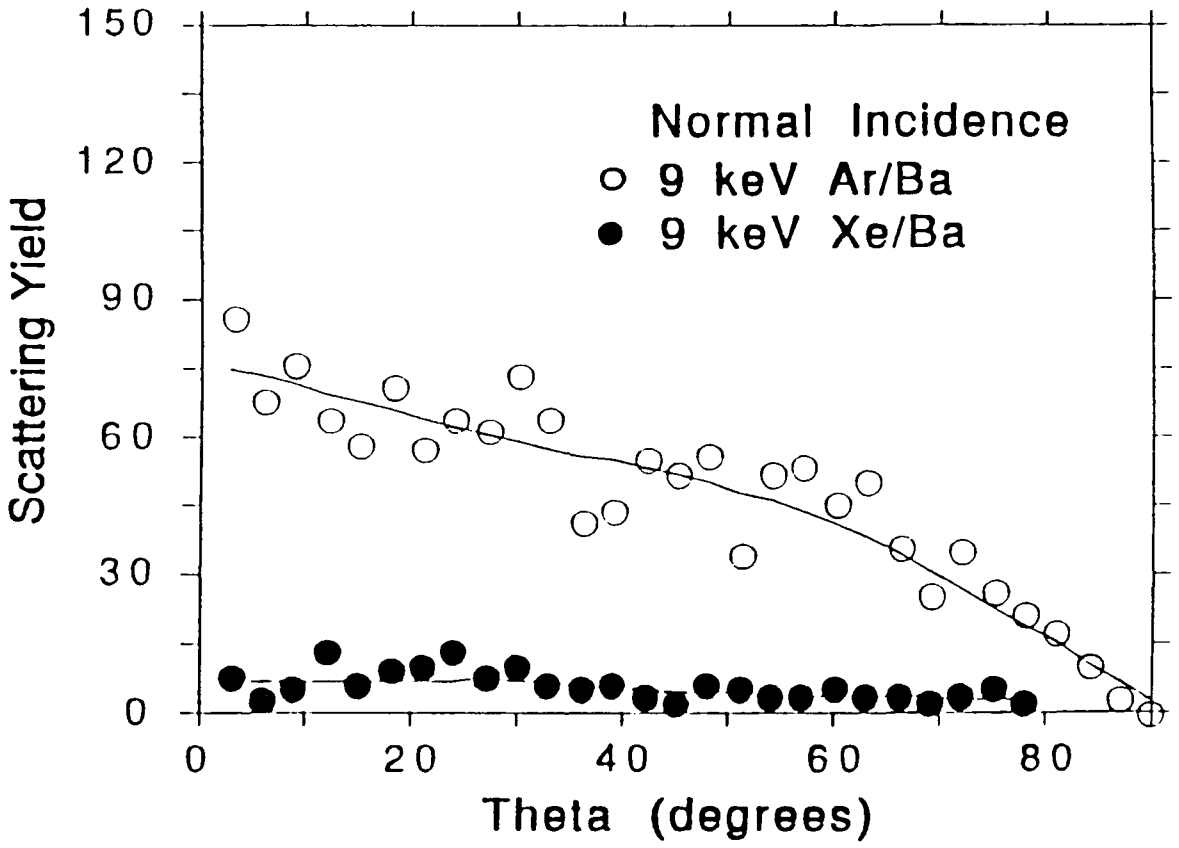
Normal Incidence
9 keV Ar/Ba
9 keV Xe/Ba
Scattering Yield
150
120
90
60
30
0
0
20
40
60
80
Theta (degrees)

Figure 29.

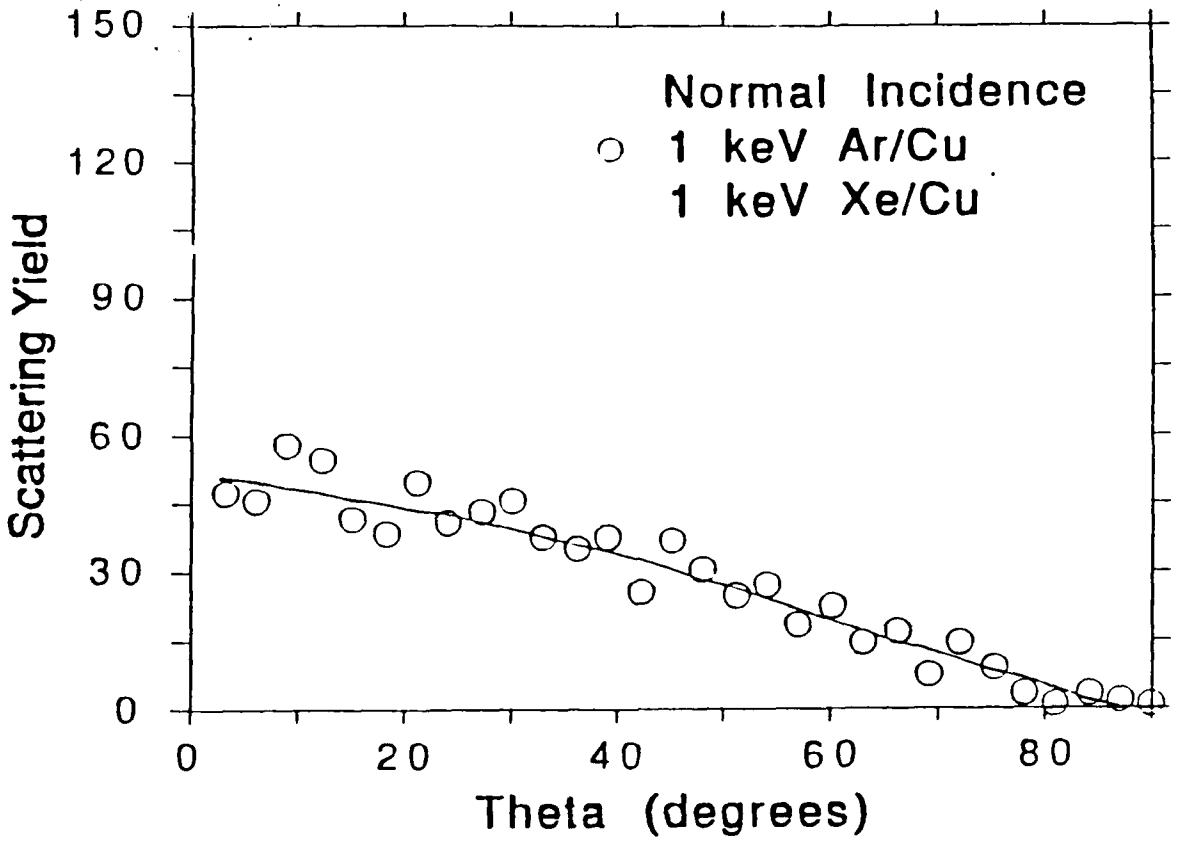
Normal Incidence
1 keV Ar/Cu
1 keV Xe/Cu
Scattering Yield
Theta (degrees)
0
30
60
90
120
150
0
20
40
60
80

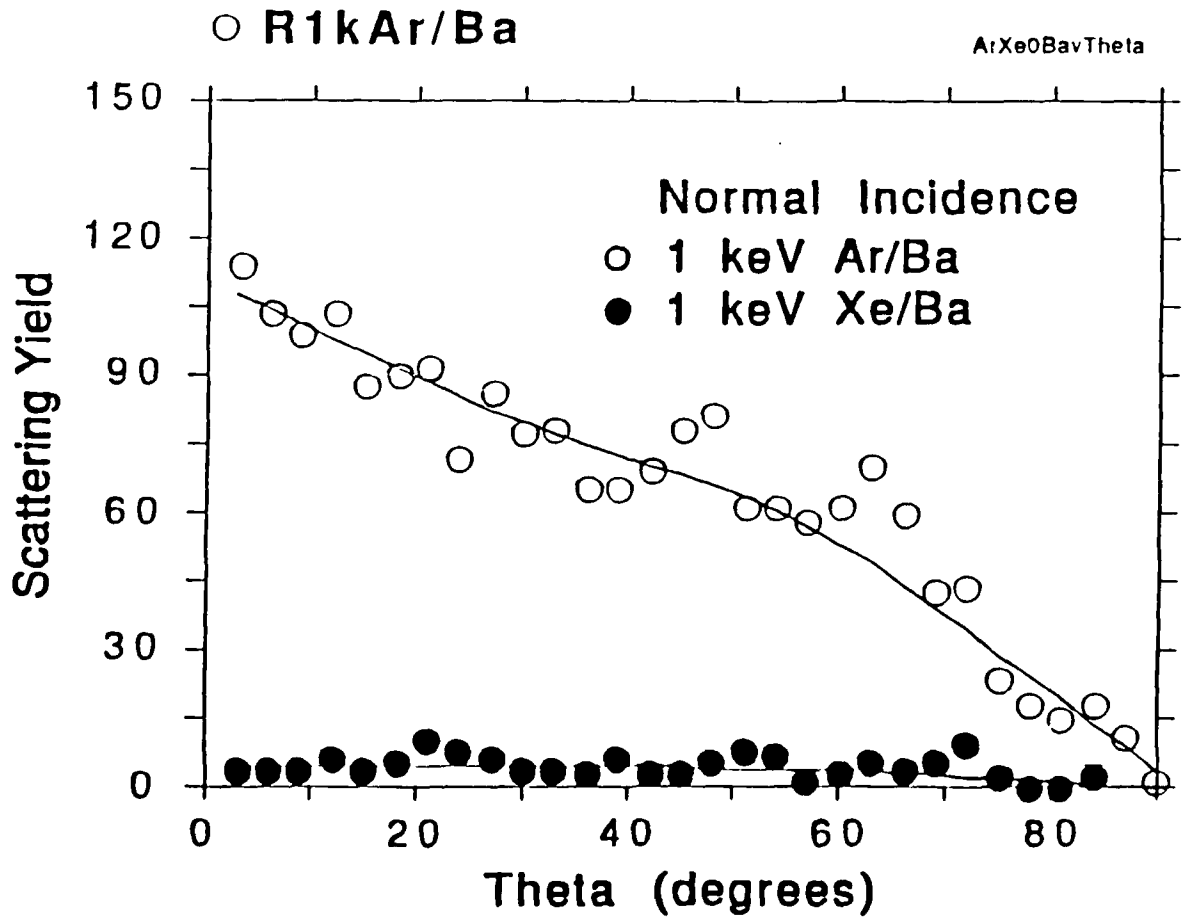
R1kAr/Ba
ArXe0BavTheta
Normal Incidence
1 keV Ar/Ba
1 keV Xe/Ba
Scattering Yield
Theta (degrees)
0
30
60
90
120
150
0
20
40
60
80

Figure 30.

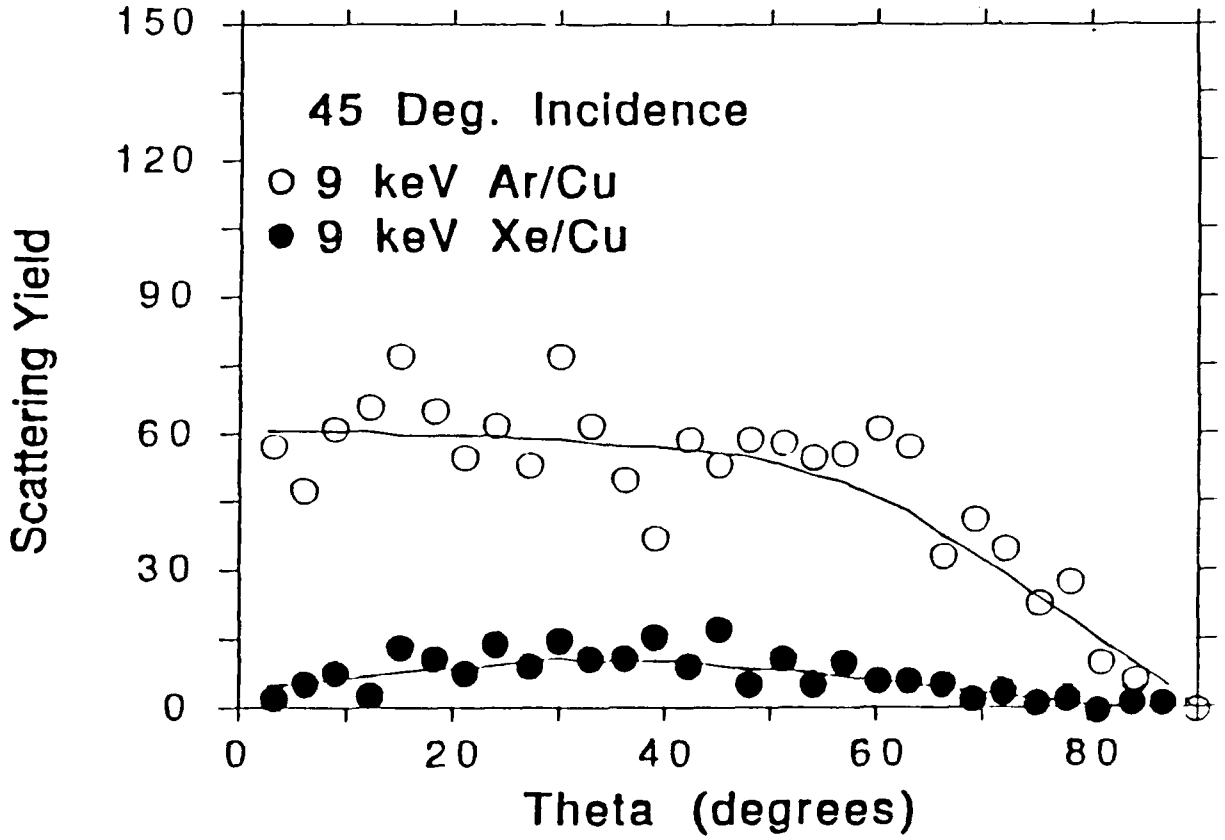
45 Deg. Incidence
9 keV Ar/Cu
9 keV Xe/Cu
Scattering Yield
Theta (degrees)
0
30
60
90
120
150
0
20
40
60
80

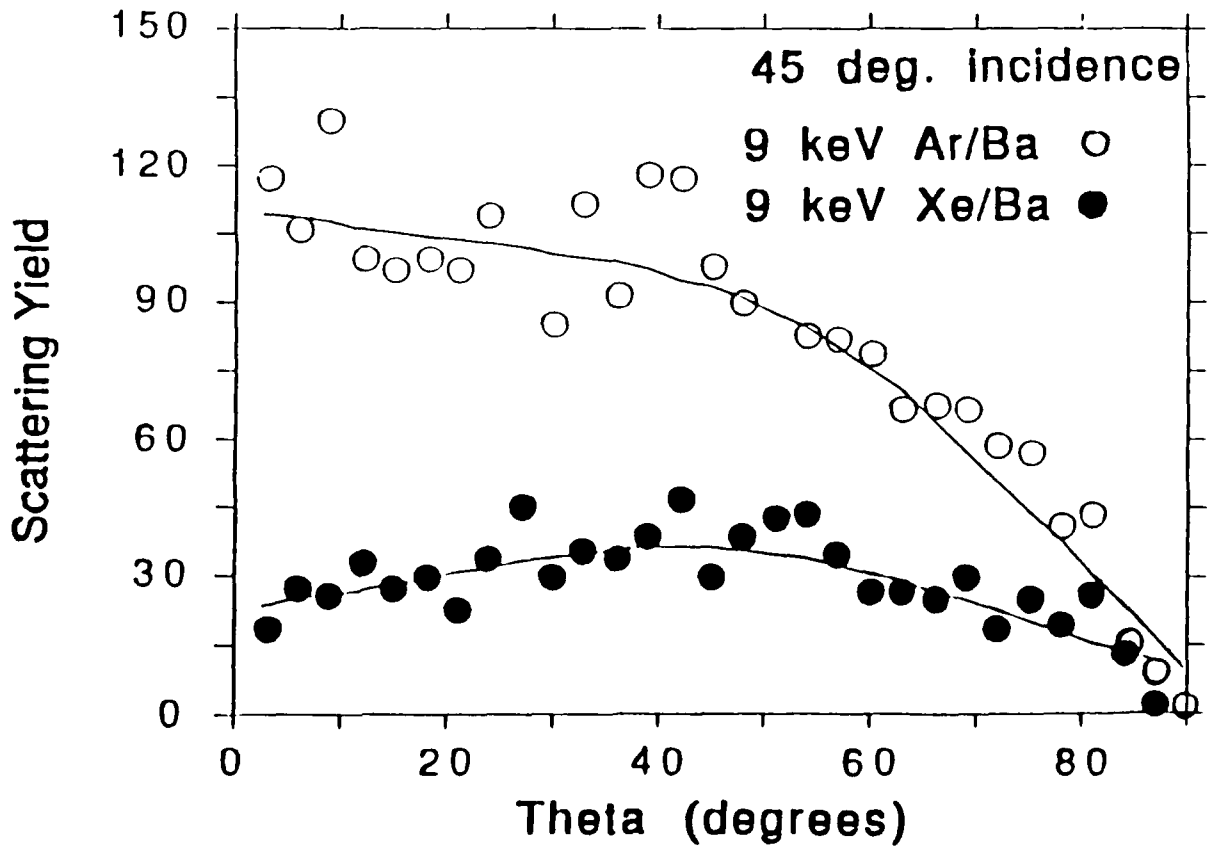
45 deg. incidence
9 keV Ar/Ba
9 keV Xe/Ba
Scattering Yield
Theta (degrees)
0
30
60
90
120
150
0
20
40
60
80

Figure 31.

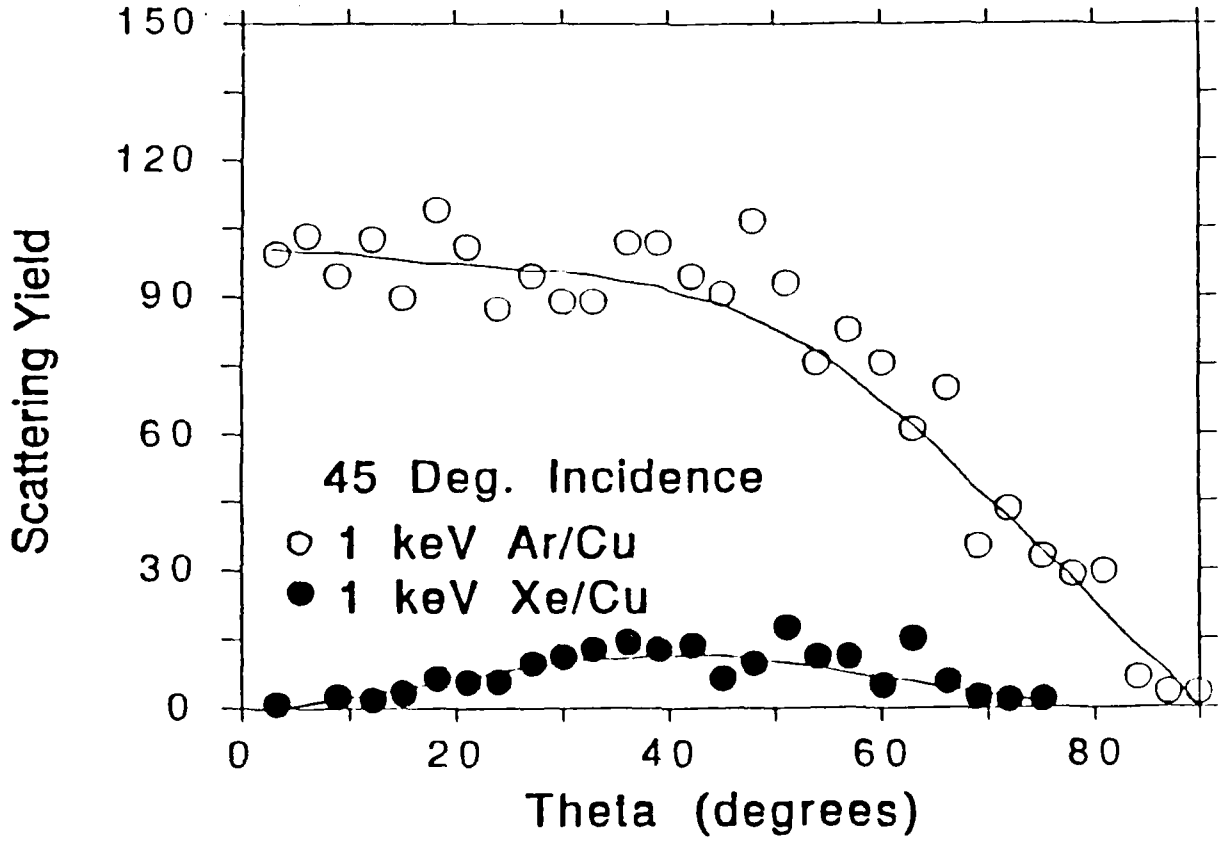
Scattering Yield
150
120
90
60
30
0
0
20
40
60
80
Theta (degrees)
45 Deg. Incidence
1 keV Ar/Cu
1 keV Xe/Cu

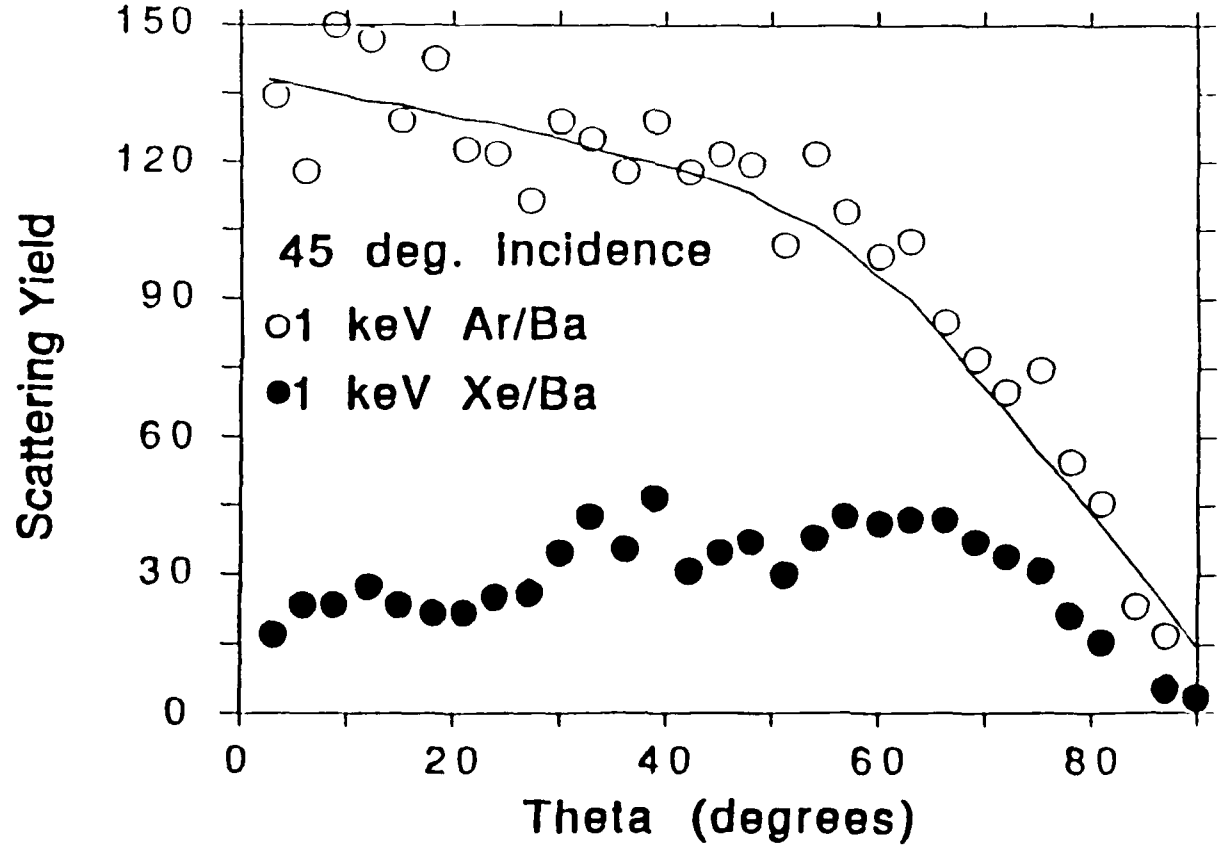
Scattering Yield
150
120
90
60
30
0
0
20
40
60
80
Theta (degrees)
45 deg. Incidence
1 keV Ar/Ba
1 keV Xe/Ba

Figure 32.

5. DEPOSITION AND CHARACTERIZATION OF $YBa_2Cu_3O_{7-\delta}$ FILMS

5.1 Background

This section describes the work related to deposition of Y-Ba-Cu-O films, including substrate preparation, deposition technique, and subsequent film analysis. Future work including the fabrication of superconducting junctions is introduced in a discussion regarding patterning of superconducting materials.

5.2. Substrate Preparation

Single crystal substrates play a very important role in thin film deposition. Substrates such as $SrTiO_3$, sapphire, Si and many others have been used to deposit superconductors. For economic reasons, and based upon structure, an acceptable lattice mismatch, and chemical stability, single crystal MgO was chosen, at least for the initial stage of the research program at NCSU, as the primary substrate for film deposition. A problem that was necessary to overcome with the MgO substrates was the large density of dislocations existing on the material surface as received from the supplier. Figure 33 shows cross section and plan view TEM micrographs of a chemically etched MgO substrate. Dislocation etch pits and a damage surface layer have been observed. The following sections describe the examination of the damaged layer and detail a preparation and cleaning procedure used to reduce the damaged layer on the surface of MgO substrates.

Dislocations on MgO substrates have been revealed by chemical etching. The etching solution was composed of 5 parts NH_4OH + 1 part H_2SO_4+ 1 part H_2O. The following procedure has been used to obtain etch pits on MgO substrates: (1) MgO substrates were immersed in the etching solution for 6 minutes, (2) they were quickly transferred to a DI water beaker to rinse out residual etching solution, (3) the substrates were then rinsed in a second DI water beaker, (4) the substrates were rinsed in methanol , and finally (5) the excess methanol was evaporated with a hot air blower.

Dislocations can be easily generated on MgO substrate surfaces during preparation . Therefore, extra care is necessary when handling the substrates. The effectiveness of dislocation reduction has been found to be proportional to increasing annealing temperatures. However, recrystallization (Figure 34) on the surface of MgO substrates tends to occur if the annealing temperature is above 1500 ^oC. Figure 33a and b compare the dislocation density on the substrate surfaces and the thickness of the damaged layers of the as-received vs. the annealed (1400 ^oC for 4 hours) substrates. Both the dislocation density on the surface and the thickness of the damaged layer is significantly reduced for the annealed substrates.

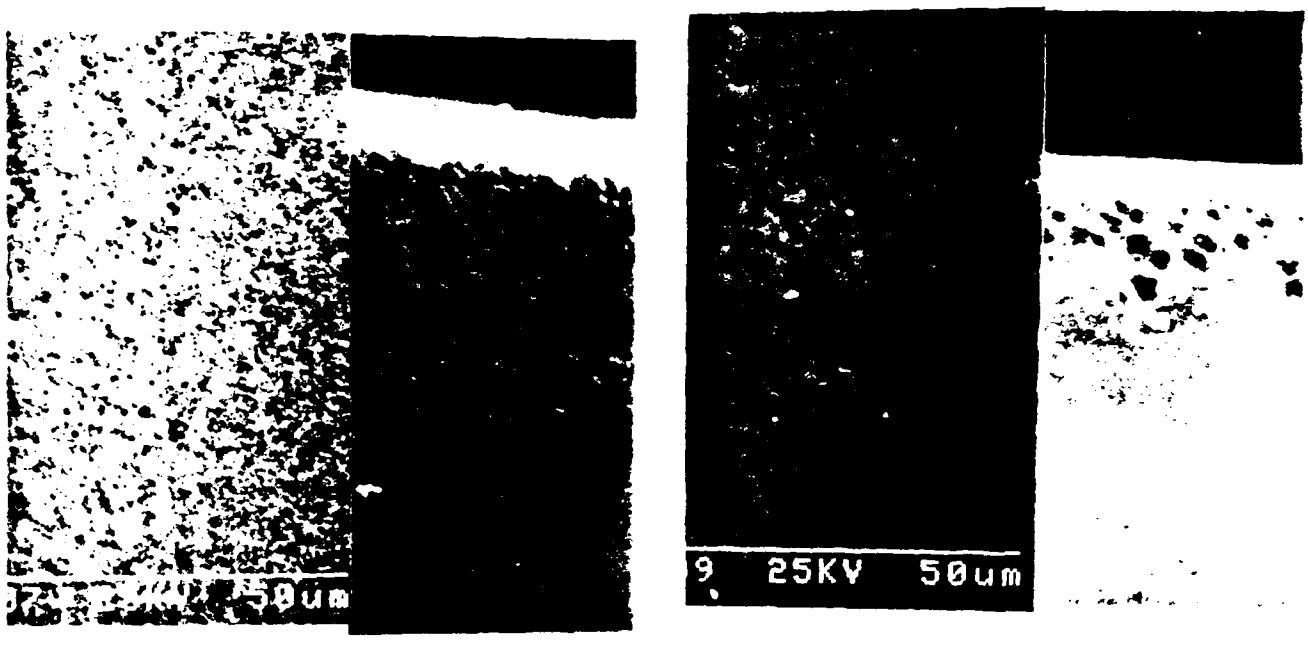

Figure 33. Cross section and plan view micrographs of MgO single crystal substrates a) as received, and b) annealed at 1400 C for 4 hours.

Figure 34. A cross section micrograph of a MgO substrate with recrystallization grains on the substrate surface.

However, the ideal substrate surface for deposition of superconducting films should be free of all dislocations. A final chemical polishing of the substrates was therefore performed to completely remove the damaged layer .

Boiling, fresh orthophosphoric acid was employed to chemically polish single crystal MgO substrates. The polishing rate was approximately 8 μm/min. A Teflon and platinum holder was designed to withstand the hot chemical polishing. Only a few background dislocations were found on the substrates polished in this manner.

The complete procedure for preparing and cleaning MgO substrates is performed in the following manner: (a) substrates are cleaved to the desired size, (b) substrates are then arranged onto two supporting MgO pieces resting on an alumina plate. The substrates are then placed with deposition surfaces perpendicular to the alumina plate to minimize particle contamination, (c) substrates are annealed at 1400 ^{o}C for 4 hours, (d) substrates are then chemically polished using the above techniques.

5.3. Deposition of Superconducting $YBa_2Cu_3O_{7-\delta}$ Films

The first superconducting $YBa_2Cu_3O_{7-\delta}$ film was produced in March 1989 using the fully implemented control program to drive the ion beam sputter-deposition system. A short description of this work will soon be published in Appl. Phys. Lett. (July 24, 1989), and details are discussed below.

Figure 2 is an schematic of the system configuration used to deposit this film, while the actual system, with the ion beam impacting on one of the targets, is shown in the photograph in Figure 35. This system configuration has now been modified as dictated by extensive experimental measurements and computer simulations of sputtering and ion scattering phenomena occurring during ion impact on the targets(see section 4) and their influence on film characteristics. A prototype system constructed using a chamber originally dedicated to other thin film work was used for deposition of this first Y-Ba-Cu-O superconducting thin film, since the chamber dedicated for the superconducting thin film project was under construction. The hardware utilized for this experiment (ion beam, rotating target holder, substrate heater, quartz crystal thin film monitor, etc.) has been described in section 3. The computer control program used for this deposition was based on the LABVIEW software package previously discussed (section 3.6).

Elemental metals (Y, Ba, Cu) and their oxides (Y_2O_3, BaO, CuO) were irradiated with an Ar^+ ion beam (1400 keV) in order to determine which of the metal or oxide targets were the most appropriate under the prevailing conditions during this film deposition. The following trends were found in these studies: (1) The sputter yield of metal targets is significantly higher than the corresponding oxide. (2) The oxides exhibit stoichiometry

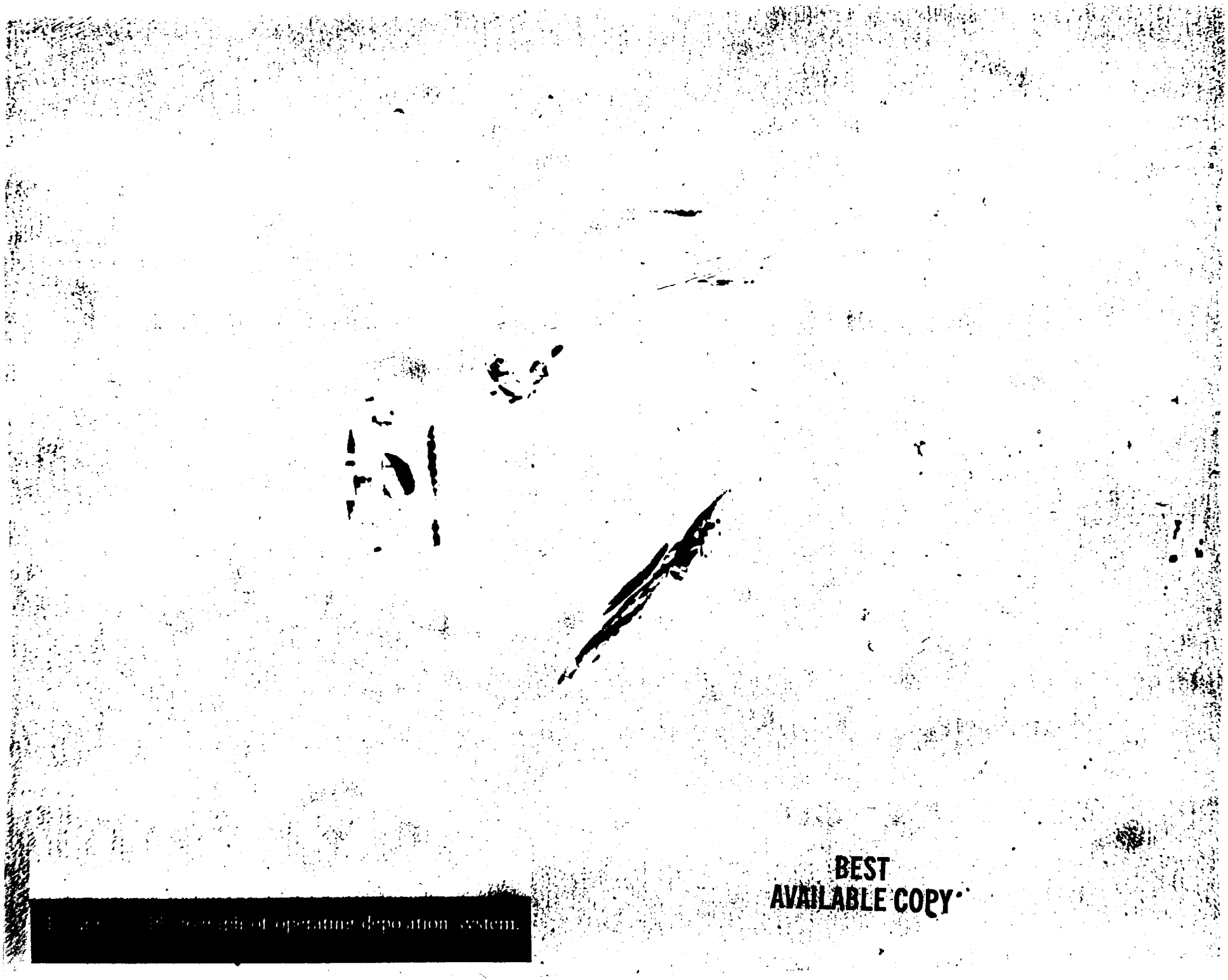

BEST
AVAILABLE COPY

changes during sputtering (which may alter the accuracy of the QCR). (3) Metal as well as oxide targets may develop topography which could result in a change in spatial distribution of sputtered species. (4) Metal targets may "poison" in the presence of oxygen, resulting in altered sputtered species and yields. For initial films, oxide precursor targets were used, mainly due to difficulties involved in maintaining a high quality Ba metal target with the temporary need for opening the target chamber to change substrates. Future investigations will include using metals, oxides, and possibly fluorides as target materials.

The experimental system shown in Figure 2 consists of a copper-lined stainless steel chamber cryo-pumped to a base pressure of about 5 x 10^{-7} torr, an ion beam of 1.4 keV and 25 mA, and a quartz lamp substrate heater. A Kr^+ ion beam was used to minimize gas incorporation into the film due to ion scattering from the targets. Gas incorporation was found to be prominent when Ar^+ ions were used, particularly for Ar^+ scattering from the BaO_2 target. This is to be expected from the physics of atomic collisions between a low mass projectile such as Ar and a high mass target atom such as Ba. Targets of Y_2O_3, BaO_2 + $Ba(OH)_2$, and CuO were prepared from oxide powders by cold pressing, followed by partial sintering. They were inserted into copper retaining rings, which subsequently were attached to the rotating target holder.

A typical deposition cycle proceeds in the following manner: The computer activates the stepper motor, positioning the first target under the beam. The QCR is then automatically programmed by the computer to the target material density value, the thickness reading is set to zero, and the ion beam is switched on. The thickness of the layer is monitored until the programmed set point is reached. The beam is switched off, and the cycle is repeated with each component until the desired film thickness is obtained. Switching the beam off during the target change minimizes possible contamination of the film that may arise from sputtering of holder material during the transition from one target to another. As a precaution the holder is constructed of copper. In the work described here, an accuracy of 3% has been achieved. Subsequent work has demonstrated point-to-point and film-to-film accuracy of better than 1%, as seen in Figure 9. Calculations were performed to determine the correct layer thicknesses required to obtain $YBa_2Cu_3O_{7-\delta}$ films. The calculated values (assuming the usual oxygen stoichiometry and literature density values for the deposited oxide layers) were about 10 Å Y_2O_3, 23.8 Å BaO_2 and 16.8 Å CuO. These, with oxygen added during the post deposition annealing, would yield the required film stoichiometry. However, the first films were slightly Cu rich and significantly Ba deficient. Empirical corrections were made to adjust the film stoichiometry. The resulting dwell time of the ion beam on each target was 11,35, and 6 seconds respectively. Films were deposited to a total thickness of about 1 μm, equivalent to 120 cycles of the three targets' exposure to the ion beam. The differences between the

calculated and empirically corrected values for the layer thicknesses, as described above, may be due to a combination of factors including deviation of the deposited oxides from their nominal stoichiometries, sticking coefficients <1, possible target charging, and ion scattering which can lead to sputtering of the growing films and/or gas incorporation, as well as variation introduced by the difference in position of the substrate and the QCR.

Films were deposited on single crystal MgO at various temperatures. In order to avoid excessive heating of the QCR under the present geometrical arrangement, a substrate temperature of 200°C was chosen for initial studies. Deposition was followed by annealing in an oxygen atmosphere at 850-910 °C and 120 minutes at 500 °C for an oxygen incorporation step in the ramp down cycle. As-deposited films were insulating and shiny black in appearance.

5.4 Film Characterization

The high T_c superconducting films were characterized by analyzing their chemical, structural, and electrical properties. Several available techniques,i.e., energy dispersion spectroscopy (EDS), scanning auger spectroscopy (SAM), and Rutherford back scattering (RBS), were utilized to analyze overall and local stoichiometric ratio of the deposited films. The superconducting thin film microstructures were examined by scanning (SEM) and transmission (TEM) electron microscopies, and X-ray diffractometry (XRD). The superconducting transition temperature (Tc) and critical current density (Jc) of the films were measured with a four point probe technique, using procedures recommended at the DARPA "Measurements Workshop".

5.4.1 Chemical Composition Analysis

Control of the chemical stoichiometry is the first and key criterion when depositing multicomponent thin films. Several techniques have been used to check the accuracy of the stoichiometric chemical composition.

The standard operating beam energy for the EDS analyzer in the SEM and TEM was 25 keV and 100 keV respectively. Energy dispersive and Auger spectra of the deposited thin films were compared with standard spectra obtained from a bulk superconductor sample. Figure 36 shows both the standard EDS spectrum and a typical EDS spectrum for a superconductor thin film with a close chemical stoichiometry. EDS and SIMS were also employed to study inert gas incorporation during deposition. RBS was used to determine the stoichiometric ratio of as-deposited and annealed films. Resolution limitations among elements as well as interdiffusion within films rendered the chemical composition

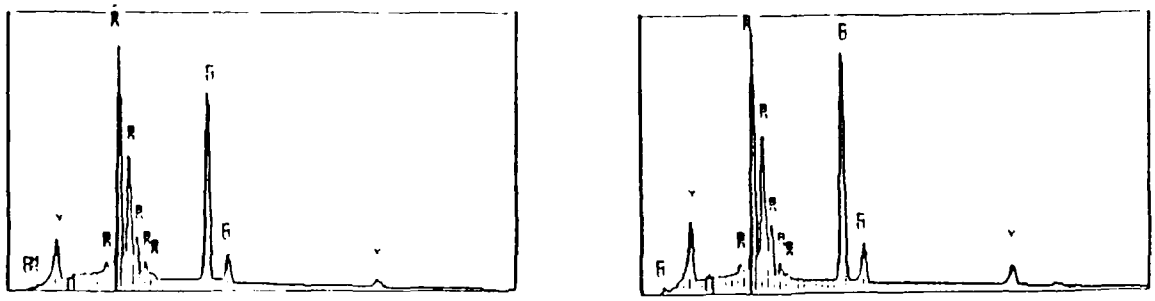

Figure 36. Energy dispersive spectra of superconductor a) thin film and b) bulk samples.

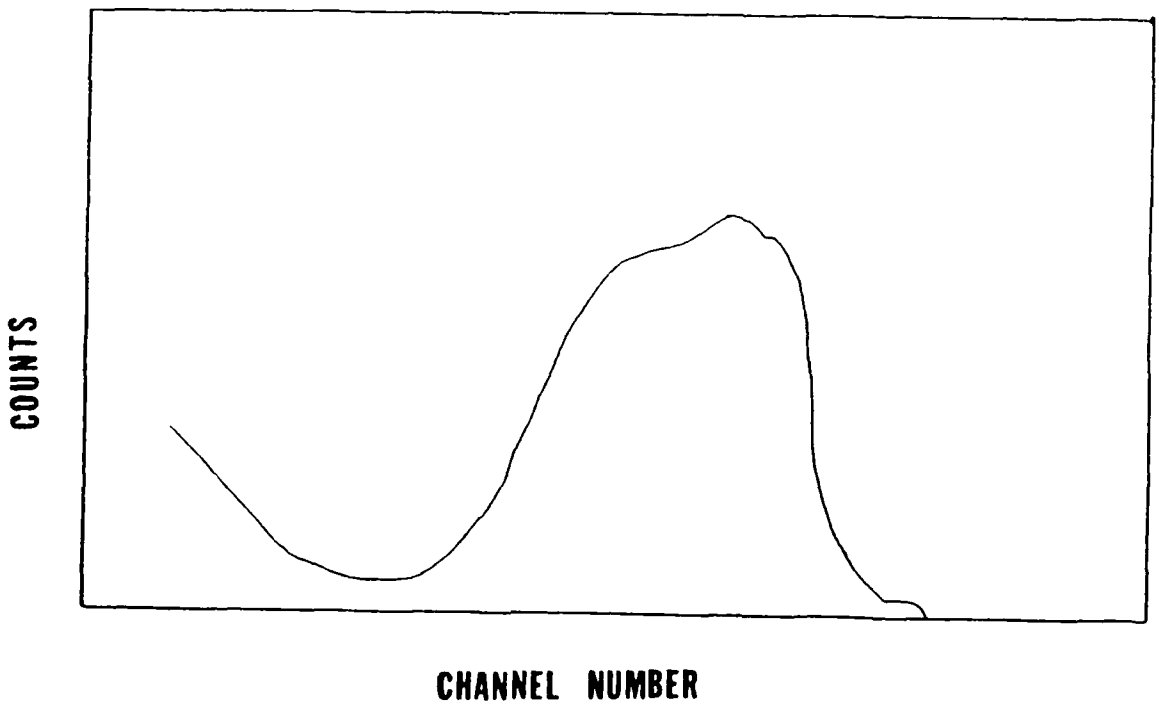

Figure 37. RBS spectrum of a yttrium barium copper oxide sample.

measurements unreliable. Further work is underway to improve the analysis conditions. A typical RBS spectrum is shown in Figure 37.

5.4.2 Structure and Microstructure Characterization

A multiphase structure has been commonly observed in the close stoichiometric superconducting thin film. Therefore, microstructure observation and phase identification are necessary to correlations and then feed back information to optimize processing parameters. SEM, TEM, and XRD were used to perform the microstructure analysis of the deposited films. Optically smooth films were obtained, which revealed an as-deposited amorphous microstructure. Subsequent annealing and oxygenation of the films produced a polycrystalline structure with an average grain size ranging from 0.1 to 0.3 μm.

SEM micrographs served to initially study gas incorporation into the films. An annealed film deposited on a room temperature substrate at 90^{o} with respect to the ion beam (see Figure 2) is shown as an example in Figure 38. The elevated surface parts of the film are blisters that were produced during the annealing process. These features were most probably generated by incorporation of scattered ions from the target during the film deposition, a phenomenon well known from extensive studies on ion implantation in solids.[9] X-ray diffraction was used to reveal the structure and the orientation of the films. In general, A large analysis area was always covered by the x-ray beam, which helped to obtain information representative of the whole film. A typical x-ray diffraction pattern, characteristic of a random oriented superconductor, is shown in Figure 39.

TEM was one of the most useful techniques used to determine the microstructure of the films, and to perform some chemical analysis. A standard procedure was used to prepare both plan view and cross section samples. Because of the cleavage plane of MgO, extra care was exercised when thinning down the test samples. Figure 40a shows the cross section morphology of superconducting film deposited on a MgO substrate. A diffraction pattern (Figure 40b) from one of the film grains is attached next to the cross section micrograph.

5.4.3 Superconducting Transition Temperature (Tc)

A four point probe technique was used to measure the film resistance as a function of temperature. A schematic drawing of the system is shown in Figure 41. Four strips of silver paint were applied on the thin films in a flowing oxygen environment immediately after the oxygen anneal. Subsequently, four gold leads were pasted on the silver strips by using silver paint. Although this is not the best procedure to obtain contacts with the lowest contact

Figure 38. Exfoliation of superconductor film due to evolution of incorporated gas.

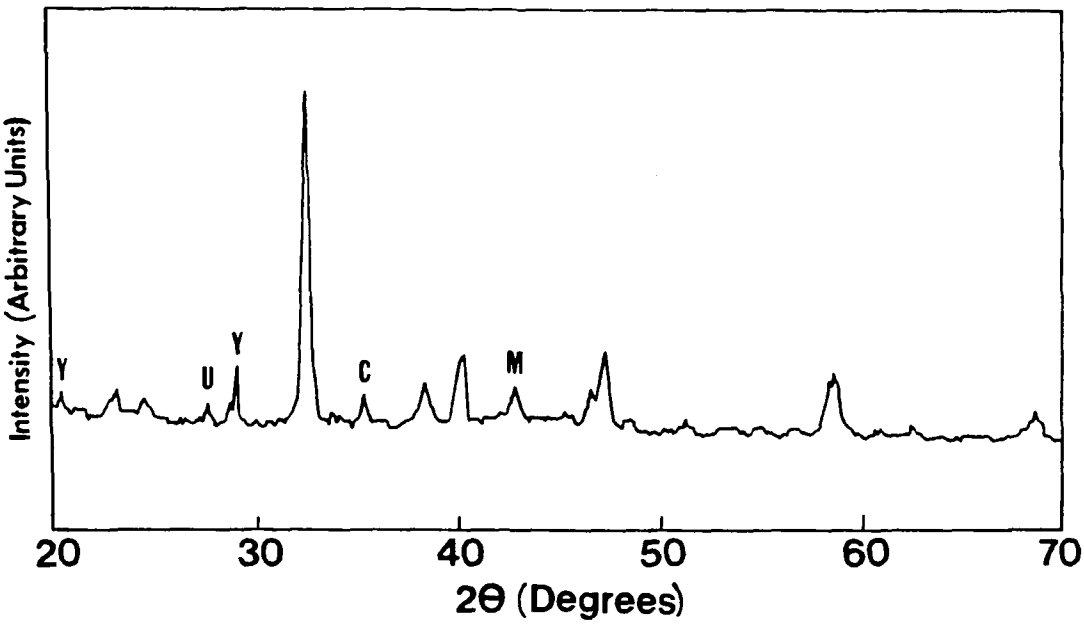

Figure 39. A typical diffraction pattern of a randomly oriented superconductor film.

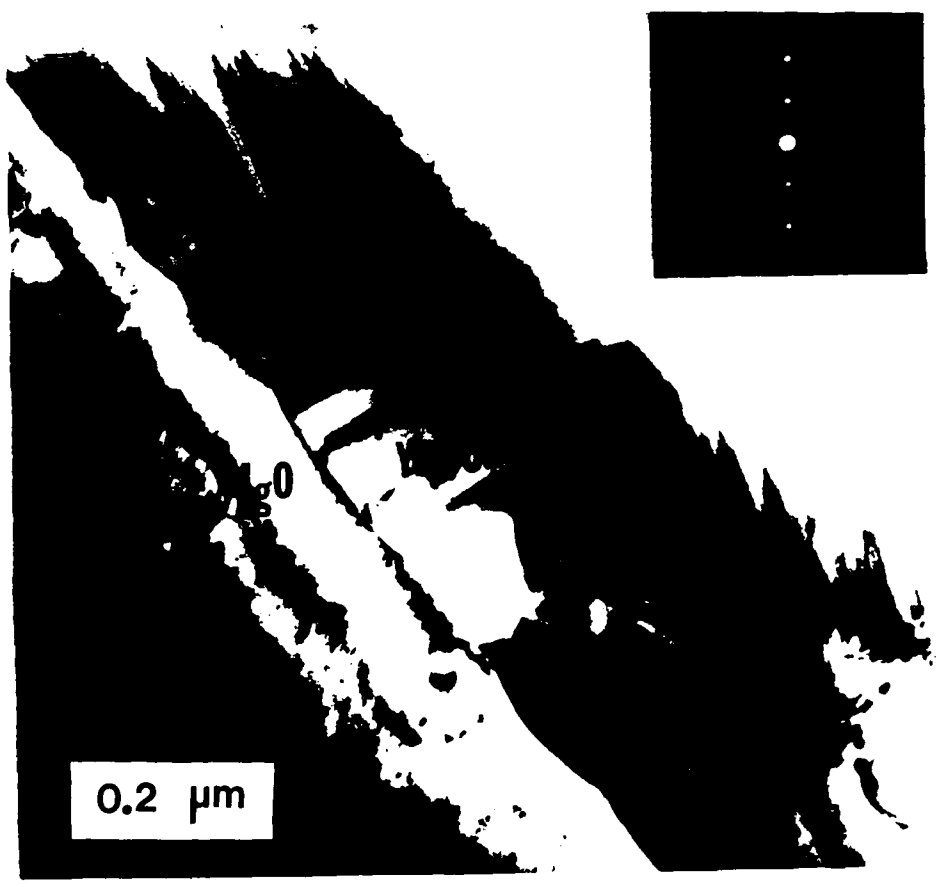

Figure 40. a) A cross section TEM micrograph of a superconductor thin film and b) an (001) pole electron diffraction pattern from one grain.

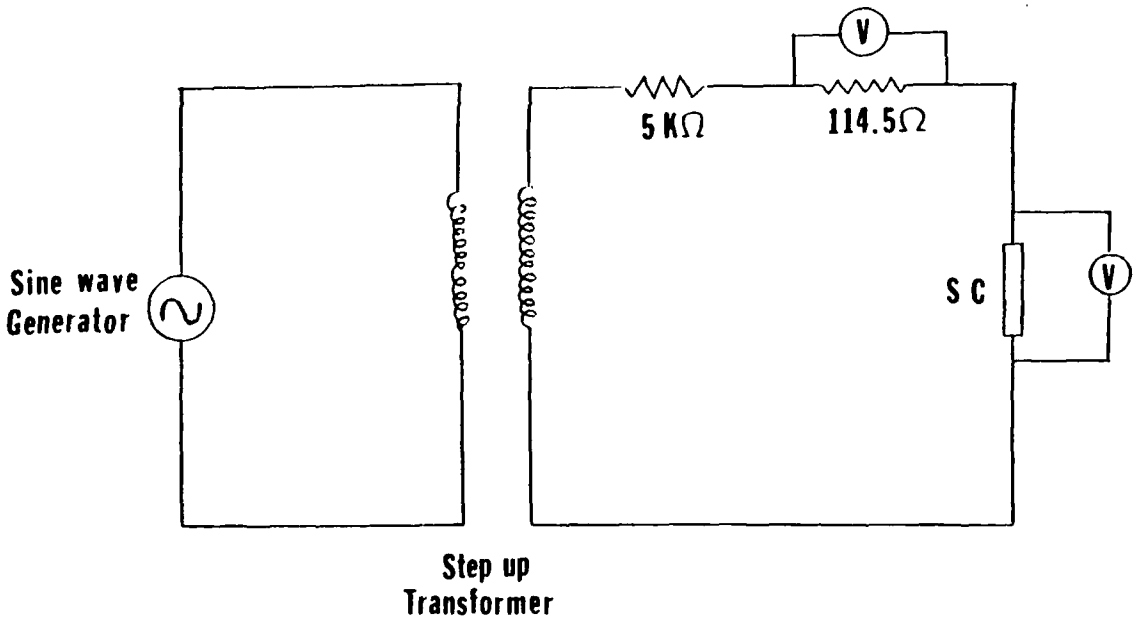

Figure 41. A schematic drawing of the four point probe T_c measurement system.

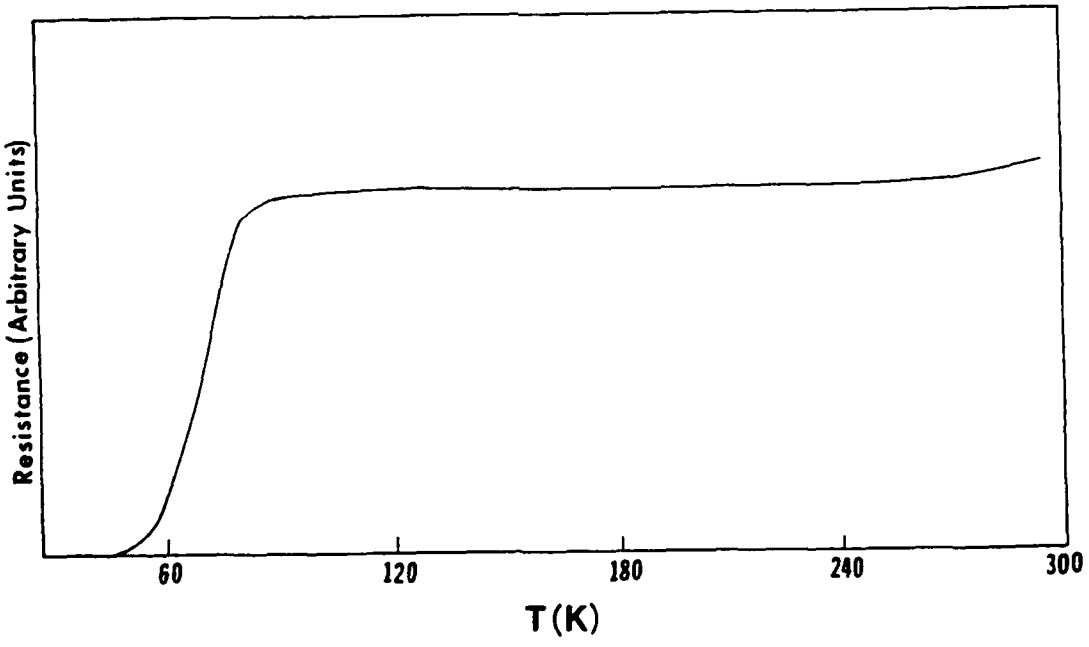

Figure 42. A resistance versus temperature plot for a superconductor sample.

resistance, it produced contacts with resistance low enough to allow performing reliable measurements. A typical resistance vs. temperature curve is shown in Figure 42.

In order to improve the contact making procedure, a metallic mask has been designed, which contains four equally spaced slots through which silver films will be deposited on top of the deposited superconducting layer to form the four contact strips necessary for the four point measuring technique. A post oxygen deposition anneal will be performed to minimize contact resistance as demonstrated by other researchers.

5.5 Patterning Procedures

The objective of producing useful devices from the superconductor films requires a patterning capability. Because of the developments in the area by other research groups, and because of the lack of need for this capability within the first year, it was decided not to utilize project manpower for this task within the first reporting period. Instead, developments have been closely monitored. In addition, one of the principle investigators undertook preliminary patterning studies by direct laser writing, under the auspices of another project[10].

A number of techniques have been applied to the patterning of high Tc superconducting films[11-13]. These have generally included resist lithography, followed by wet or dry etching. These techniques have the advantage of being amenable to large throughput processes. Disadvantages relate to adverse chemical interactions between etchants and films. This becomes particularly important as film thicknesses are reduced, and if etching processes are performed between steps in an SIS or SNS fabrication procedure. Even standard methods for removing the photoresist masks, e. g. by the use of acetone, is potentially unsuitable.

We[10] and others [14,15] have demonstrated the feasibility of direct laser writing. It should be noted that the choice of laser wavelength affects the ultimate feature dimensions.

The above techniques are limited to feature dimensions greater than one micron. Harriott et. al.[16] have demonstrated high resolution patterning of $YBa_2Cu_3O_{7-\delta}$ films with dimensions down to 0.3 μm by focussed ion beam etching. The technique has been used to pattern microbridges, and is useful as a developmental tool.

6. VERY THIN LAYER-BY-LAYER GROWTH

In order to reach a program goal of high quality film deposition at low substrate temperatures using an automated ion beam sputter-deposition system, a method of detecting either the flux of sputtered species from the targets or the mass of material being deposited is required. The device must have the ability to detect these changes with resolution on the order of a monolayer or less for successful layer-by-layer growth of material. Additionally, the technology must possess proper speed and reproducibility in order for an automated feedback mechanism to operate satisfactorily.

We have been investigating a commercially available quartz crystal resonator (QCR) for use in this application. This commercial QCR offers several advantages and disadvantages as enumerated in the following discussion. The QCR can be easily interfaced to the computer that control the experiment for efficient data transfer to the control program. The instrument can be externally programmed by the computer for a zero reset, a setting at which the resolution of the output voltage is 1 Å. The film density as well as other physical characteristics may be programmed, allowing for higher accuracy while depositing from a given target. We describe below a few of the experiments we have performed to test the accuracy and reproducibility of the QCR for very thin layers of materials.

A limitation of the QCR is that a temperature difference exists between the substrate, which is heated by a lamp, and the resonator, which is water cooled. This will cause discrepancy between the measured and actual amount of deposited film due to the thermal dependence of the sticking coefficient. This problem is currently circumvented by calibrating the QCR verses films deposited at temperature. We are also looking into the possibility of using a heated QCR. The geometrical issue of having the QCR in an offset position from the substrate has been investigated through a series of depositions aimed at determining the spatial distribution of sputtered species with respect to the target position, as seen in Figure 43. These results indicate that a symmetric positioning of the substrate and QCR with respect to the target surface normal is essential, in order to assure that films with equivalent thickness are deposited on both the QCR and the substrate. Another problem is the speed at which the data is collected in the QCR control circuit. This number, presently 1 data point per 0.25 seconds, is slow compared to the flux rate of sputtered material produced by useful ion beam currents and energies. Future work will include possible improvements in the performance of the QCR to obtain precise control over the amount of material being deposited.

Our current work has focused on determining the accuracy with which very thin films of metals and oxides can be reproducibly deposited. Figures 44 and 45 show an Auger depth

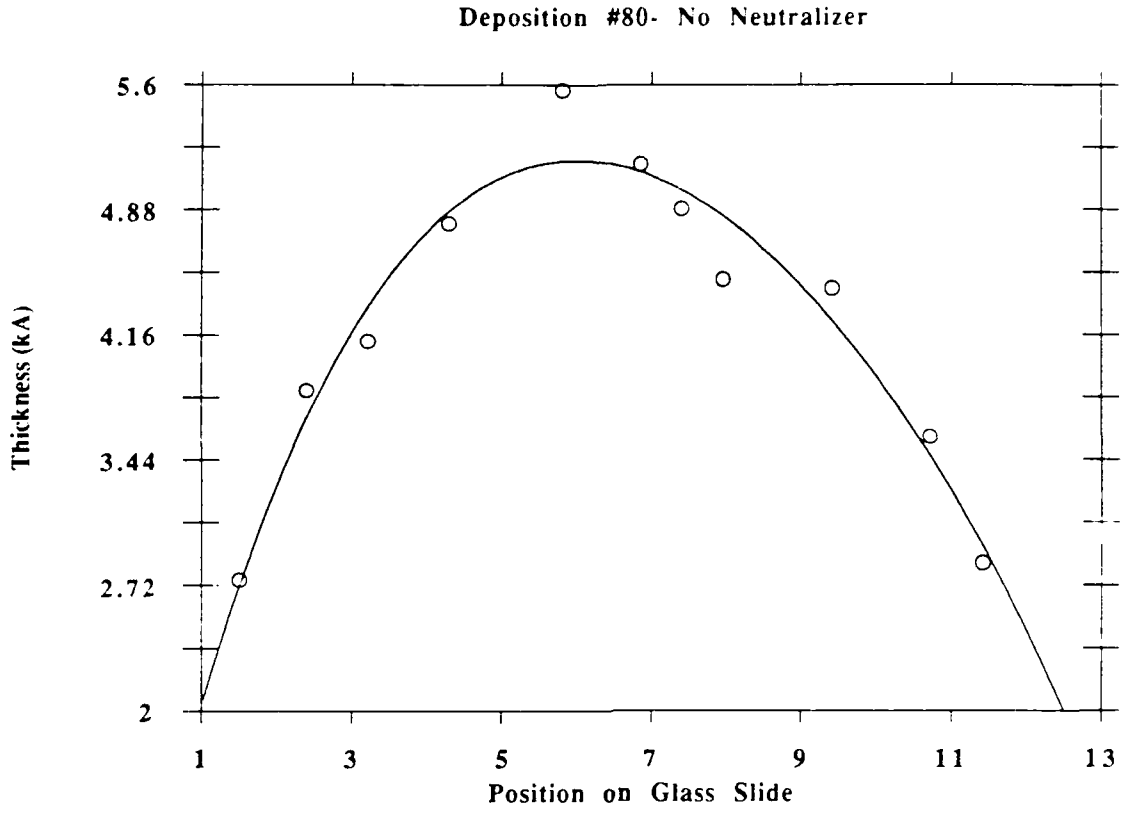

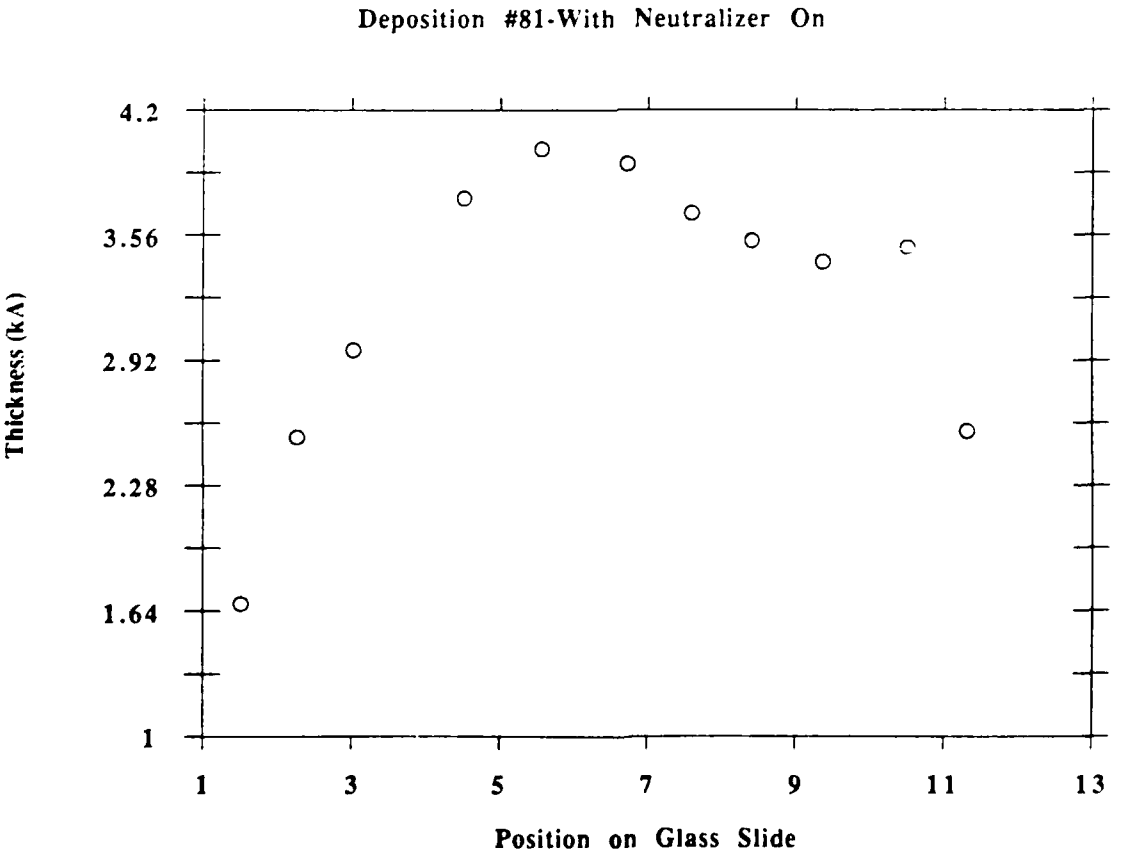

Figure 43. Lateral variation of deposited film thickness, used to determine the optimum position of the quartz crystal resonator. (A) Beam Neutralizer off. (B) Beam neutralizer on.

profiling study of Cu-Nb-Cu sandwich layer structures which were deposited using the QCR controlled by the computer program. Figure 44 shows a multilayer structure of several different thickness deposited using the program. There was an error in the timing sequence of the program that has been corrected, and the actual layer thicknesses are in doubt. However, distinct interfaces can be discerned. Layers of Nb of thickness 100 Å, 50 Å, and 10 Å where deposited in between Cu layers of approximately 500 Å,as seen in Figure 45. The results indicate that the Nb thickness can be controlled to these thicknesses accurately with the QCR. Also, the oxygen peak that follows the Nb indicates a contaminated Nb surface, which should be pre-sputtered. We are currently using field-emission SEM and high resolution TEM to determine the accuracy of the layer thicknesses on an atomic scale.

Smoothed ; at%

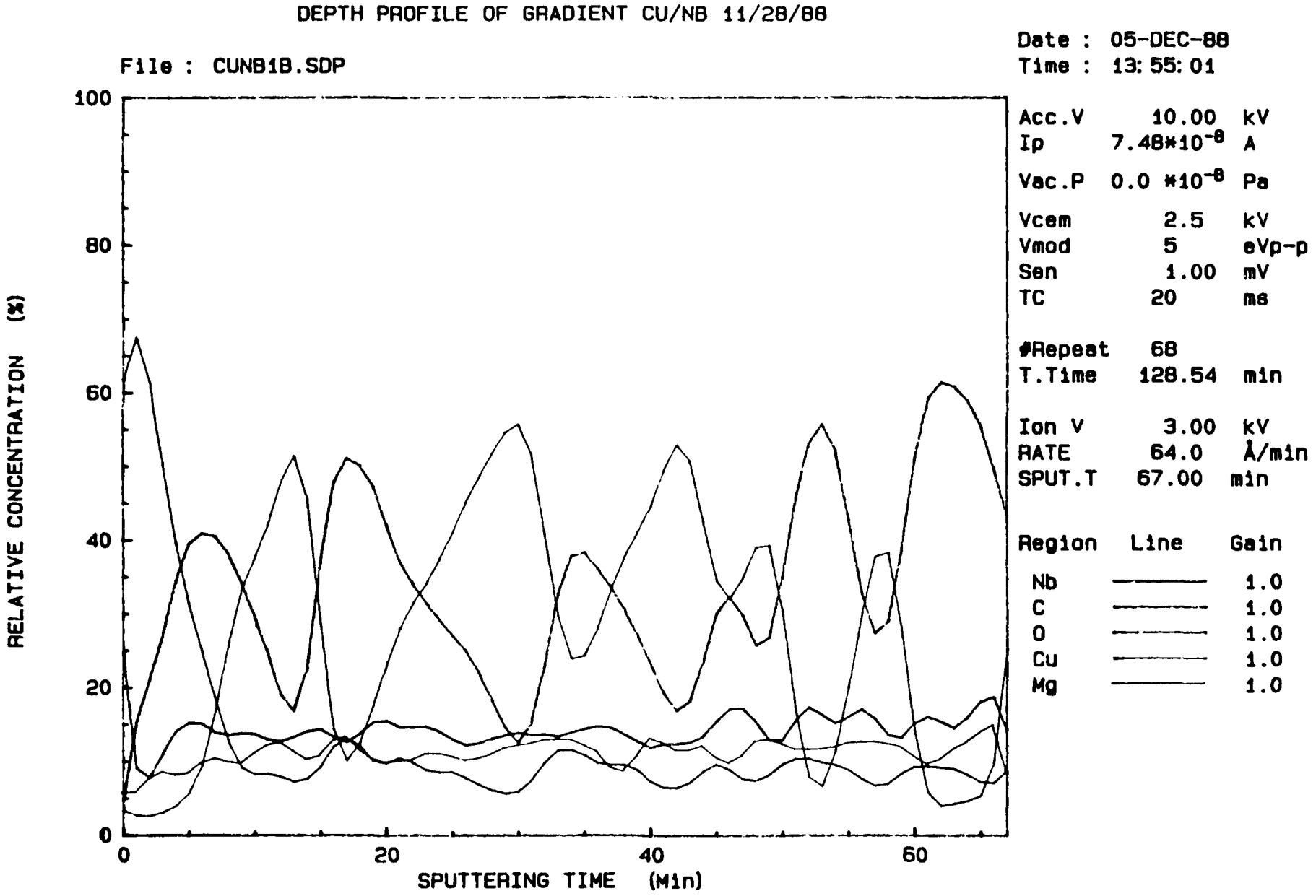

Figure 44. Auger depth profile study of a Cu/Nb multilayer structure with varying Cu and Nb thicknesses.

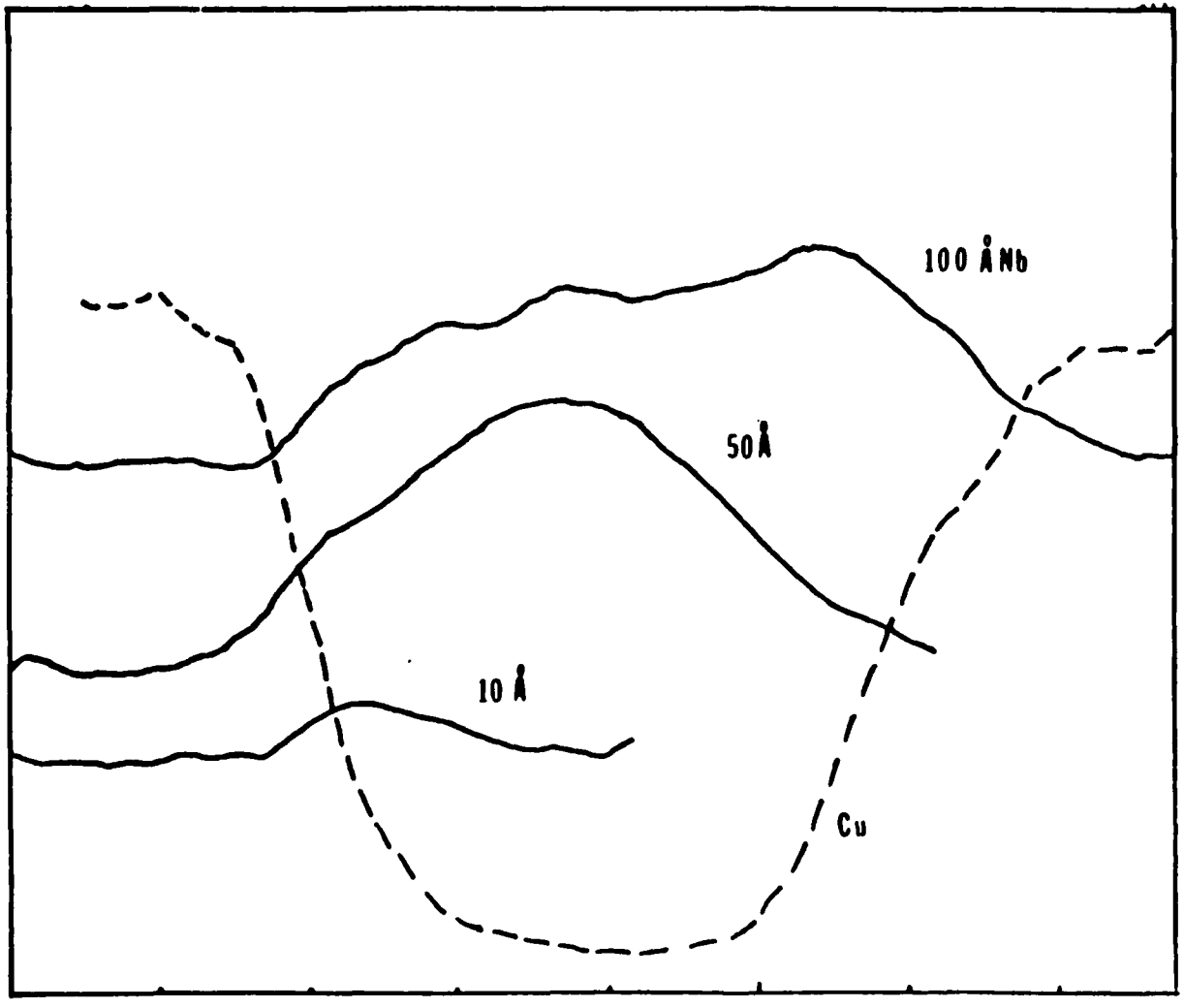

Figure 45. Auger depth profile study of Cu/Nb/Cu heterolayer structures deposited using the ion beam deposition system. The Cu profile was for the 100 Å Nb curve.

7. REFERENCES

1. O. Auciello, M. Ameen, S.H Rou, C.S. Soble, T.M. Graettinger, and A.I. Kingon, Amer. Inst. of Phys. Conf. Proc. No 167,1989.

2. D. D. Berkely, B. R. Johnson, N. Anand, K. M. Beauchamp, L. E. Conroy, A. M. Golman, J. Maps, K. Mauersberger, M. L. Mecartney, J. Morton, M. Touminen, Y. Y-J. Zhang, Appl. Phys. Lett. **53**, 1973(1988).

3. J.M.E. Harper, R.J. Colton, and L.C. Feldman (Eds.), Thin Film Processing and Characterization of High Temperature Superconductors, Amer. Inst. of Phys. Conf. Proc. No. 165, 1988.

4. J.M.E. Harper, J.J. Cuomo, R.J. Gambino, and H.R. Kaufman, Ch.4 in "Ion Bombardment Modification of Surfaces: Fundamentals and Applications", O. Auciello and R. Kelly (Eds),Elsevier Publishers, 1984.

5. J.W. Coburn, Ch.1 in "Plasma Diagnostics:Surface Analysis and Interactions" vol. 2, O. Auciello and D.L. Flamm (Eds.), Academic Press, 1989.

6. P. Sigmund, in "Sputtering by Particle Bombardment, vol. I", R. Bericsh (Ed.), Springer Verlag, p.9, 1981.

7. J.P. Biersack and W. Eckstein, Appl. Phys. **A34**, 73 (1984).

8. O. Auciello, Rad. Eff. **61,** 1 (1981).

9. O. Auciello, Ch. 1 in "Ion Bombardment Modification of Surfaces: Fundamentals and Applications", O. Auciello and R. Kelly (Eds.), Elsevier Science Publishers, 1984.

10. U. Varshney, R. J. Churchill, H. P. Groger, and A. I. Kingon, "CO2 laser patterning of plasma-deposited High Tc superconducting thick films," accepted for publication in J. Appl. Phys.

11. S. Matsui, Y. Ochiai, Y. Kojima, H. Tsuge, N. Takado, K. Asakawa, H. Matsutera, J. Fujita, T. Yoshitake, and Y. Kubo, J. Vac. Sci. Technol. B**6**, 900 (1988).

12. H. Tsuge, S. Matsui, N. Matsukura, Y. Kojima, and Y. Wada, Extended Abstracts Int. Conf. on Solid State Devices and Materials, Tokyo, 1988.

13. I. Shih and C. X. Qiu, Appl. Phys.Lett. **52**, 1523 (1988).

14. S. Matsui, N. Takado, H. Tsuge, and K. Asakawa, Appl. Phys. Lett. **52**, 69 (1988).

15. A. Gupta and G. Koren, Appl. Phys. Lett. **52**, 665 (1988).

16. A. Inam, X. D. Wu, T. V. Venkatesan, S. B. Ogale, C. C. Cheng, and D. Dijkamp, Appl. Phys. Lett. **51**, 1112 (1987).

17. L. R. Harriott, P. A. Polakos, and C. E. Rice, Appl. Phys. Lett, accepted for publication August , 1989.

8. ACKNOWLEDGMENTS

We would like to acknowledge useful discussions with the following individuals: Robert Stokes, for help with the MgO substrate characterization and cleaning procedures, David Haase for aid with the Tc and Jc measurements, and Alan Krauss, as a collaborator in the development of the deposition system.

9. PUBLICATIONS AND PRESENTATIONS, JUNE 1988-JUNE 1989

1. "$YBa_2Cu_3O_{7-\delta}$ Films Deposited by a Novel Ion Beam Sputtering Technique,"A. I. Kingon, O. Auciello, M. S. Ameen, S. H. Rou, and A. R. Krauss, accepted for publication in Applied Physics Letters, July 24, 1989.

2. "Ion Beam Sputter Deposition of $YBa_2Cu_3O_{7-\delta}$: Beam Induced Target Changes and Their Effect on Deposited Film Composition," O. Auciello, M. S. Ameen, T. M. Graettinger, S. H. Rou, C. N. Soble, and A. I. Kingon, American Inst. of Phys. Conf. Proc. **167**, 1989.

3. "Computer Controlled Ion Beam Sputter Deposition of Multicomponent Oxides," A. I. Kingon, M. S. Ameen, O. Auciello, C. N. Soble, T. M. Graettinger, S. H. Rou, Amer. Cer. Soc. Conf. Proc. (in press, 1989).

4. "A Critical Analysis of Deposition Techniques and Basic Phenomena Related to High Temperature Superconducting Thin Films," O. Auciello, A.R. Krauss and A.I. Kingon (Invited Review, Scanning Electron Microscopy International Journal, in preparation, 1989).

5. "Studies on Ion Scattering and Sputtering Processes in Ion Beam Sputter-Deposition of High Tc Superconducting Films: Their Importance For Optimization of Deposition Parameters," O. Auciello, M.S. Ameen, A. R. Krauss, and A. I. Kingon, submitted to AVS Fall Meeting Symposium on High Tc Superconductors.

Presentations

1. "A Critical Analysis of Deposition Techniques and Basic Phenomena Related to High Temperature Superconducting Thin Films", by O. Auciello (Invited), Scanning Electron Microscopy International Conference, Utah, 1989.

2. "Computer Controlled Ion Beam Sputter-Deposition of Multicomponent Oxides", by A.I. Kingon (Invited), Amer. Cer. Soc. Annual Symposium, Indianapolis, IN, 1988.